AD NUMBER

AD818448

LIMITATION CHANGES

TO:

Approved for public release; distribution is unlimited. Document partially illegible.

FROM:

Distribution authorized to U.S. Gov't. agencies and their contractors; Critical Technology; MAR 1967. Other requests shall be referred to Air Force Cambridge Research Laboratory, OAR(CRDM), Hanscom AFB, MA 01730. Document partially illegible. This document contains export-controlled technical data.

AUTHORITY

afcrl ltr, 22 dec 1971

UNCLASSIFIED

AFCRL-67-0348

STUDY OF ECM ANTENNA OPTIMIZATION

AUTHORS
P.F. SFORZA, S.N. SAMADDAR,
E. ROLFE, J.G. WEISS

RAYTHEON COMPANY
SPACE AND INFORMATION SYSTEMS DIVISION
SUDBURY, MASSACHUSETTS

CONTRACT NO. AF19(628)-5519
PROJECT NO. 8671
FINAL REPORT

CONTRACT MONITOR
WALTER ROTMAN
MICROWAVE PHYSICS LABORATORY

U67-4138

JUNE 1965 - MARCH 1967

RAYTHEON

RAYTHEON COMPANY

SPACE AND INFORMATION SYSTEMS DIVISION

RAYTHEON COMPANY

SPACE AND INFORMATION SYSTEMS DIVISION

AFCRL-67-0348

STUDY OF ECM ANTENNA OPTIMIZATION

AUTHORS
P.F. SFORZA, S.N. SAMADDAR,
E. ROLFE, J.G. WEISS

RAYTHEON COMPANY
SPACE AND INFORMATION SYSTEMS DIVISION
SUDBURY, MASSACHUSETTS

CONTRACT No. AF19(628)-5519
PROJECT No. 8671
FINAL REPORT

U67-4138

JUNE 1965 - MARCH 1967

THIS RESEARCH WAS SPONSORED BY THE
ADVANCED RESEARCH PROJECTS AGENCY
ARPA ORDER No. 693

PREPARED FOR

AIR FORCE CAMBRIDGE RESEARCH LABORATORIES
OFFICE OF AEROSPACE RESEARCH
UNITED STATES AIR FORCE
BEDFORD, MASSACHUSETTS

This document is subject to special export controls and each transmittal to foreign governments or foreign nationals may be made only with prior approval of

Hq. AFCRL OAR
(CRDM) USAF, L.G. Hanscom Field
Bedford, Massachusetts

ACKNOWLEDGMENT

This research was supported by the
Advanced Research Projects Agency
Project DEFENDER
and was monitored by the
Air Force Cambridge Research Laboratories
under Contract No. AF 19(628)-5519

RAYTHEON COMPANY
SPACE AND INFORMATION SYSTEMS DIVISION

PROGRAM CONTRIBUTORS

R. Maartmannmoe	Program Manager
J. G. Weiss	Manager of Advanced Reentry Technology
E. Rolfe	Technical Director
P. F. Sforza	Project Leader
Dr. S. N. Samaddar	Senior Engineer
J. C. L. Shabeck	Staff Engineer
J. Whelpton	Senior Engineer
R. Young	Engineering Assistant
J. Bancewicz	Engineering Assistant

ABSTRACT

Measurements on the effects of a conical plasma sheath on two orthogonally oriented slot antennas flush-mounted on the surface of a conical vehicle model were made. The plasma parameters were varied over the range $13 < \omega p/\omega < 23$, $.007 < \nu/\omega < .026$. The measurements were performed at 2700 MC with input powers of 100 milliwatts and 10 watts.

The antenna patterns show strong interference effects and signal attenuation on the order of 30db. Isolation between the slot antennas is found to decrease 20 db for $\omega p/\omega > 20$ and $\nu/\omega < .008$. The antenna input impedance is observed to be appreciably affected by pressure changes of 1 Torr in argon for high input power (i.e., 10 watts). The impedance is also observed to undergo an appreciable change for high power but constant pressure. The greatest change in input impedance is produced by an RF sustained plasma at the antenna aperture at high power. The plasma sheath produced a maximum VSWR of 4.5 indicating that the major loss of power was due to absorption in the plasma. The RF sustained plasma produced a maximum VSWR of 7.8.

Developments in progress to extend the operating range of the simulator are described.

The analytical problem of determining the input impedance and radiation field pattern of a slot antenna on the surface of an infinite conducting cone covered by a plasma sheath is formulated.

A summary of a systems analysis is presented.

TABLE OF CONTENTS

TABLE OF CONTENTS (CONT.)

LIST OF ILLUSTRATIONS

LIST OF ILLUSTRATIONS (CONT.)

LIST OF ILLUSTRATIONS (CONT.)

LIST OF ILLUSTRATIONS (CONT.)

SECTION 1

INTRODUCTION

This report describes the work performed during the final quarter by the Space and Information Systems Division of the Raytheon Company on Contract AF19(628)-5519 for the Air Force Electronic Systems Division (ESKK), Systems Command, under ARPA Project Defender.

The purpose of the program was to use a laboratory reentry plasma simulation technique to study the effect of the plasma sheath on various types of practically realizable ECM vehicle antennas. On the basis of this study an optimum antenna configuration for penetrating through the plasma sheath was to be recommended. Due to the difficulties encountered in developing the plasma simulation technique, time and funds permitted the detailed investigation of only one type of antenna configuration. The experimental and analytical studies were concerned with the effects of the plasma sheath on two orthogonally oriented slot antennas flush-mounted on the surface of a conical reentry vehicle model.

The analytical problem of determining the antenna input impedance and radiation-field pattern was formulated, and the field amplitude coefficients were in the process of being evaluated. At this point, the analytical effort was terminated to conserve funds and place more emphasis on the experimental effort. The experimental program was carried out in great detail, producing many useful results.

A systems study was performed to guide the program towards reentry systems problems and requirements.

1.1 Summary of Experimental Effort

A dc discharge plasma simulator was constructed which produced a conical plasma sheath whose overall dimensions were approximately equal to those of a typical ECM reentry plasma sheath. Inside the simulator was mounted a copper cone whose dimensions were typical of a full-size ECM vehicle nose cone. Antennas were mounted in the conical surface. A photograph of the setup appears in Figure 2-4, page 2-5.

Electron densities and electron temperatures in the plasma were measured with Langmuir probes. Useful plasma sheaths could be generated with argon gas in the pressure range from 2.4 Torr to 3.5 Torr. The electron-neutral particle collision frequencies were less than 5×10^{8} $(sec)^{-1}$ and electron densities were greater than 10^{13} $(cm)^{-3}$. An anechoic chamber was constructed around the simulator facility for making antenna pattern measurements. The chamber was modified until satisfactory "no plasma" antenna patterns were obtained. This modification process proved to be more difficult than expected, and substantial work was needed to achieve satisfactory results.

An S-Band coaxial system was constructed which produced very little RF leakage. A low RF leakage background was required to obtain meaningful antenna patterns. Antenna patterns, antenna isolation, input impedance and input VSWR were measured at low power (i.e., 100 milliwatts) and high power (i.e, 10 watts.).

In the actual reentry case, electromagnetic energy propagated towards the rear of the vehicle becomes trapped in the wake of

the plasma sheath. This aspect of the wake was simulated by properly terminating the vehicle model at the base with microwave absorber material.

SECTION 2

REENTRY PLASMA SIMULATOR

A dc discharge plasma facility developed in an earlier program by the Raytheon Company was used to generate a conical plasma sheath whose overall dimensions were approximately equal to those of a typical ECM vehicle reentry plasma sheath. The plasma facility is shown schematically in Figures 2-1 and 2-2.

2.1 Construction

The simulator envelope was constructed from two glass cones which were joined at their bases. The apex of the outer cone was connected to 1 1/2" D glass tube which contained a water-cooled anode and two Langmuir probes. Four externally heated cathodes were located near the base of the outer cone, spaced 90° apart. The ac heater supply for the cathodes and the dc discharge power supply are shown schematically in Figure 2-1. The principle dimensions of the simulator are given in Figure 2-3. A photograph of the simulator mounted in the anechoic chamber is shown in Figure 2-4.

The main dc supply was a welding generator capable of supplying 600 amperes of dc current. A dc power supply was put in series with the welding generator to obtain the necessary striking anode-to-cathode voltage required to initiate the discharge. Each cathode stem was air-cooled to prevent excessive thermal stresses in the glass. The cathodes were operated between 900°C and 1000°C; the cathodes were observed to "flicker" at lower operating temperatures. The Langmuir probes were constructed from .010" tungsten wire encased in a glass sleeve. Each probe extended to the

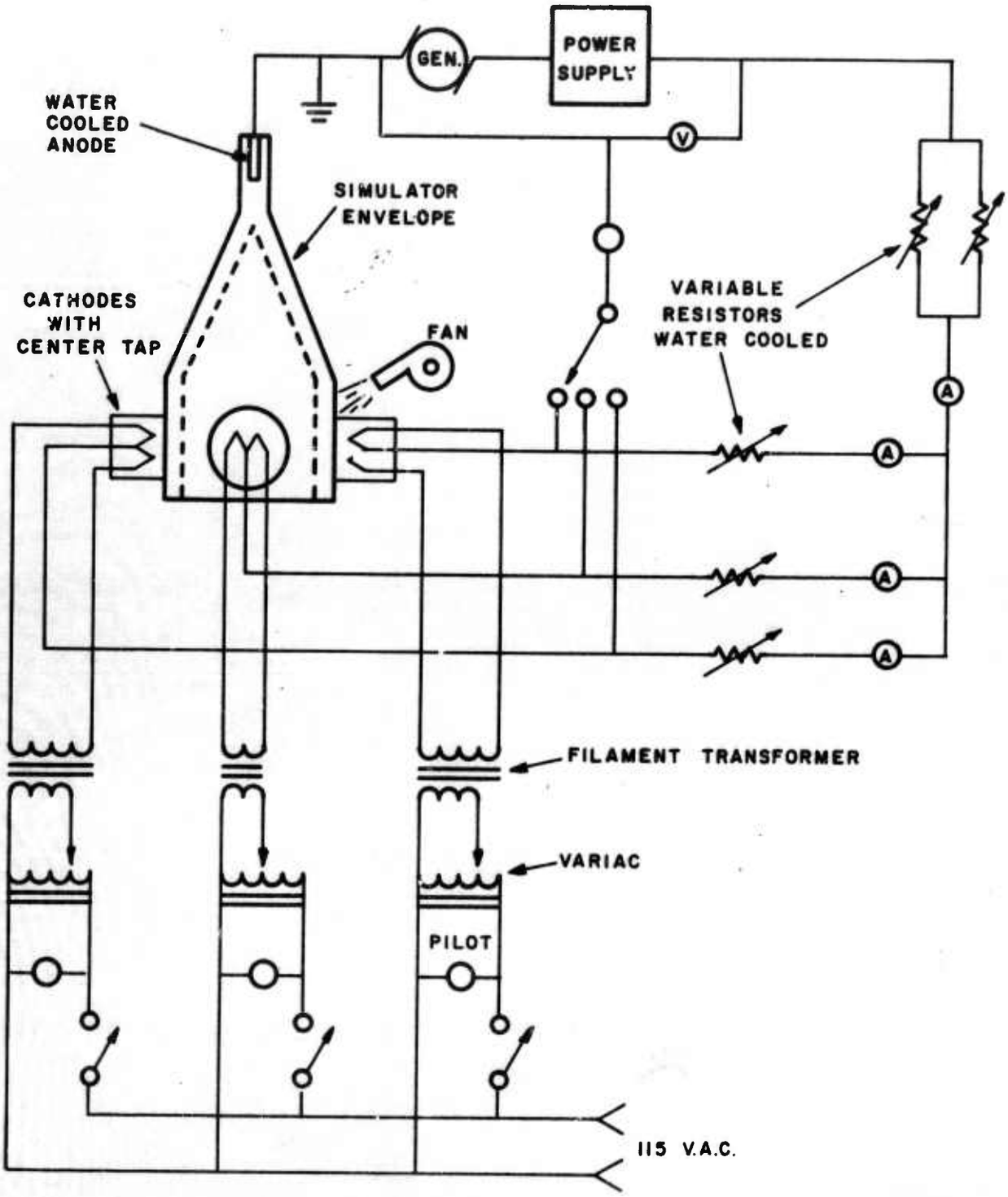

Figure 2-1 Plasma Simulator - Electrical Schematic

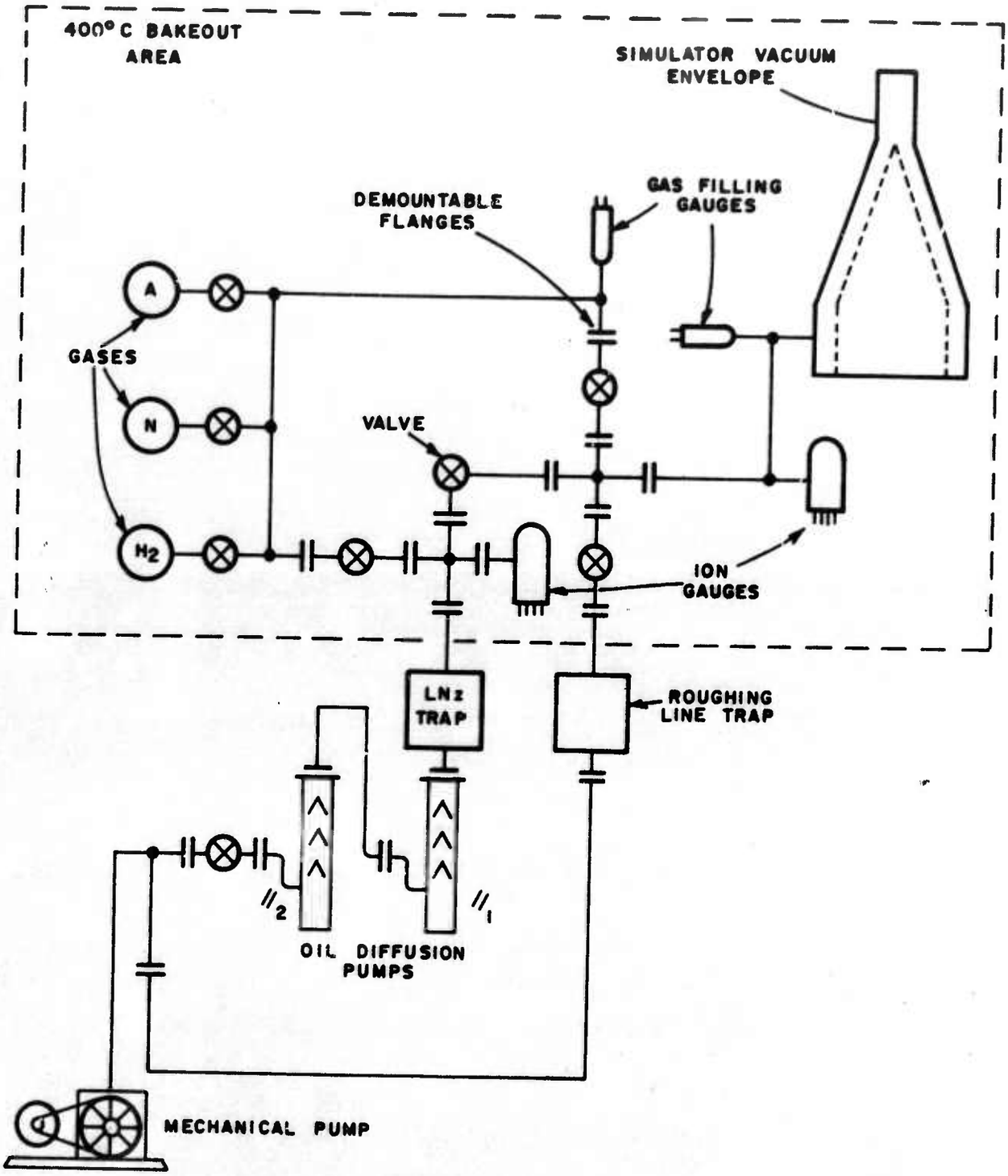

Figure 2-2 Simulator - Vacuum and Gas Schematic

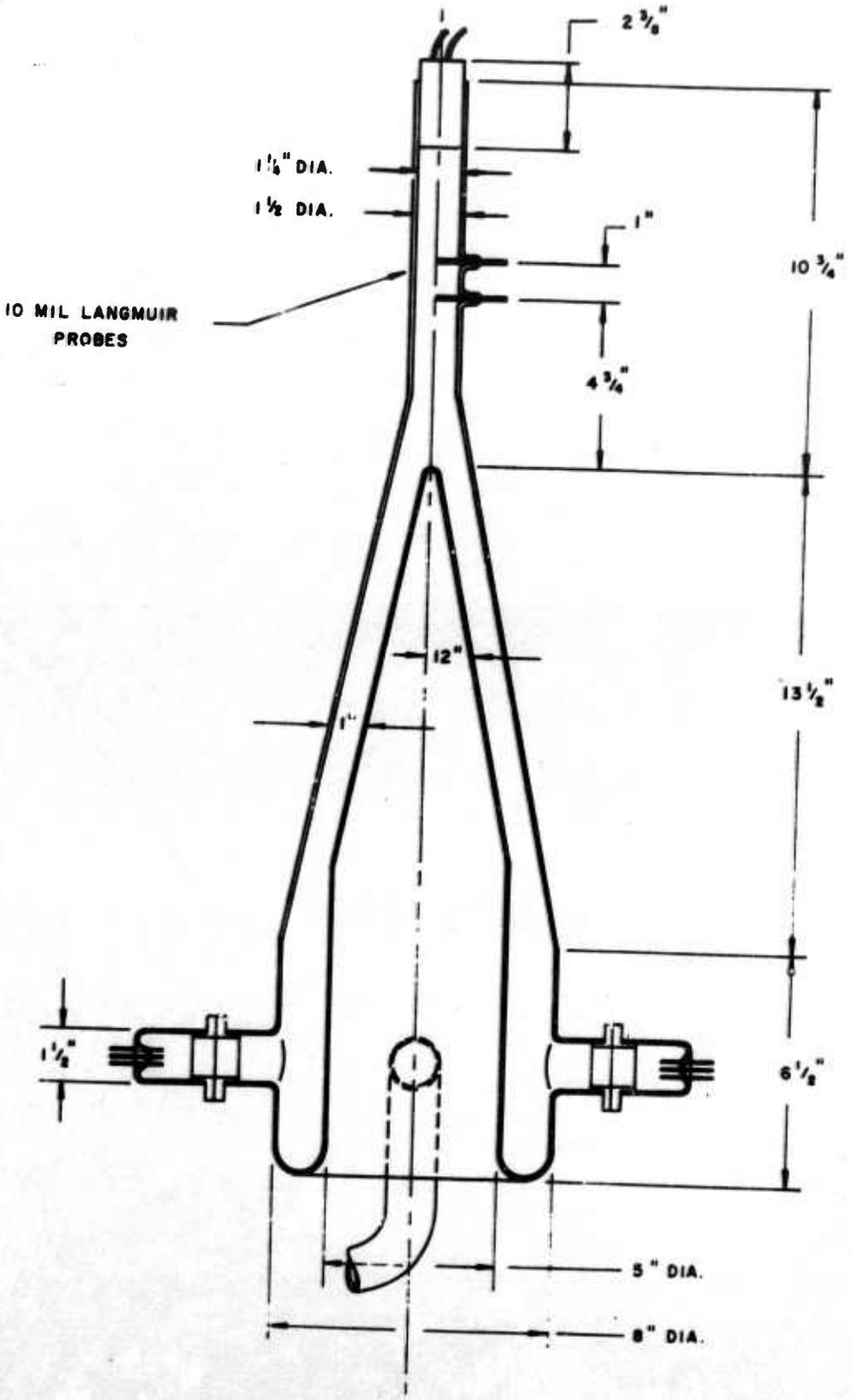

Figure 2-3 Principal Dimensions of Plasma Simulator

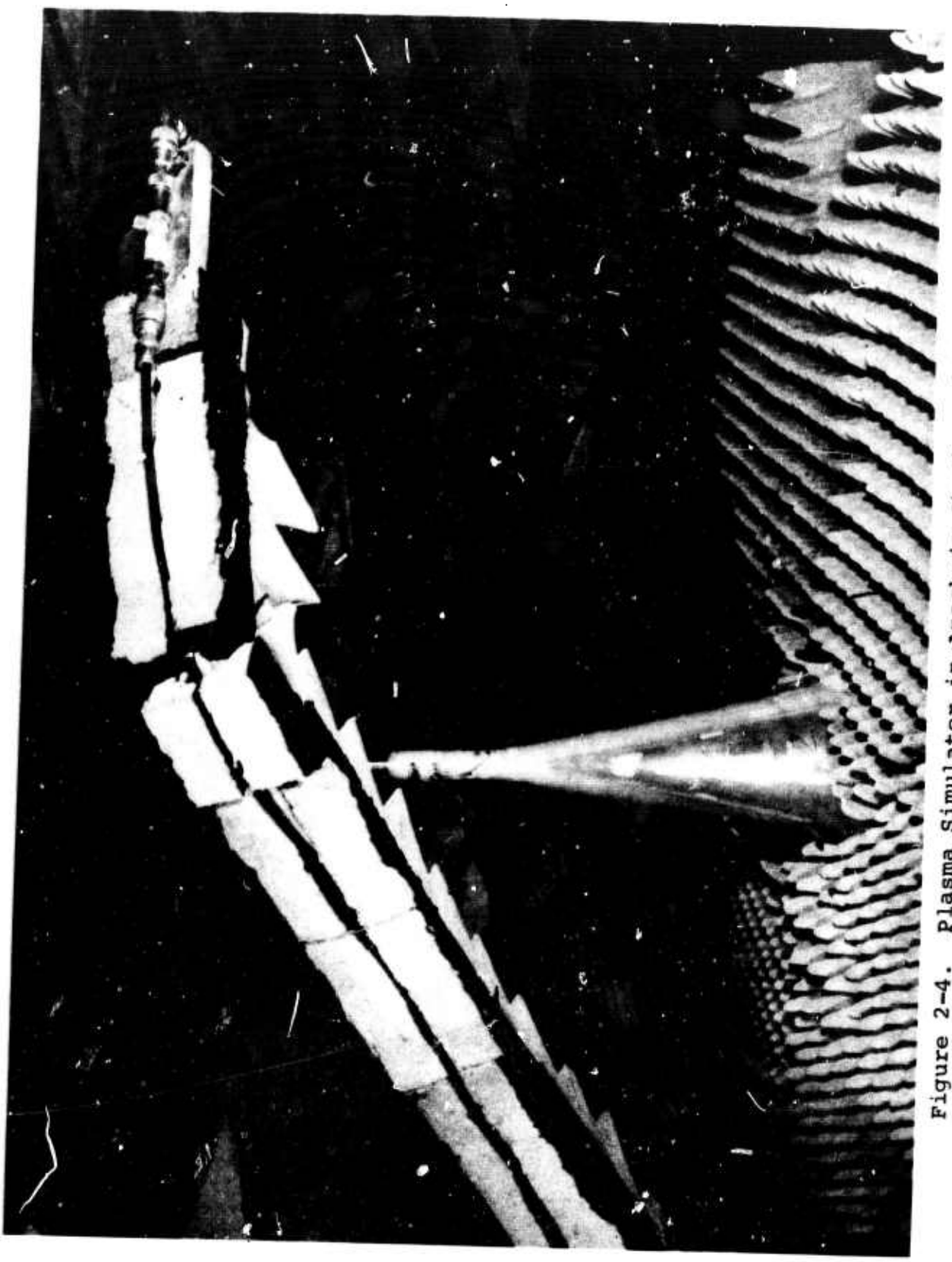

Figure 2-4. Plasma Simulator in Anechoic Chamber with Vehicle Model in Position

center of the discharge column. The use of two probes enabled one to measure the electric field strength in the plasma.

The entire glass system was baked for several days to 350°C to drive impurities out of the glass walls. After bake-out the simulator was pumped down tc 10^{-8} Torr. A very clean system was necessary for steady operation of the discharge, for long cathode life and reproducibility of plasma conditions. The gas pressure could be held at a constant value over a period of several months without adding or subtracting gas. Before making measurements the simulator was run for several hours to further clean the system by particle bombardment, and obtain a stable discharge of a pinkish glow characteristic of a pure argon discharge.

The all-glass gas-mixing section enabled one to mix any three spectroscopically pure gases in any proportion desired (Figure 2-2).

2.2 Operational Characteristics

The electric field in the plasma for gas discharges with externally heated cathodes is constant and close to zero along the distance between the cathode and the anode, except across the cathode fall space which is usually very short, on the crder of 10^{-4} cm (Reference 1). A constant electric field distribution in the plasma is very convenient for determining the drift velocity of electrons at any point in the plasma, since the drift velocity is a function of E/p where E is the electric field strength and p is the gas pressure (Reference 2). Thus the electron drift velocity is a constant along the distance between the cathode and the anode, except for the cathode fall space. For a constant drift velocity of electrons along a discharge vessel of varying cross-sectional area the electron density at some cross-section is related to the electron density at some other

cross-section through the relationship

$$n_e = \frac{I}{A_D e V_d} \qquad (2\text{-}1)$$

where I is discharge current; A_D the cross-sectional area of the discharge vessel; e the charge of the electron and V_d the drift velocity of electrons in the gas being used. Equation (2-1) was used to determine the electron density in the region of the slot antenna (Figure 3-1, page 3-2) as discussed above.

Filling of the simulator envelope with plasma was investigated experimentally over a wide range of gas pressures and discharge currents. One hundred percent argon was used in all experiments. The percentage filling of the simulator depended critically on the gas pressure and to a lesser extent, on the magnitude of the discharge current. At very low pressures (i.e., approximately 25 microns) the gas pressure dropped to zero in about 35 minutes, indicating that argon was being driven into the simulator walls by the discharge. In the current range from 24 amps to 50 amps, however, the simulator was completely filled and the discharge appeared to be very stable. At 50 microns cold pressure the simulator was completely filled and the discharge very stable in the current range from 24 amps to 50 amps. Below 24 amps the discharge became unstable and the percentage filling decreased rapidly with decreasing discharge current. For 215 microns cold pressure complete filling was never achieved. Maximum filling of approximately 75% of the simulator envelope occurred at 48 amps. Below 34 amps the percentage filling decreased rapidly and the discharge became highly unstable. Between 215 microns and approximately 2 Torr the discharge was highly unstable. At 3 Torr cold pressure the percentage filling increased with increasing current

and was almost completely filled (i.e., approximately 95%) at 45 amps discharge current. No attempt was made to run the simulator above 48 amps since the apex temperature of the inner glass cone became very hot at high discharge currents. The percentage filling dropped to about 50% at 25 amps. It was discovered that about 75% filling could be achieved by running the simulator on only three cathodes. With only three cathodes the unfilled portion of the simulator was essentially confined to the region directly above the "turned-off" cathode; whereas the plasma filling in the region over the operating cathodes was increased. This mode of operation of the simulator was found to be most useful when making antenna measurements, since both slot antennas were located on one side of the simulator. At pressures of about 13 Torr the discharge constricted to a strip of plasma about 5 inches wide at 50 amps and 1 inch wide at 4 amps. Such a constricted plasma was useless for antenna measurements.

From the above observations it was concluded that the only useful pressures of operation would be at about 50 microns and 3 Torr. Operation at 50 microns was later excluded when it was discovered that the discharge was fluctuating at a rapid rate, as discussed below.

The supply voltage required to initiate the discharge was typically about 120 volts with the aid of a Teslar coil. The average anode-to-cathode voltage required to sustain the discharge varied between 70 volts at low current and 33 volts at high current. The simulator was run with each cathode drawing equal dc current to obtain a uniform plasma in the azimuthal direction.

Heating of the apex of the inner glass cone required the discharge current to be maintained below 48 amps. Cooling of the apex was provided by a jet of compressed air fed through the ECM vehicle model and directed to one side of the apex. A thermocouple was placed at the apex during the heat tests to obtain a correlation between discharge current and the temperature of the apex. The outer glass cone was cooled by a high capacity blower mounted several feet above the anode.

2.2.1 Plasma Instability

Preliminary antenna patterns taken with argon gas at 60 microns in the simulator showed approximately 3 db of attenuation due to the plasma sheath, but no noticeable pattern distortion. This led us to suspect that the discharge was unstable even though it appeared very stable visually.

A CW S-Band signal was fed into one of the slot antennas, and the signal transmitted through the plasma sheath was detected and displayed on an oscilloscope using the circuit shown in Figure 2-5. The amplitude modulation superimposed on the signal by the plasma is shown in Figure 2-6 and Figure 2-7. In each case it is noted that the mean height of the top of the pulse corresponds to zero db of signal attenuation and the mean height of the bottom of the pulse corresponds to signal attenuation greater than 10 db. The almost square-wave modulation due to the plasma explains the approximate 3 db of attenuation observed from the antenna pattern measurements and the absence of pattern distortion.

At a gas pressure of 620 microns or greater the plasma did not modulate the signal, thus indicating a stable plasma. This is shown in Figure 2-8 and Figure 2-9.

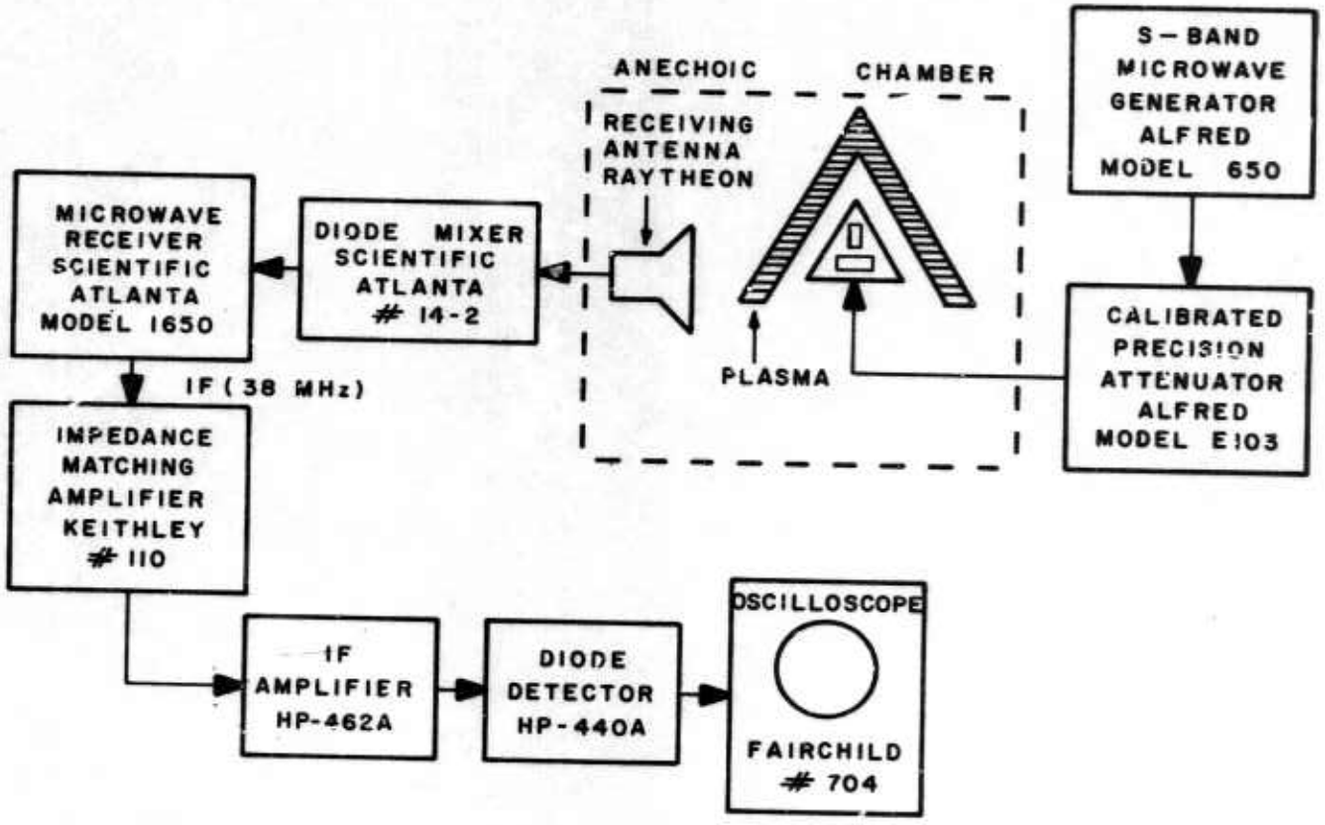

Figure 2-5 Plasma Instability Measurement System

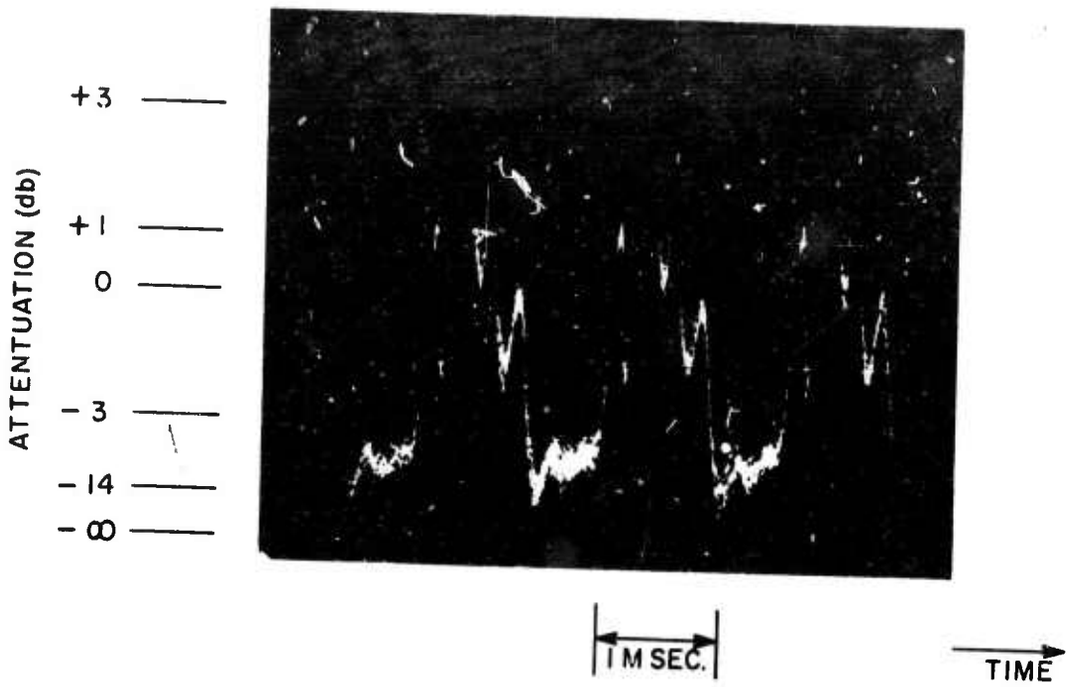

Figure 2-6 Modulation of 2700 MC CW Signal Due to Plasma Instabilities for Argon at 70 Microns and I=35 amps.

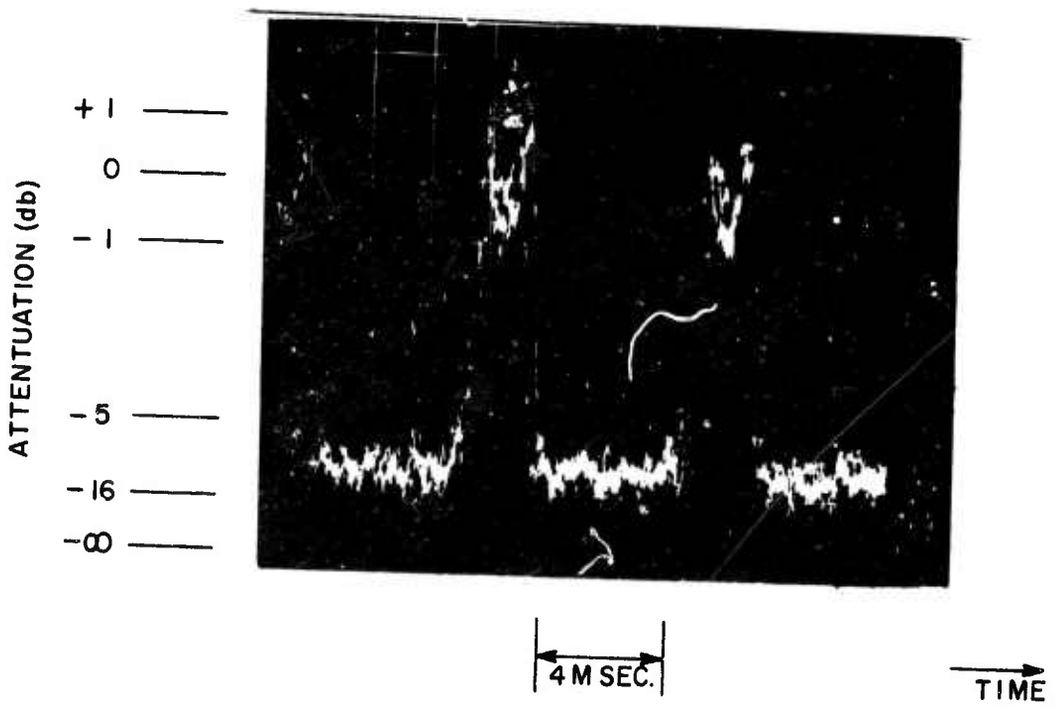

Figure 2-7 Modulation of 2700 MC CW Signal Due to Plasma Instability for Argon at 105 Microns and I=35 amps.

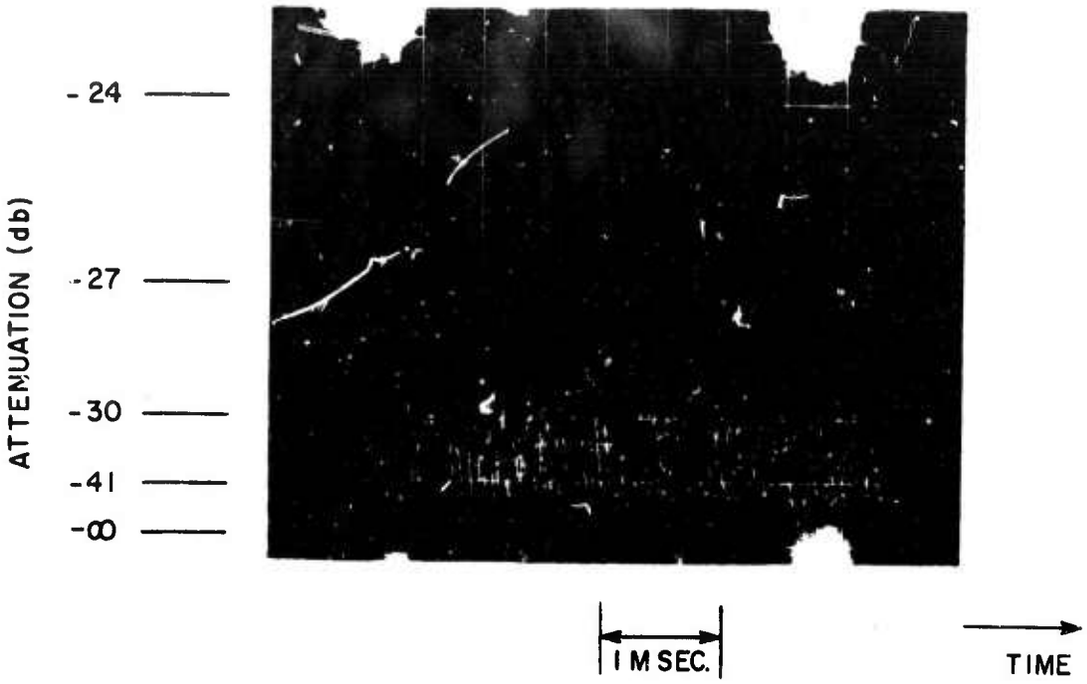

Figure 2-8 Attenuation of 2700 MC CW Signal Due to Plasma Sheath for Argon at 620 Microns and I=35 Amps.

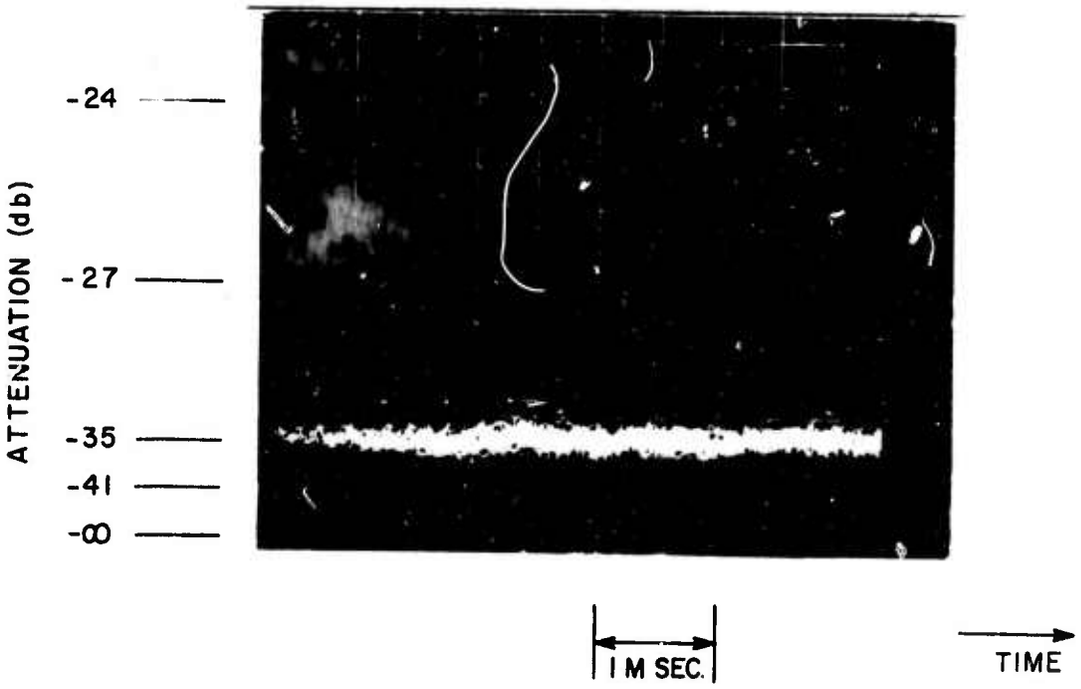

Figure 2-9. Attenuation of 2700 MC CW Signal Due to Plasma Sheath for Argon at 3.0 Torr and I=35 Amps.

No measurements of plasma modulation effects were made for gas pressures below 620 microns and above 200 microns, since the plasma was visually highly unstable, in this pressure range, as discussed in the previous section.

From the above observations on plasma filling of the simulator envelope and plasma stability it was decided to make all antenna measurements at 2.4 Torr and 3.5 Torr.

2.2.2 Plasma Parameters

The electron density and electron temperature at the apex of the simulator were determined from Langmuir probe measurements. The electron density in the vicinity of the slot antennas was obtained by applying equation (2-1) and the measured values of the electron density at the apex of the simulator. To determine the electron-neutral particle collision frequency the gas temperature was measured by noting the change in pressure when the discharge was turned off and applying the ideal gas law.

Since the percentage filling of the simulator with plasma decreased appreciable for discharge currents below 25 amps, the plasma parameters were not measured for currents below 25 amps.

A detailed discussion of Langmuir probe theory, and corrections to Langmuir probe data required at the higher pressures (i.e., above 1 Torr) is given in References 3 and 4. A description of the Langmuir probe circuit used in the experiments is described in Reference 4. A typical Langmuir probe characteristic obtained with the probe nearest the simulator anode is shown in Figure 2-10. The probe current I_p is measured on the vertical axis and the probe voltage V_p (i.e. with respect to the anode) is measured on the horizontal axis. The distance of the

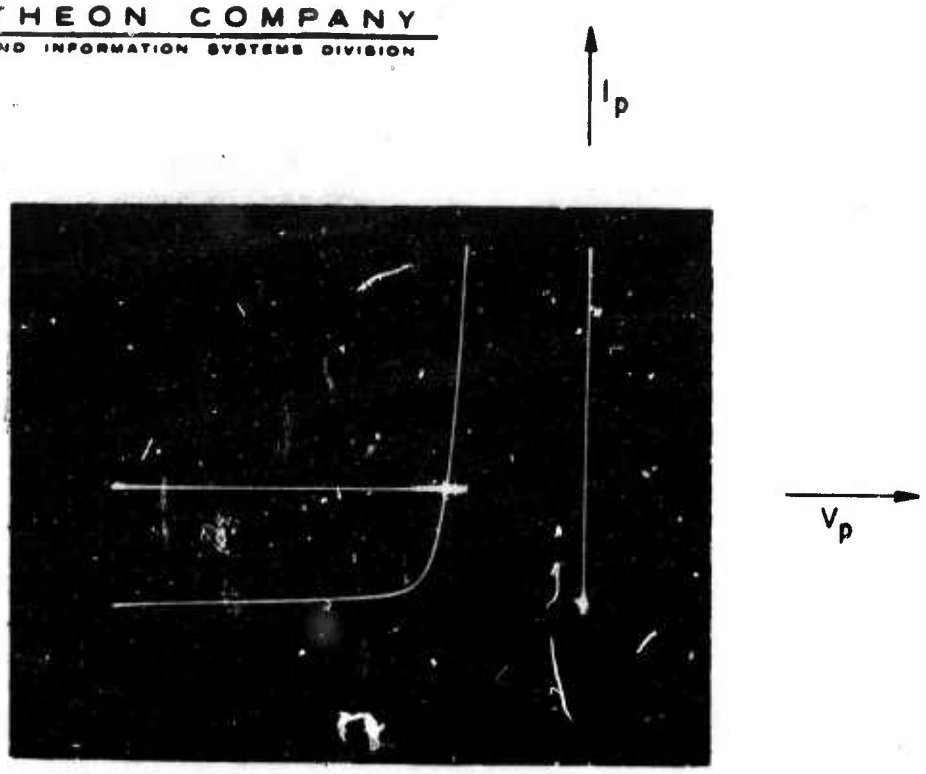

Figure 2-10 Langmuir Probe Characteristic for 25 Ampere Discharge in Argon at 3.5 Torr.

flat bottom portion of the characteristic from the horizontal axis is a measure of the ion saturation current to the probe when the probe voltage is sufficiently negative. The intersection of the characteristic with the voltage axis is the floating potential of the probe ($f_p = 0$). The floating potential was found to be negative in all measurements. The electron saturation portion of the curve could not be obtained since it would have required the probe to draw a large electron current causing the probe to burn out.

2.2.2.1 Electron Density

The electron density at the probe is given by (Reference 4)

$$n_e = \frac{I_{es}}{eA_p \times 1.67 \times 10^5} \frac{e}{kT_e}^{1/2} \quad (m^{-3}) \qquad (2\text{-}2)$$

where,

I_{es} = electron saturation current to the probe (amp)

A_p = probe area (m^2)

T_e = electron temperature (^oK)

e = electronic charge = 1.6×10^{-19} coulombs

k = Boltzmann's constant = 1.38×10^{23} joules/^oK

After substituting the numerical values of e, k and A_p, for the probe used, Equation (2-2) can be re-written in the form:

$$n_e = (23.144)\ (I_{is})\ \left(\frac{I_{es}}{I_{is}}\right) \times \frac{10^{20}}{T_e} \quad (m^{-3}) \qquad (2\text{-}3)$$

where I_{is} is the ion saturation current to the probe. The numerical value of I_{is} is obtained from the Langmuir probe characteristic and the ratio $\left(\frac{I_{es}}{I_{is}}\right)$ is given by Figure 59 of Reference 3.

For $p = 2.4$ Torr $\left(\frac{I_{es}}{I_{is}}\right) = 680$ (2-4)

and for $p = 3.5$ Torr $\left(\frac{I_{es}}{I_{is}}\right) = 840$ (2-5)

The electron temperature is obtained from the slope of the vertical portion of the Langmuir probe characteristic and the

relation (Reference 4)

$$\frac{d(\ln I_p)}{dV_p} = \frac{e}{kT_e} \qquad (2\text{-}6)$$

where I_p is the probe current and V_p the probe voltage with respect to the anode.

From the point of view of antenna measurements, the electron density in the vicinity of the slot antennas is of interest. Let the cross-sectional area of the discharge at the probe be denoted by A_{D1} and the cross-section at a point midway between the two slot antennas by A_{D2}, then from Equation (2-1) of Section 2.2

$$n_{e1} A_{D1} = \frac{I}{eV_d} = n_{e2} A_{D2} \qquad (2\text{-}7)$$

since the total discharge current I and electron drift velocity V_d are independent of the discharge cross-section (Section 2.2). n_{e1} and n_{e2} are the electron densities at A_{D1} and A_{D2}, respectively. If the discharge extends to the simulator walls, A_{D1} and A_{D2} are obtained from the dimensions of the simulator envelope.

In the experiments the discharge was observed to extend to the walls of the simulator, and A_{D1} and A_{D2} were computed simply from geometrical considerations. Substituting for A_{D1} and A_{D2} in Equation (2-7).

$$n_{e2} = \frac{A_{D1}}{A_{D2}} n_{e1} = (.137)\, n_{e2} \qquad (2\text{-}8)$$

From equations (2-3), (2-4), (2-5) and (2-6) the electron density at the probe was calculated for three discharge currents. The

electron density at the slot antennas was then computed from Equation (2-8) and plotted as a function of discharge current in Figure 2-11. The electron temperature calculated from Equation (2-6) is given as a function of electron density in Figure 2-12.

2.2.2.2 Electron-Neutral Particle Collision Frequency

The collision frequency of electrons with gas atoms is given by (Reference 2)

$$\nu = \frac{\overline{V}}{\lambda} \qquad (2\text{-}9)$$

where, $\overline{V}$ is the average speed of the electron and λ is the electron mean free path. For a maxwell-Boltzmann distribution of velocities, $\overline{V}$ is given by (Reference 1):

$$\overline{V} = \left(8\ k\ T_{e/m\pi}\right)^{1/2} \qquad (2\text{-}10)$$

where k is Boltzmann's constant in joules per degree Kelvin, m is the mass of the electron in kilograms and T_e is the electron temperature in degrees Kelvin. The general expression for the mean-free path is given by:

$$\lambda = \frac{1}{p_o P_c} = \frac{1}{\frac{273\ p\ P_c}{T_g}} \qquad (2\text{-}11)$$

or, $$\lambda = \frac{T_g}{273 p P_c}$$

where, T_g is the gas temperature in degrees Kelvin; p is the pressure in mm Hg,; P_c is the probability of collision in $(\text{mm Hg})^{-1}\ \text{cm}^{-1}$, and p_o is the "reduced" pressure. Combining Equations (2-9), (2-10) and (2-11) the collision frequency reduces to:

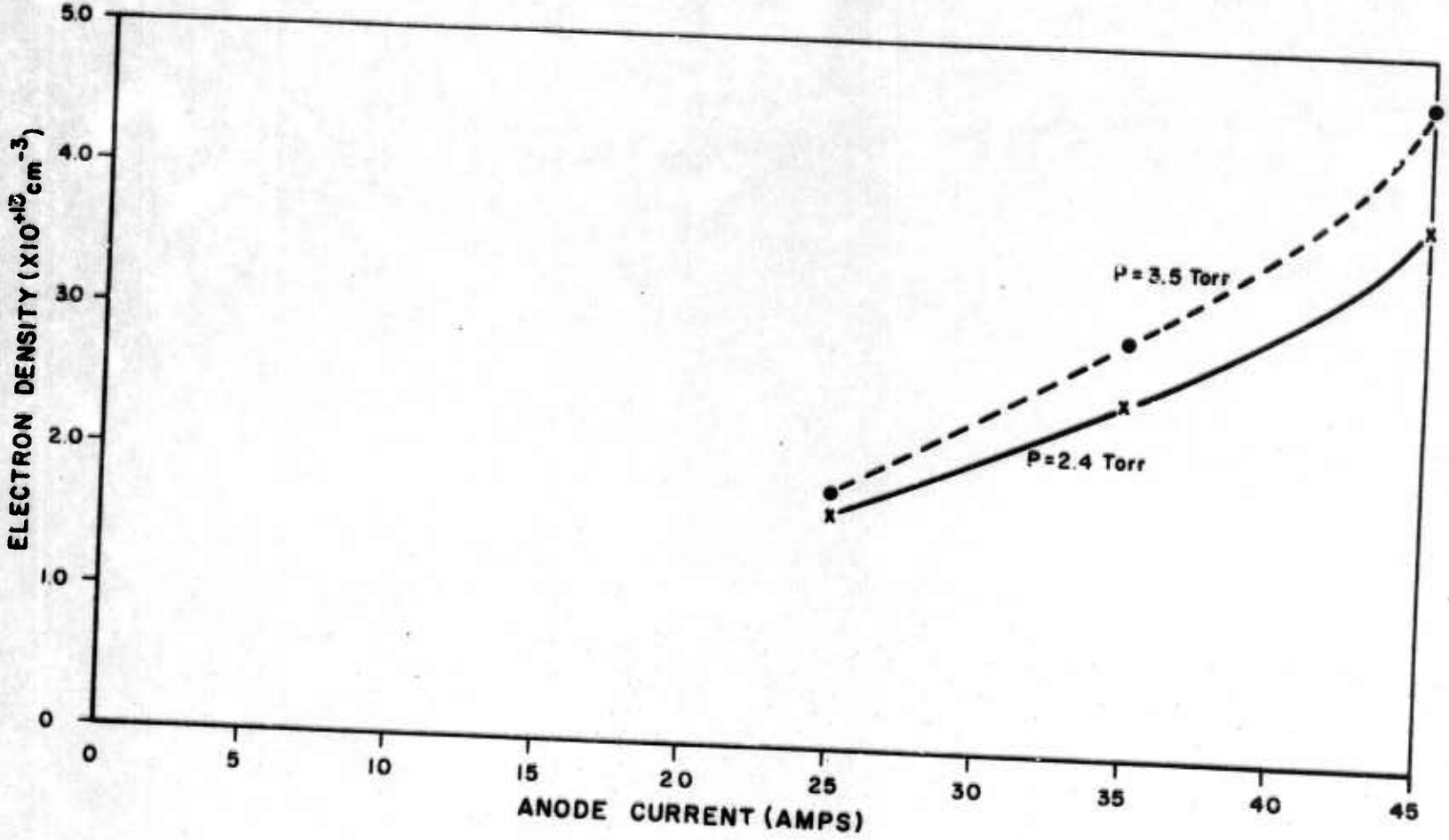

Figure 2-11 Electron Density Vs Simulator Discharge Current

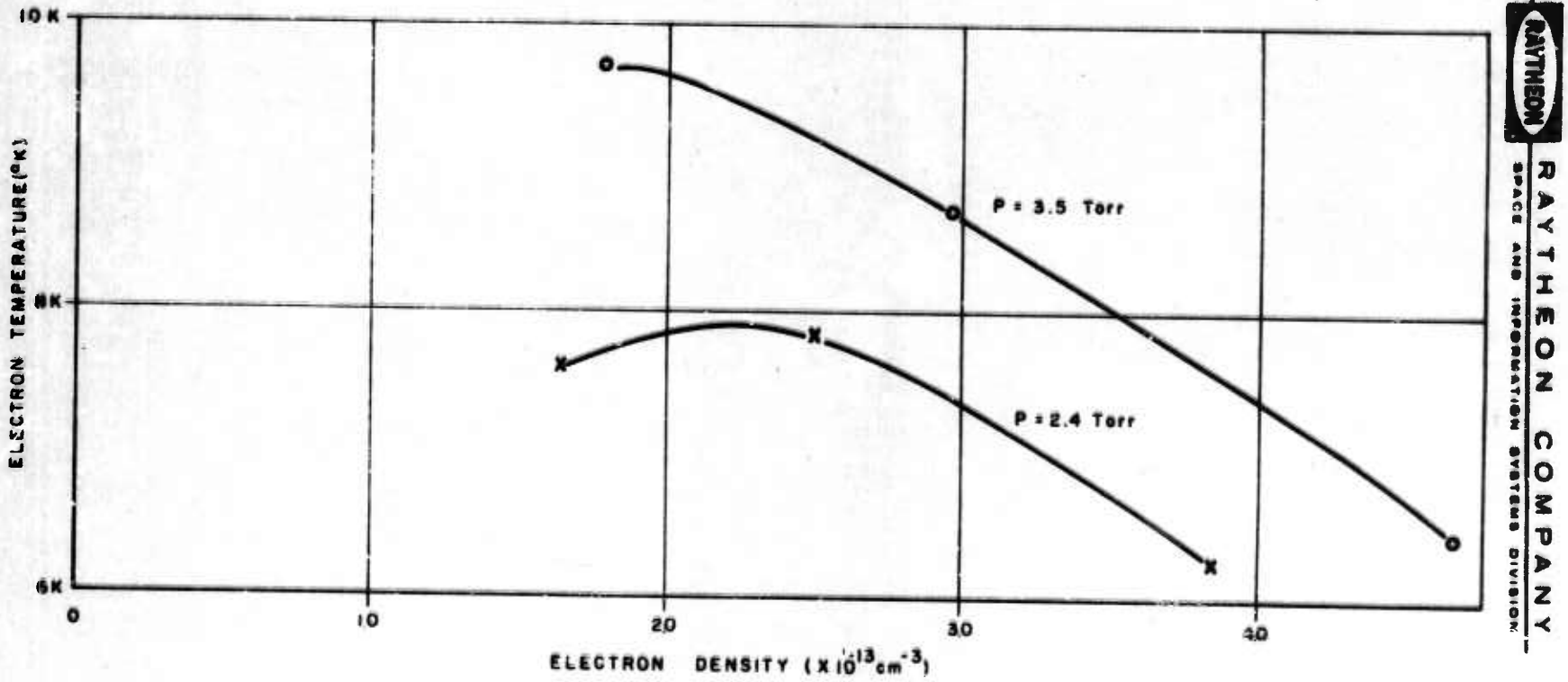

Figure 2-12 Plasma Simulator Electron Temperature Vs Electron Density Characteristics

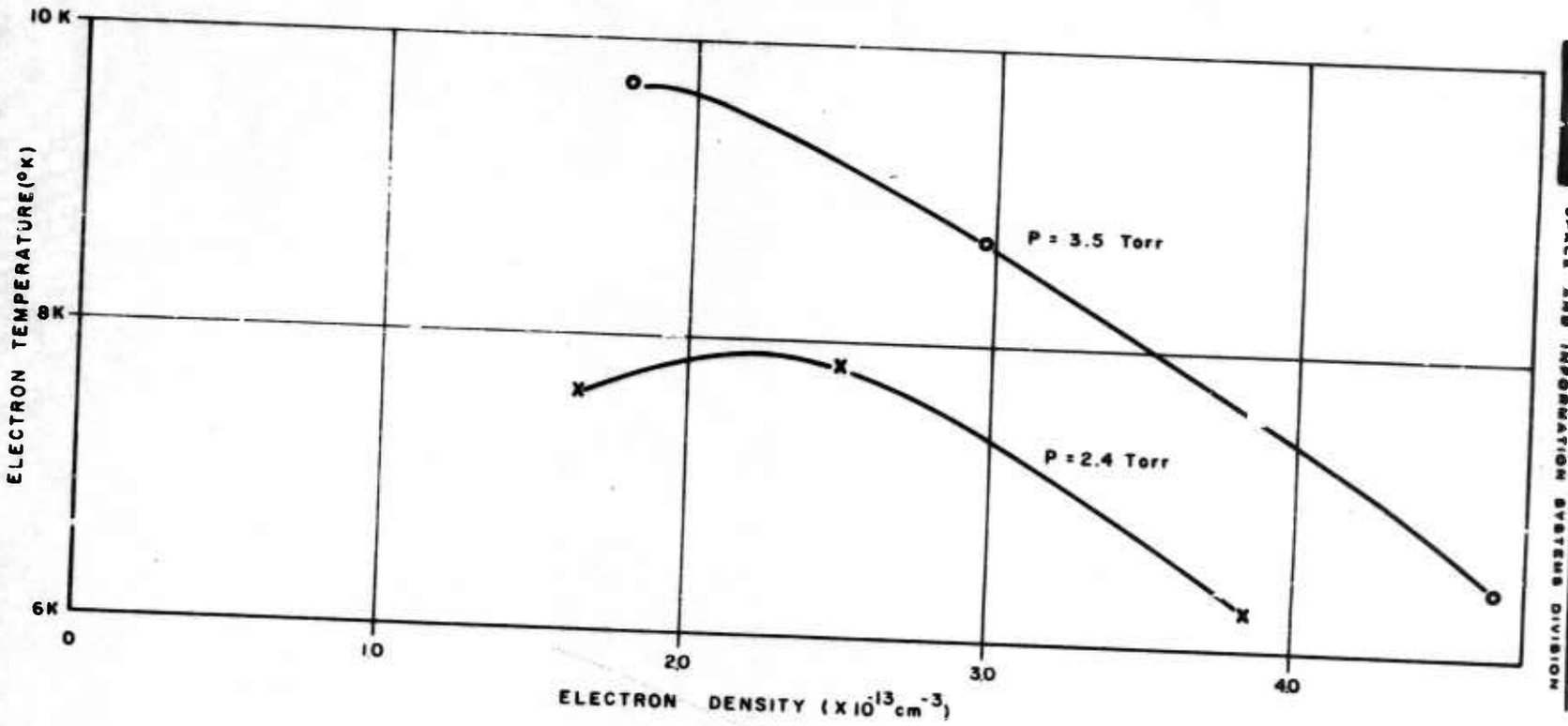

Figure 2-12 Plasma Simulator Electron Temperature Vs Electron Density Characteristics

$$\nu = 1.696 \times 10^{8}\ p\ P_c\ \frac{T_e^{1/2}}{T_g} \qquad (2\text{-}12)$$

The values of P_c were obtained from Reference 2. T_g was determined by noting the change in pressure when the discharge was turned off. The collision frequency is plotted as a function of electron density in Figure 2-13.

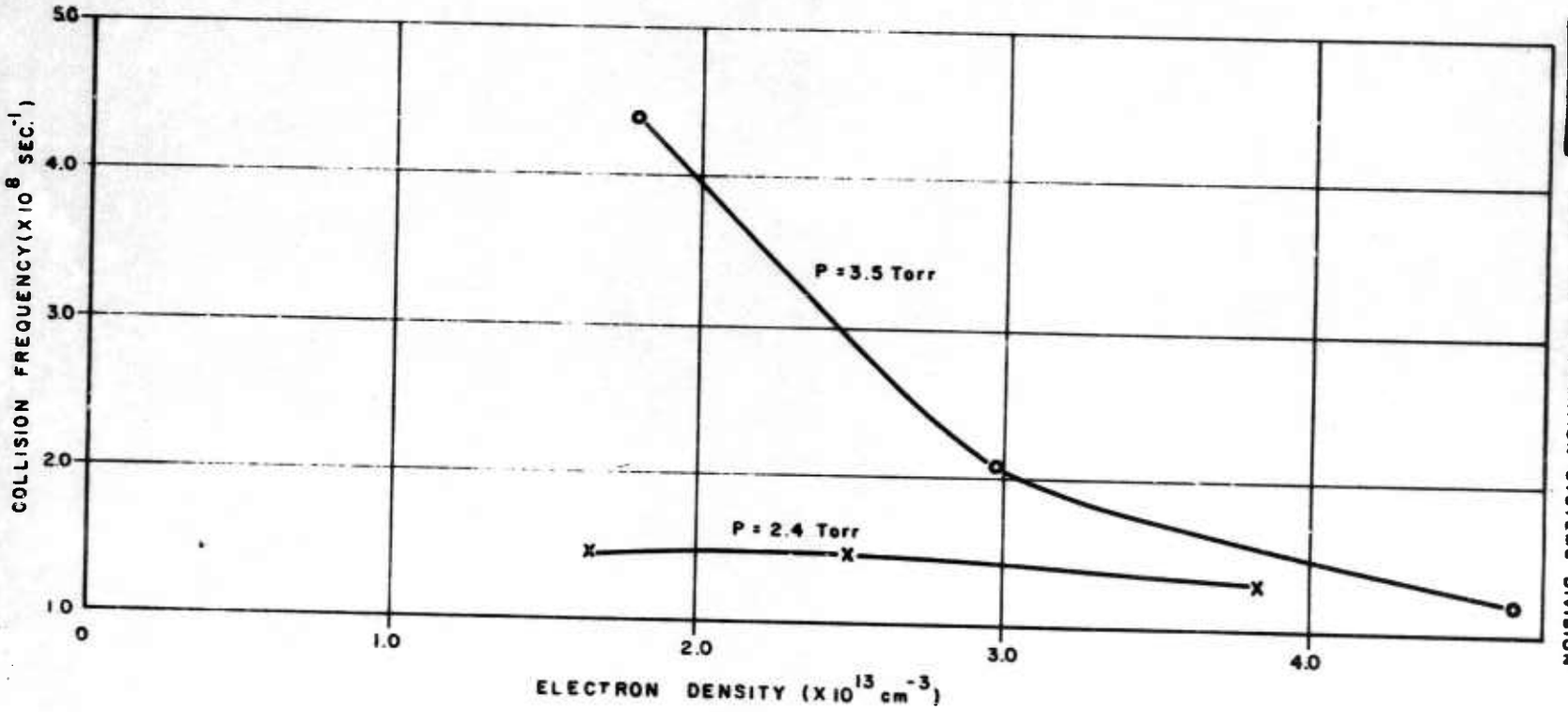

RAYTHEON COMPANY
SPACE AND INFORMATION SYSTEMS DIVISION

Figure 2-13 Plasma Simulator Collision Frequency Vs Electron Density Characteristics

SECTION 3

ECM VEHICLE MODEL

The vehicle model used in the experiments was constructed from a copper cone 10 1/2 inches high with an apex angle of 21 degrees. Two orthogonally oriented slot antennas were flush mounted on the conical surface approximately 4 1/2 inches from the base of the cone, measured to a point midway between the slots. A copper cylinder about 12 inches long was soldered to the base of the cone to support it in the simulator and to confine reflected RF power from the plasma interface as well as surface wave radiation from the plasma discontinuity to the microwave absorber material at the base of the simulator (Section 4). An air jet was passed through the nose of the cone to cool the apex of the inner glass surface of the simulator. 1/4 inch holes were drilled into the copper cylinder wall to permit air from the jet to flow down between the cone and the inner glass surface of the simulator. The copper cone was cooled by passing water through copper tubing soldered around the base. A sketch of the model is shown in Figure 3-1, and a photograph is shown in Figure 3-2.

3.1 Antenna Construction

The slot antennas were constructed from dielectrically loaded C-band waveguide terminated at one end by a metal plate. The waveguides were fed by coaxial cables whose outer shields were soldered to the waveguides. Because of the mismatch between the coaxial cables and the waveguides, and the mismatch due to the glass walls of the simulator, coaxial stub tuners were put on the ends of the feed cables. The cut-off frequency of the dielectrically loaded waveguide was about 2.6 GHz.

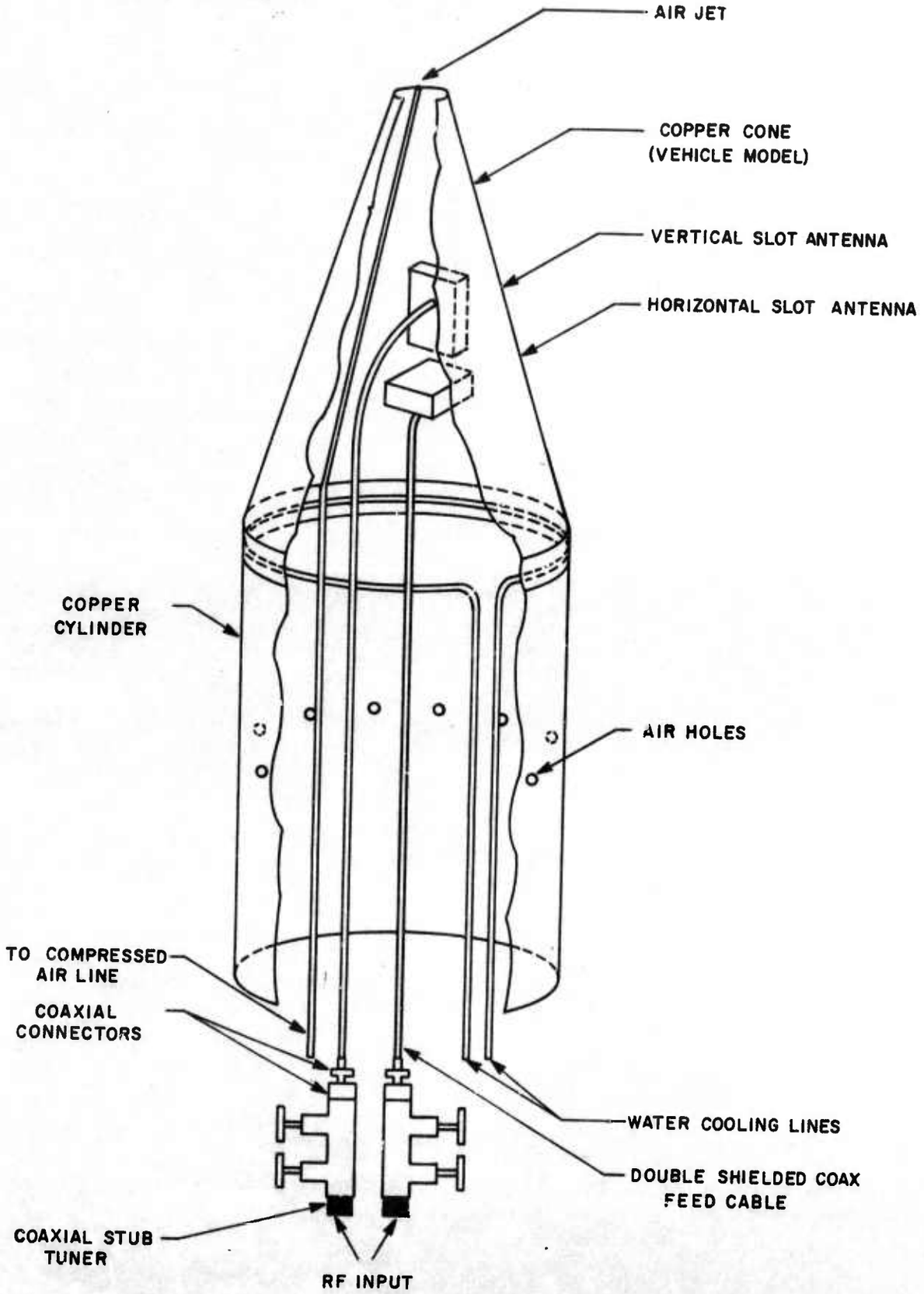

Figure 3-1 Sketch of ECM Vehicle Model with S-Band Slot Antennas

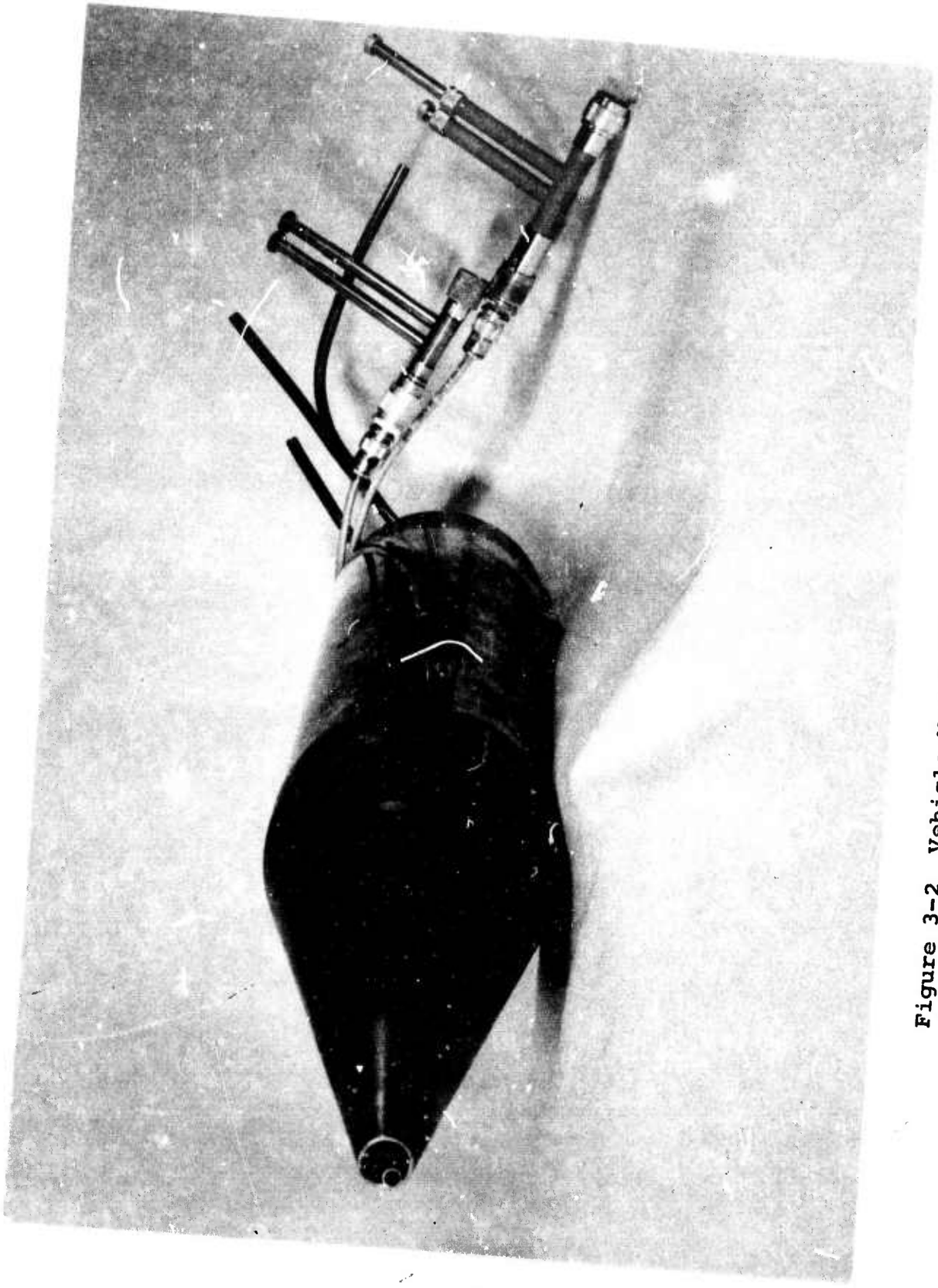

Figure 3-2 Vehicle Model with S-Band Slot Antennas

3.2 Antenna Characteristics

With no plasma in the simulator, the stub tuners could be adjusted so that the VSWR at the input of the tuners was less than 1.10. The internal loss of the antennas was estimated by covering the slot apertures with aluminum tape and noting the change in the input VSWR. The vertical slot antenna had about a 4 db loss and the horizontal slot antenna had less than a 1 db loss. The high internal loss of the vertical slot antenna was due to a weak connection between the coaxial feed cable and the waveguide. It would have been necessary to take almost the entire vehicle model apart to repair the antenna. Since time did not permit undertaking such a major task, the outer shield of the feed cable was soldered to the inside surface of the copper cylinder to prevent the antenna input impedance from changing due to mechanical stresses in the feed cable. Since the tuning was highly sensitive to frequency variations, the output frequency of the transmitter had to be controlled to within a few megacycles. A small change in VSWR was observed due to heating of the antennas by the plasma. The affect of heating on the VSWR was measured by measuring the VSWR immediately after the discharge was turned off.

SECTION 4

S-BAND MICROWAVE SYSTEM

A block diagram of the coaxial S-Band system is shown in Figure 4-1. The frequency of the Alfred oscillator could be adjusted from 2.0 GHz to 4.0 GHz with a maximum power output of 80 milliwatts at 2.0 GHz and 220 milliwatts at 4.0 GC. The frequency was monitored by displaying the output of the frequency meter on the vertical plates of the oscilloscope. During a frequency adjustment, the output power was held constant by a correction signal fed back to the oscillator from the RF sampler. Two isolators prevented the output frequency of the oscillator from drifting when large changes in load impedance occurred due to the plasma. Since the antenna input impedance was highly sensitive to frequency changes (Section 3.2), a large surge of reflected power was obtained if the RF coaxial switch was not used. This effect was due to the transient frequency output of the oscillator immediately after turning it on. Since the thermoelectric power head on the reflected power coupler could take a maximum of one milliwatt, a surge of reflected power caused the head to burn out before the coaxial switch was put in the circuit.

A TWT amplifier was used to deliver 10 watts of power at the inputs of the antennas. The angle of the reflection coefficient was obtained directly by feeding the outputs from the sidearms of the dual directional coupler into a phase bridge. The VSWR was obtained by measuring the incident and reflected powers. The reflected power was measured with a thermoelectric power meter. With the one milliwatt power head reflected power as small as

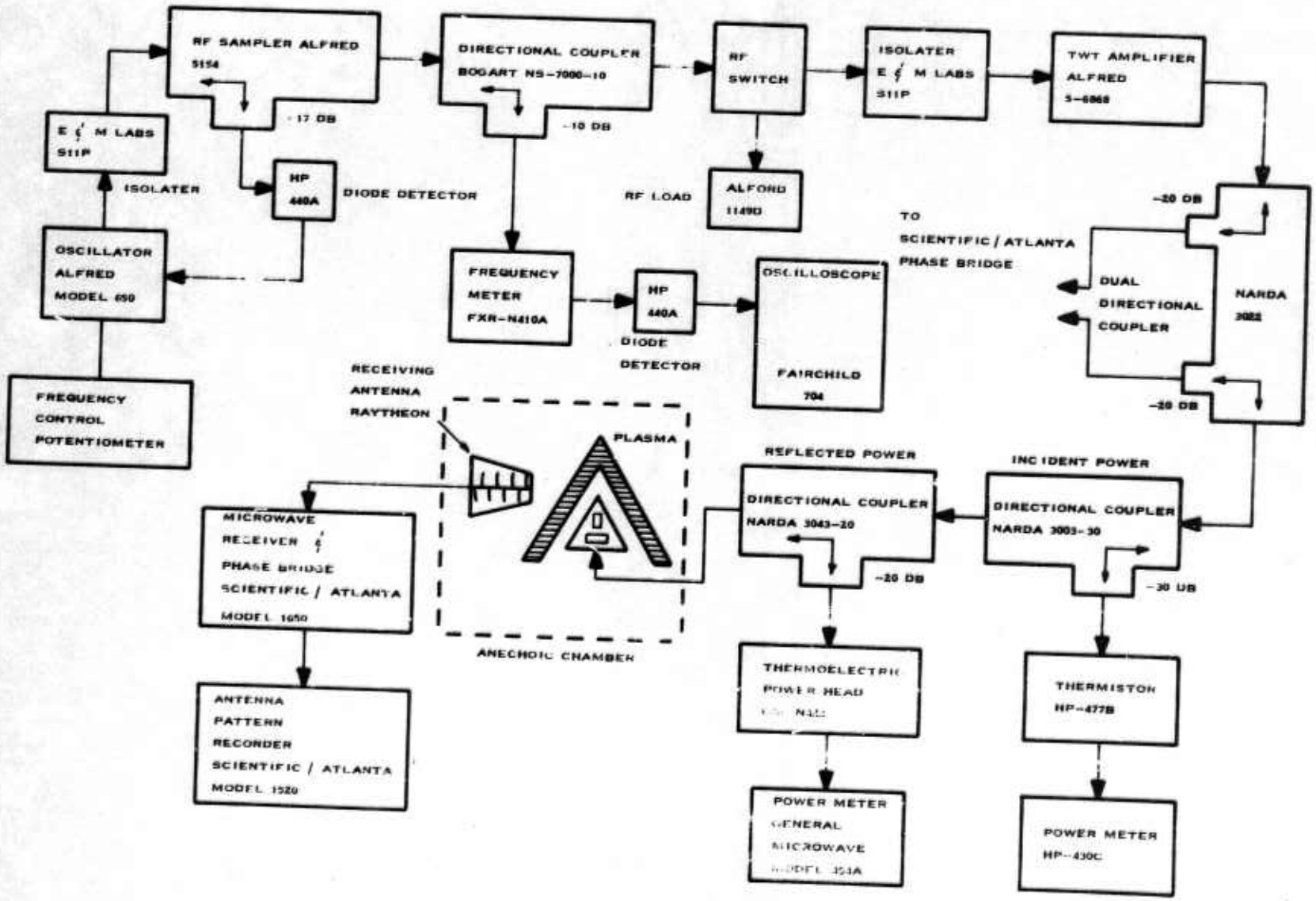

Figure 4-1 S-Band Microwave System

30 microwatts could be measured. This sensitivity enabled the tuning of the antennas for input VSWR's less than 1.1 for incident powers below 100 milliwatts.

The transmitted signal was detected with a Scientific/Atlanta microwave receiver. The receiver was connected to an antenna pattern recorder which gave relative power directly in decibels. A potentiometer circuit was built to externally control the frequency output of the oscillator. With this device the frequency could easily be adjusted to within a megacycle.

4.1 Vehicle Model Microwave Termination

In the actual reentry case the wake of the plasma sheath tends to constrict towards the vehicle axis forming a trap for electromagnetic energy. This aspect of the wake was simulated in the laboratory by mounting the plasma simulator on a ring of "pack-in-place" microwave absorber and surrounding the base of the simulator, up to the base of the cone, with panels of absorber which were specially cut to fit the contours of the simulator base. A sketch of the microwave termination is shown in Figure 4-2. The simulator and absorber rested on a copper ground plane approximately 3' x 3'. The vehicle model was inserted up into the simulator through a hole in the ground plane. A copper cylinder was soldered to the hole and slotted at one end for clamping the model in position. The cylinder also extended one inch above the ground plane to hold the "pack-in-place" absorber in place. The absorber panels which were cut to fit around the simulator also shielded the steel flanges of the cathodes from the RF field. The flanges produced scattering in the field of the antennas when exposed.

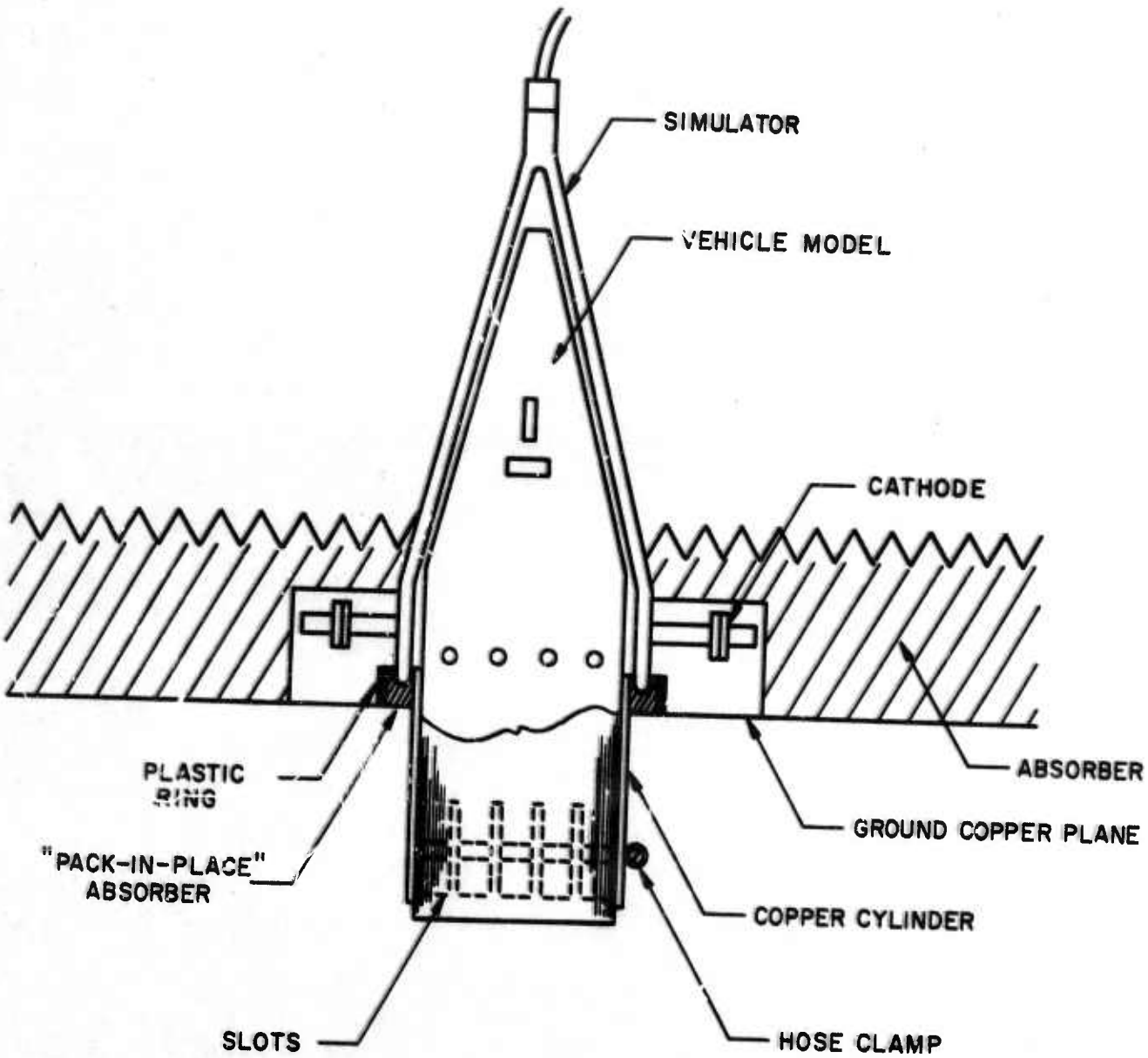

Figure 4-2 Sketch of Vehicle Model With Microwave Termination

4.2 RF Shielding

Since the plasma attenuated the incident signal more than 30 db (Section 5.4), the field at the receiving antenna due to RF leakage from coaxial cables and connectors had to be made small compared to the received signal from the plasma. In a preliminary set-up of the system the transmitter was located close to the anechoic chamber to keep the length of coax between the transmitter and the inputs to the antennas to a minimum. Doubly shielded coaxial cables, about 10 feet long were used between the transmitter and the antenna inputs. Microwave components at the transmitter such as isolators, couplers etc. were connected together in many cases with the same type of coaxial cable. With this set-up preliminary antenna patterns indicated that the field detected due to RF leakage was comparable to the signal received from the plasma. The leakage level was measured by terminating the coax from the transmitter with a dummy load and noting the change in signal level on the antenna pattern recorder.

To obtain a meaningful measurement of the small signal from the plasma, the background RF level had to be reduced to at least 50 db below the signal received with no plasma in the simulator. The oscillator, the TWT and components connected on the outputs of these devices were grouped together on two tables and moved to a distance about 15 feet from the slot antennas. The components were connected together with short lengths of solid coaxial cables and solid coaxial connectors. The cables between the transmitter and the antenna inputs had to be lengthened to 18 feet. RF leakage from these cables and the connector junctions at each end was eliminated by encasing the cables in 3/8" flexible

steel conduit and taping the ends of the conduit with aluminum tape, with conducting adhesive, to the bodies of the connectors. The transmitter assembly is shown on the left in Figure 4-3. The shielded cables can be seen along the floor. The anechoic chamber (not shown in the photo) is to the far right. The Scientific/Atlanta receiver and phase bridge is located in the center of the photo and the pattern recorded to its right.

The RF shielding was quite successful. Background RF was reduced to -65 dB below the signal received with no plasma in the simulator. This isolation was maintained even at 10 watts input power.

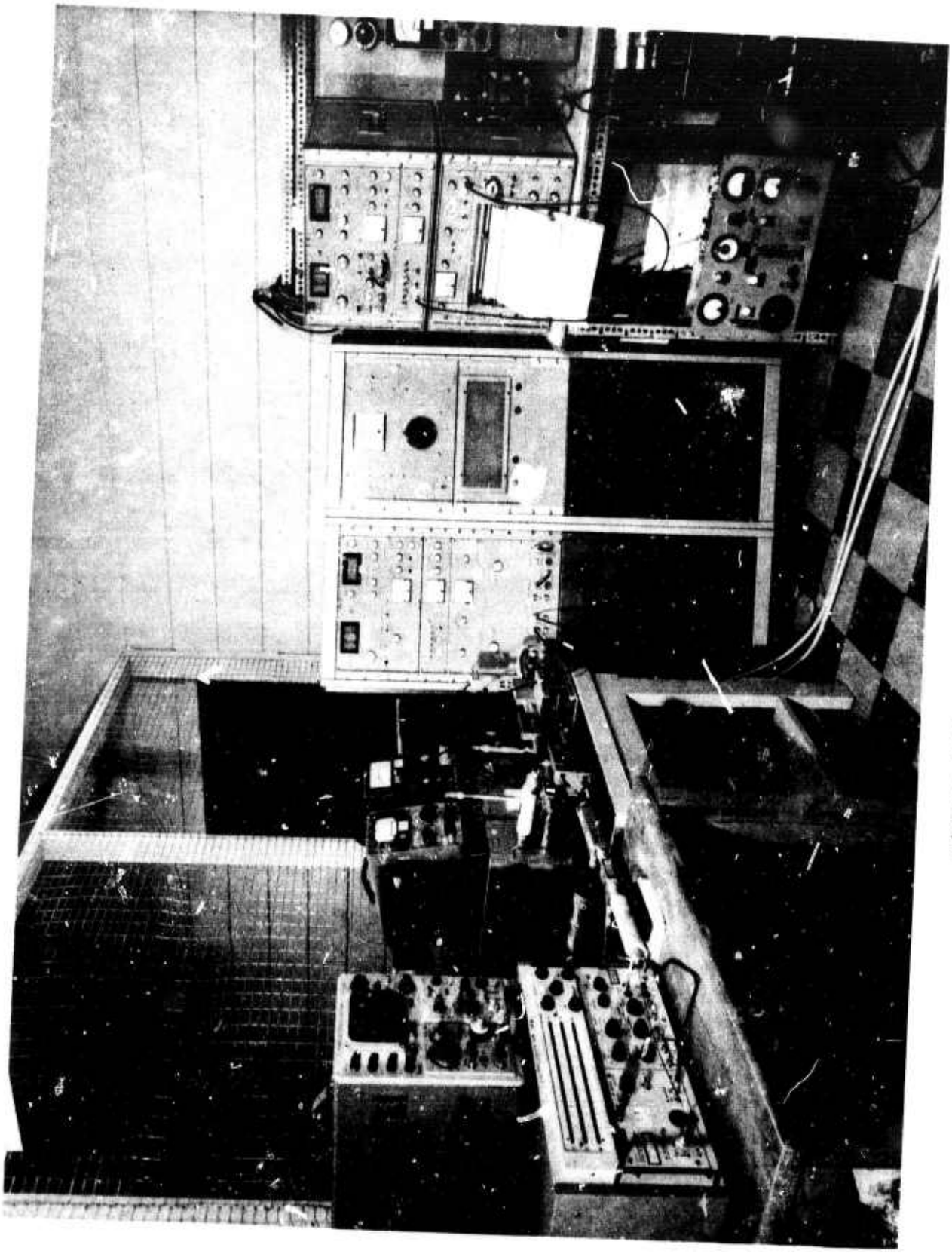

Figure 4-3. S-Band Coaxial System

SECTION 5

ANTENNA MEASUREMENTS

Preliminary measurements showed that the perturbation of the plasma on the antenna measurements discussed in the following sections varied by a negligible amount as the frequency was varied from 2700 MHz to 3900 MHz. Since one of the requirements of this program was to make measurements at low frequencies, all measurements were made at 2700 MHz. The slot antennas were "cut-off" at approximately 2600 MHz and thus a lower frequency could not be used.

The operational characteristics of the simulator defined the upper and lower limits of gas pressure and discharge current that could be used to obtain meaningful antenna measurements (see Sections 2.2 and 2.2.1). Therefore all measurements were performed at 2.4 Torr and 3.5 Torr, and at currents between 25 amperes and 45 amperes. The procedure used in taking the measurements was to set the gas pressure at 2.4 Torr or 3.5 Torr with the simulator current set at 35 amperes. The current was then varied between 25 amperes and 45 amperes to make antenna measurements under different plasma conditions. The small pressure variation due to changing the current was observed to have no measurable effect on the antenna measurements.

With 10 watts input power to the slot antennas, a small plasma could be sustained around the antenna apertures with the RF power alone. The plasma had to be initiated by applying a high voltage from a Tesla coil near the simulator. With the RF plasma alone, the input VSWR to the antennas was high and the

reactive component of the input impedance was large and negative. When the dc discharge was turned on the VSWR decreased and the reactance became less negative. A photograph of the RF plasma around the aperture of the horizontal slot antenna is shown in Figure 5-1. The measured values of the input VSWR and input impedance are given in the sections below.

To facilitate the presentation of the experimental data, the electromagnetic parameters (i.e., VSWR, impedance, etc.) were plotted as a function of the simulator discharge current for parametric values of gas pressure and input power. The experimental results given in the following sections may be related to the ratios ω_p/ω and ν/ω by Table 5-1.

TABLE 5-1

Relation of Simulator Gas Pressure and Discharge Current to Ratios ω_p/ω and ν/ω.

	P = 2.4 TORR		P = 3.5 TORR	
ANODE CURRENT (AMPS)	ω_p/ω	ν/ω	ω_p/ω	ν/ω
0	0	0	0	0
25	13.50	.009	14.00	.026
35	16.64	.009	18.09	.012
45	20.54	.008	22.61	.007

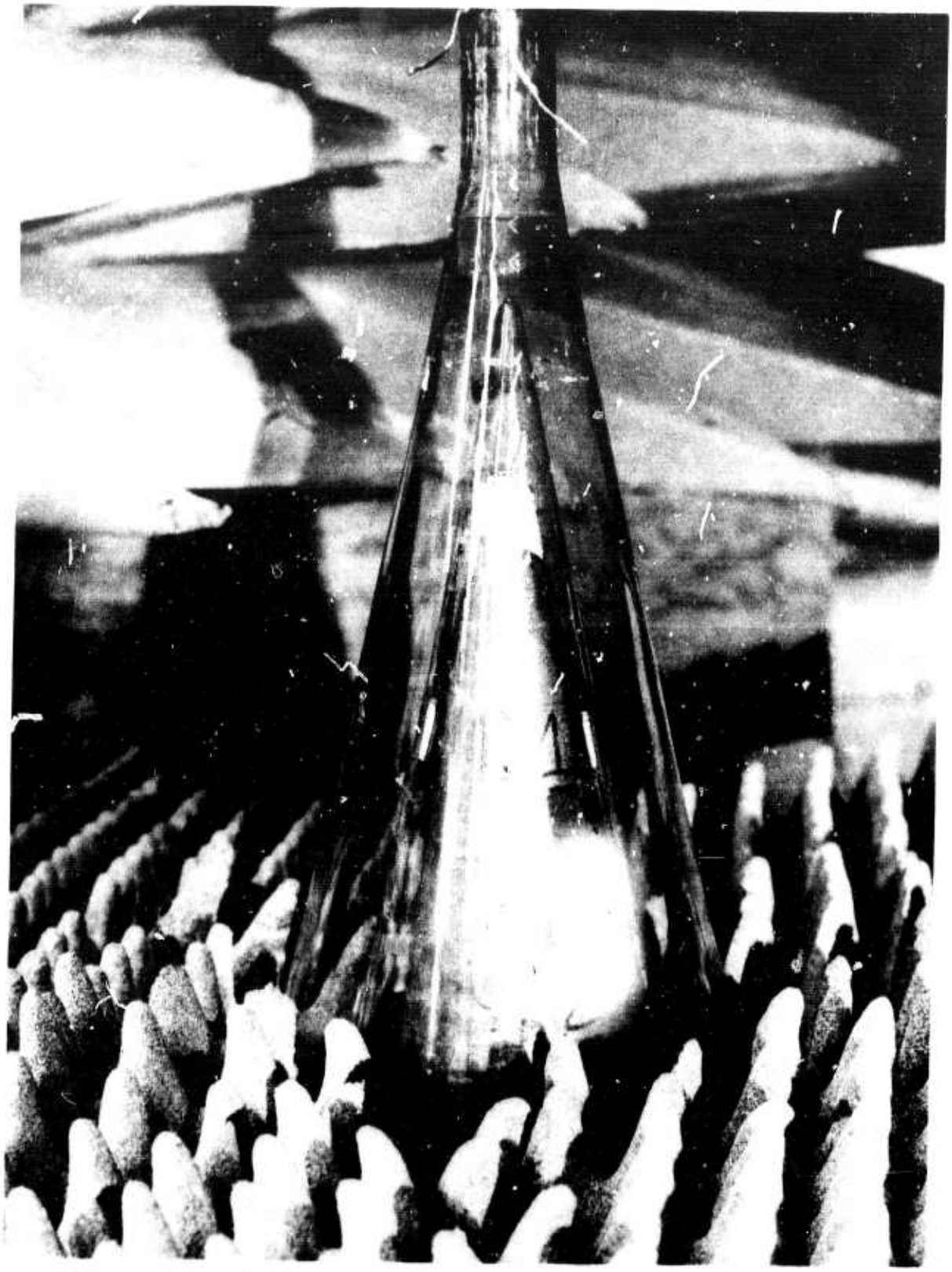

Figure 5-1 RF Plasma Produced by Horizontal Slot Antenna at 10 Watts Input Power.

5.1 Antenna Input VSWR

The VSWR at the antenna inputs was determined by measuring the incident and reflected powers with directional couplers (Figure 4-1). The reflection coefficient is related to the incident and reflected powers by

$$\left|\Gamma_C\right| = \left(\frac{P_r}{P_i}\right)^{1/2} \qquad (5.1)$$

where Γ_C is the reflection coefficient at the couplers, and P_r and P_i are the reflected and incident powers, respectively at the couplers. Due to transmission line attenuation, the reflection coefficient at the couplers is smaller than the reflection coefficient at the antenna inputs. If Γ_A is the reflection coefficient at the antenna inputs, then

$$\text{line attenuation (db)} = 10 \log_{10} \left(\frac{\left|\Gamma_C\right|}{\left|\Gamma_A\right|}\right) \qquad (5.2)$$

The input VSWR, S_A, is given by

$$S_A = \frac{1 + \left|\Gamma_A\right|}{1 - \left|\Gamma_A\right|} \qquad (5.3)$$

The line attenuation was measured by terminating the transmission lines to the antennas with known RF loads, and measuring the reflection coefficient at the couplers. Due to discontinuities at the connectors, an <u>effective</u> attenuation was measured. The effective attenuation was found to be different for low and high VSWR's. To facilitate the measurements, an average value of the effective attenuation was used. The input VSWR's measured were accurate to within approximately 15%.

The input VSWR is plotted in Figures 5-2 and 5-3. For the horizontal slot, the VSWR was appreciably affected by increasing the input power to 10 watts. The VSWR was only slightly affected by changing the pressure from 2.4 Torr to 3.5 Torr. The RF sustained plasma produced the highest VSWR. The maximum VSWR obtained for the vertical slot was much lower than the maximum VSWR for the horizontal plot. This effect was due to the high internal loss (4 db) of the vertical slot antenna. A VSWR of 2.14 was measured when the vertical slot aperture was covered with aluminum tape. Therefore, the plasma could not produce a VSWR much greater than 2.0.

5.2 Antenna Patterns

An anechoic chamber was built around the simulator, part of which is shown in Figure 2-4. The receiving antenna was log-periodic with a beamwidth of about 110° in the H-plane and about 90° in the E-plane. It was mounted on a boom that could be swung through an angle of 90° from the simulator axis. A photo of the antenna on the boom is shown in Figure 2-4. The boom was covered with absorber material to reduce spurious reflections. The plane in which the antenna patterns were taken is defined in Figure 5-4. The receiving antenna was about five feet from the axis of rotation of the boom.

The received signal was detected with a microwave receiver (Figure 4-1) whose sensitivity was -95 dbm. The output of the receiver drove a chart recorder which recorded the field intensity directly in db as a function of the "off-axis" angle θ (Figure 5-4). The chart drive was monitored by a 1:1 synchro motor on the boom axis of rotation.

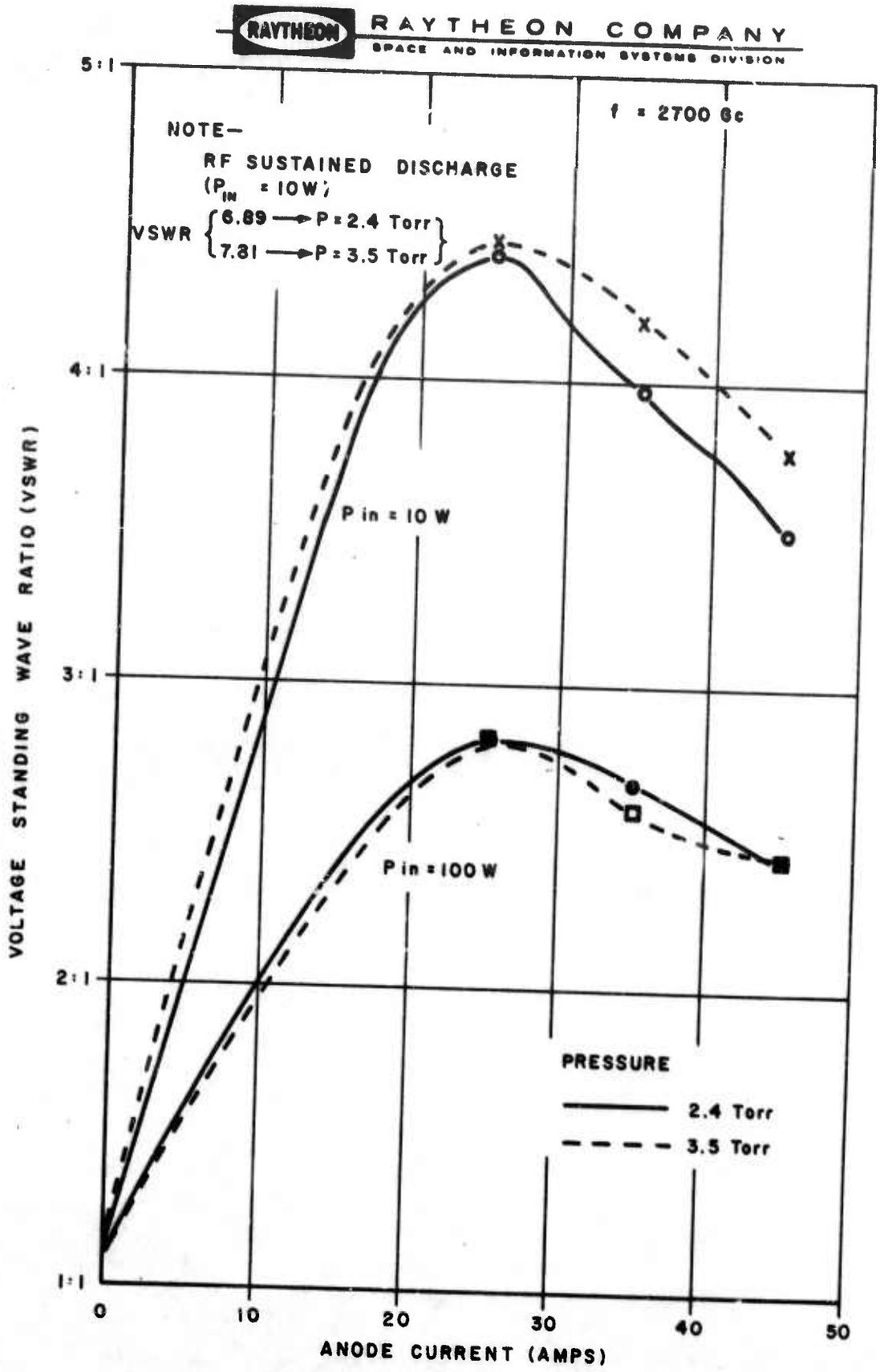

Figure 5-2. Horizontal Slot Antenna Input VSWR vs. Simulator Discharge Current

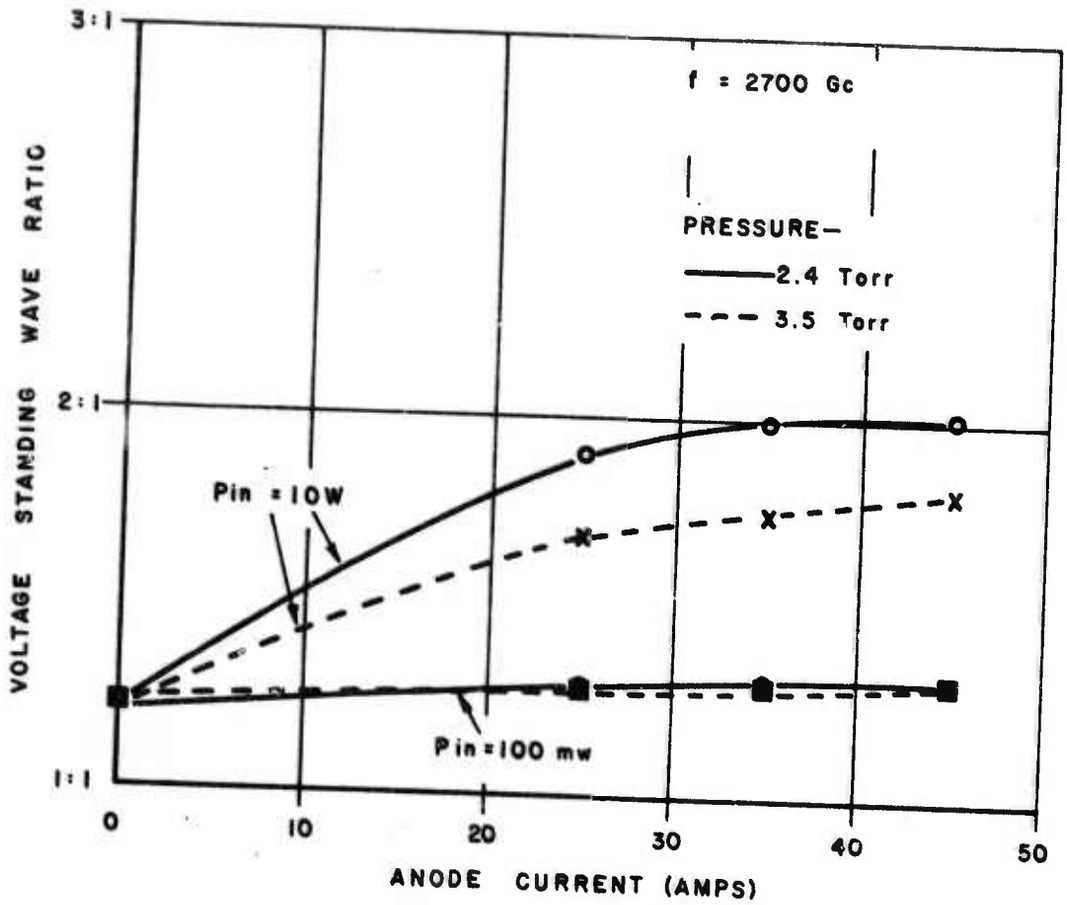

Figure 5-3. Vertical Slot Antenna Input VSWR vs. Simulator Discharge Current

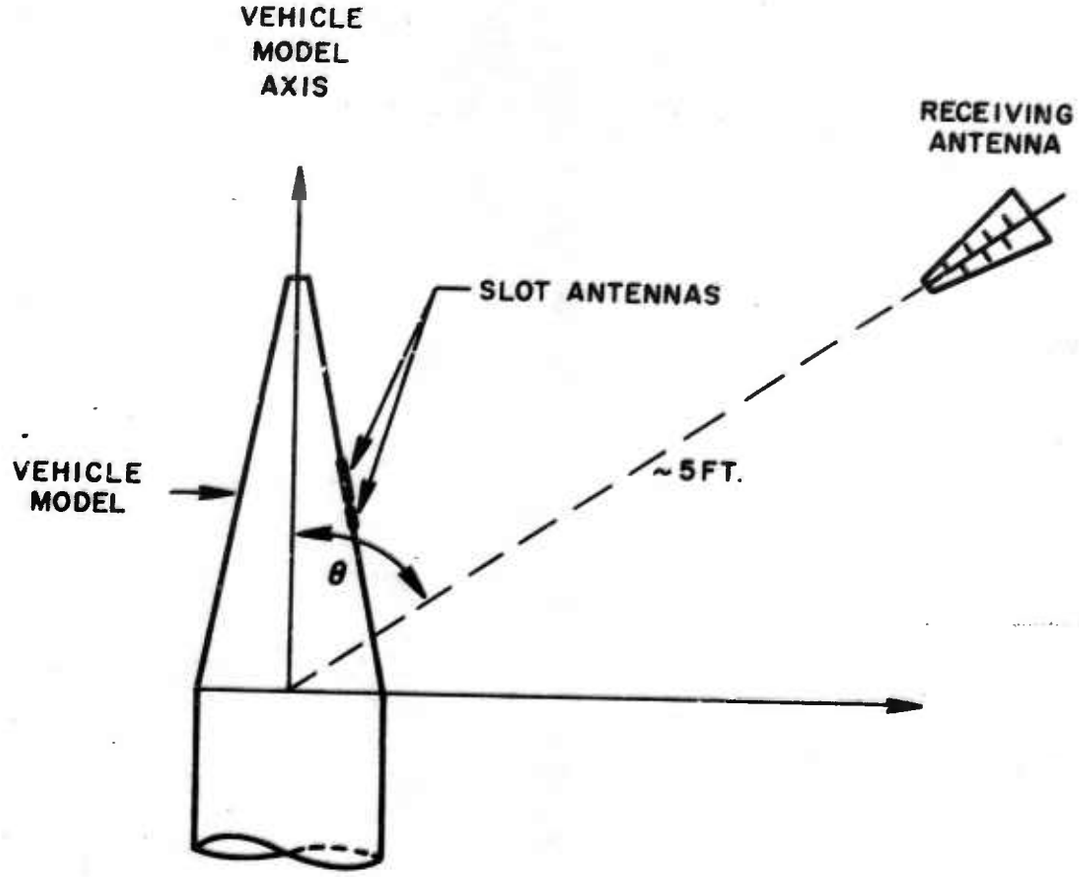

Figure 5-4 Antenna Pattern Measurement Plane

The H-plane patterns of the vertical slot are given in Figures 5-5 through 5-6d, and the E-plane patterns of the horizontal slot are given in Figures 5-7 through 5-8d. All patterns (except the "no plasma"patterns) exhibit strong interference effects. Since the plasma was highly overdense (i.e., $\omega_p/\omega >> 1$) in all cases most of the RF power was radiated from the discontinuities of the plasma including the partially unfilled portion of the simulator behind the slots (Section 2.2). This assumption was confirmed by covering the simulator with aluminum foil just up to the discontinuities of the plasma sheath, and taking antenna patterns. The antenna patterns showed no change in the average attenuation, and no appreciable pattern distortion due to the aluminum foil. Radiation from the spatially separated discontinuities (i.e., radiation sources) gave rise to constructive and destructive interference at various points in the field, resulting in antenna patterns with strong interference effects. Interference effects due to spurious radiation from cables, connectors, etc., was negligible since the level of this radiation (-65 db) (see Section 4.2) was far below the level of the received radiation. This fact was further checked by repeating the "no plasma" patterns with a 50 db pad inserted at the inputs of the slot antennas. The resulting patterns were identical in shape to the patterns obtained without the pad. A small probe was placed at the base of the vehicle model (i.e., a plasma discontinuity) to detect surface wave radiation. When the plasma was "turned-on" no increase in signal was observed. However, this may have been because the probe was not in the optimum position to detect surface waves, so that this result is inconclusive.

If the interference structure of the patterns is neglected some general observations of the effects due to polarization and

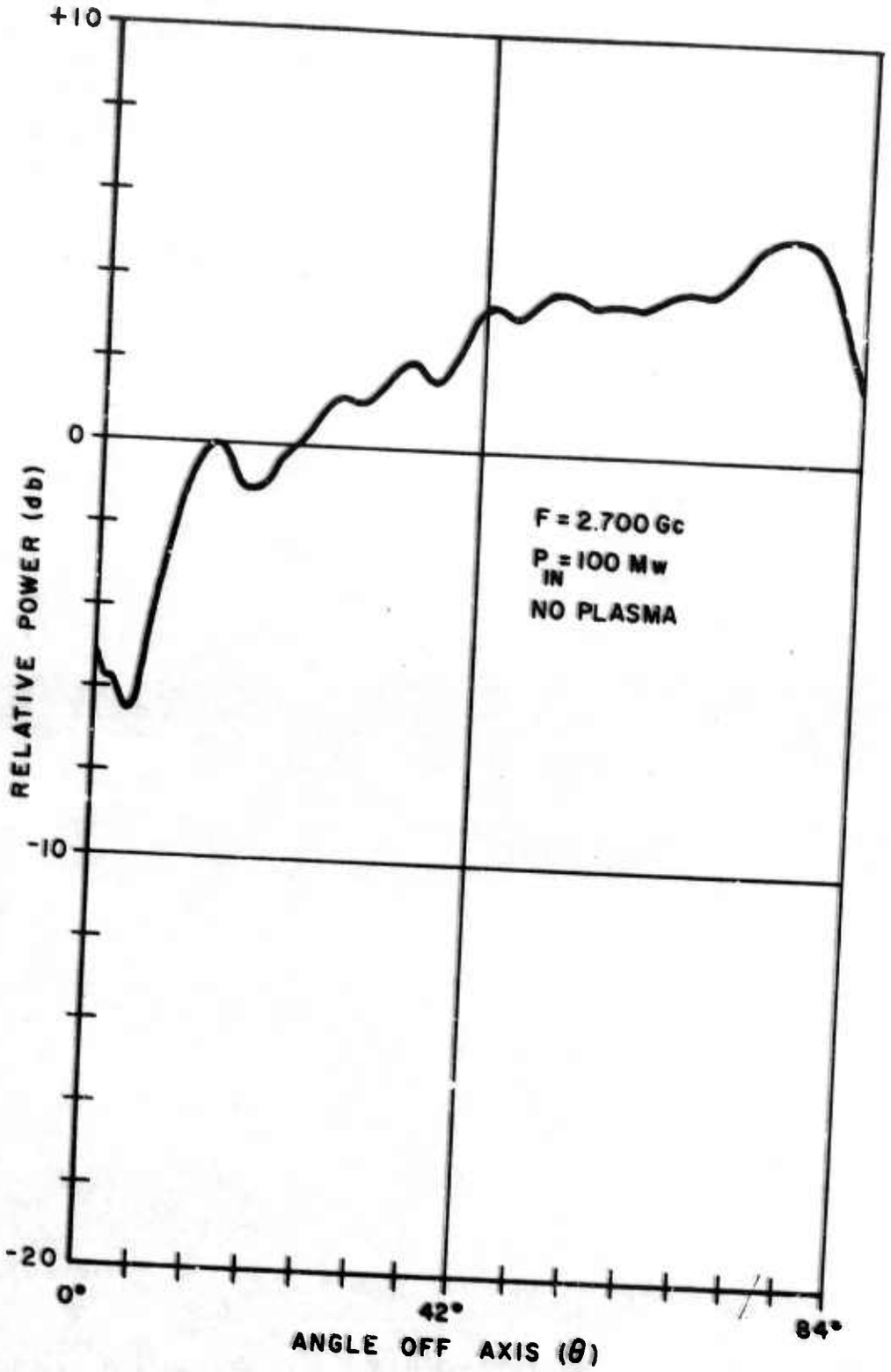

Figure 5-5 H-Plane Pattern of Vertical Slot Antenna

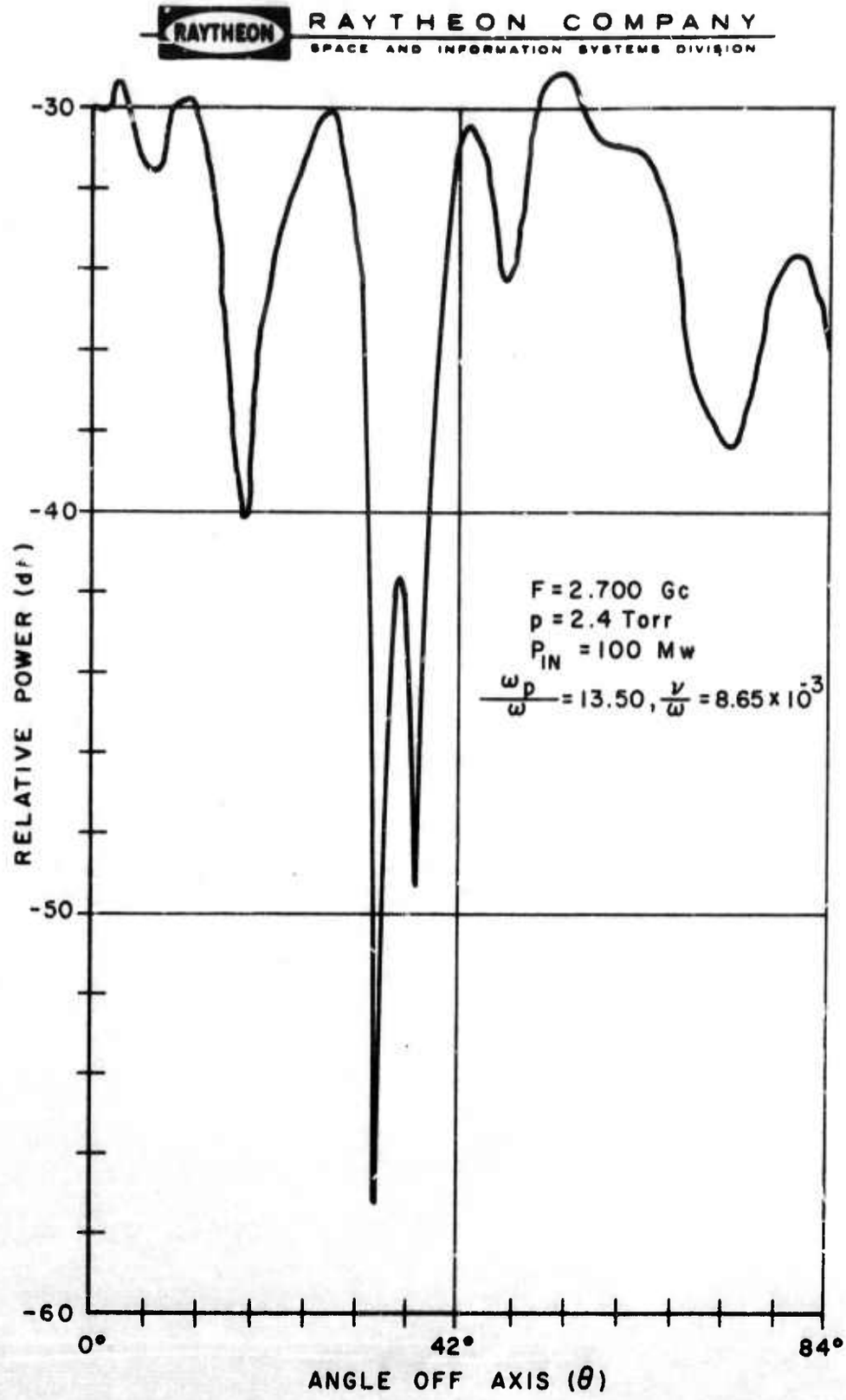

Figure 5-5a H-Plane Pattern of Vertical Slot Antenna

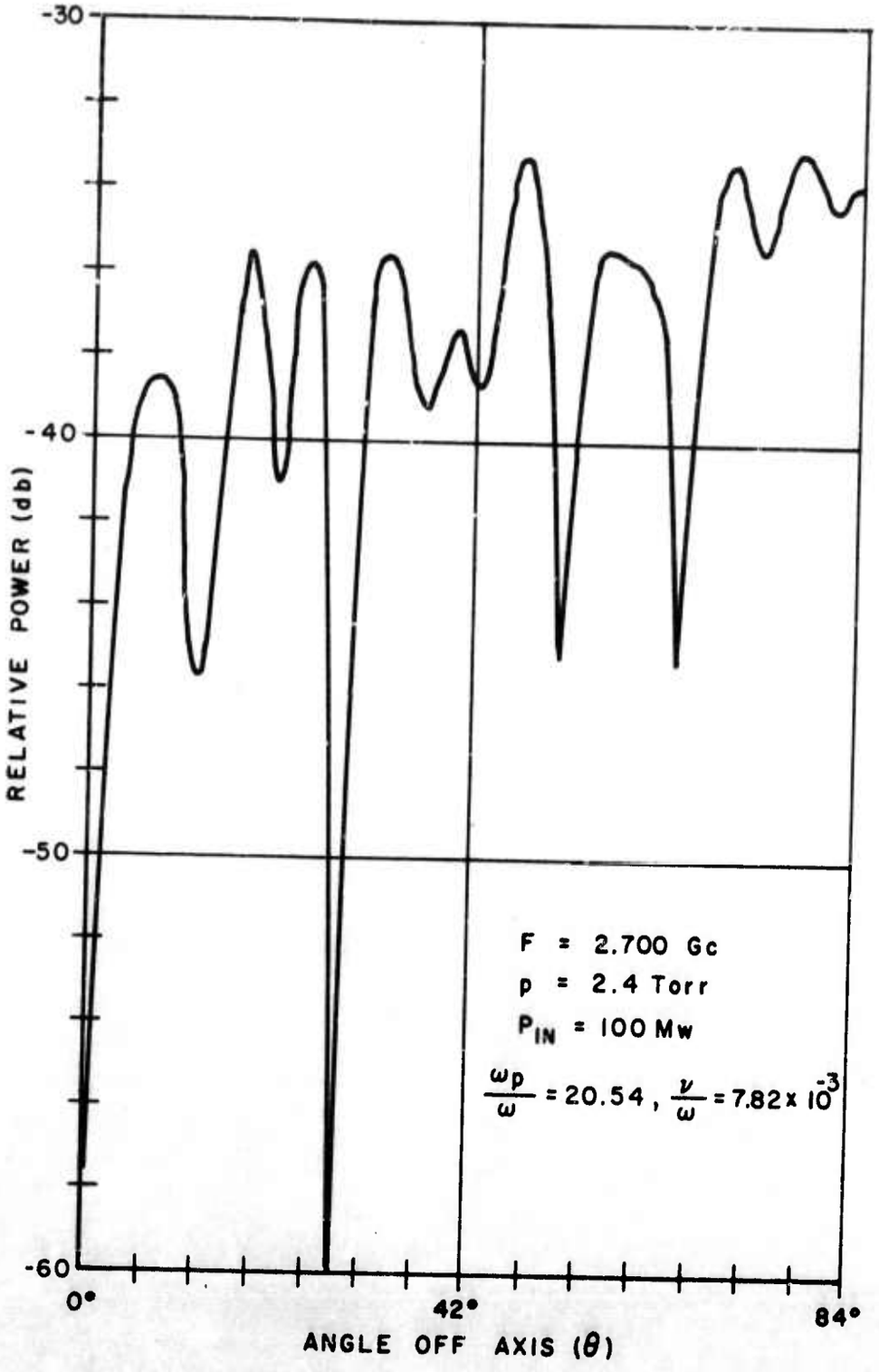

Figure 5-5b H-Plane Pattern of Vertical Slot Antenna

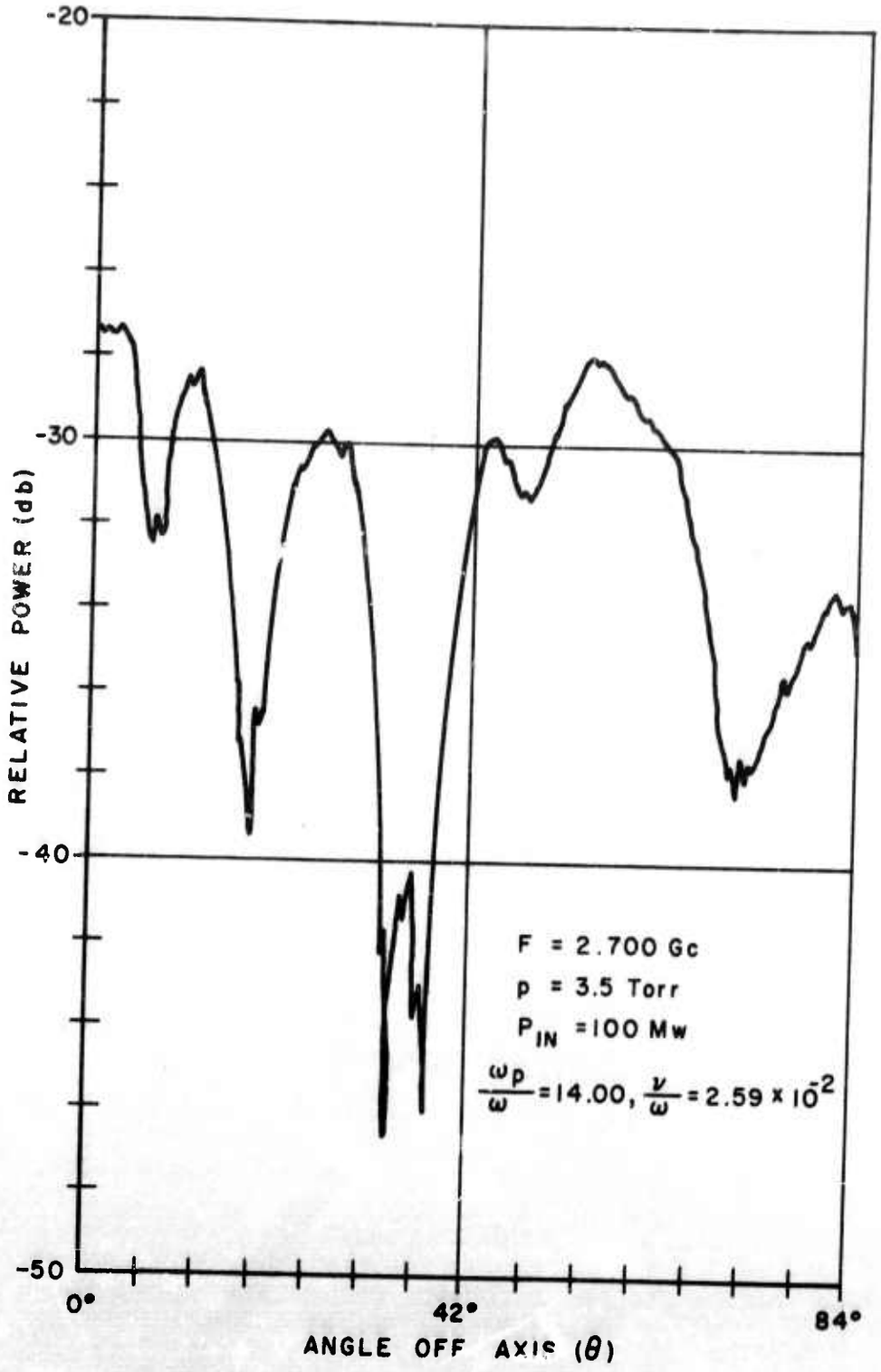

Figure 5-5c H-Plane Pattern of Vertical Slot Antenna

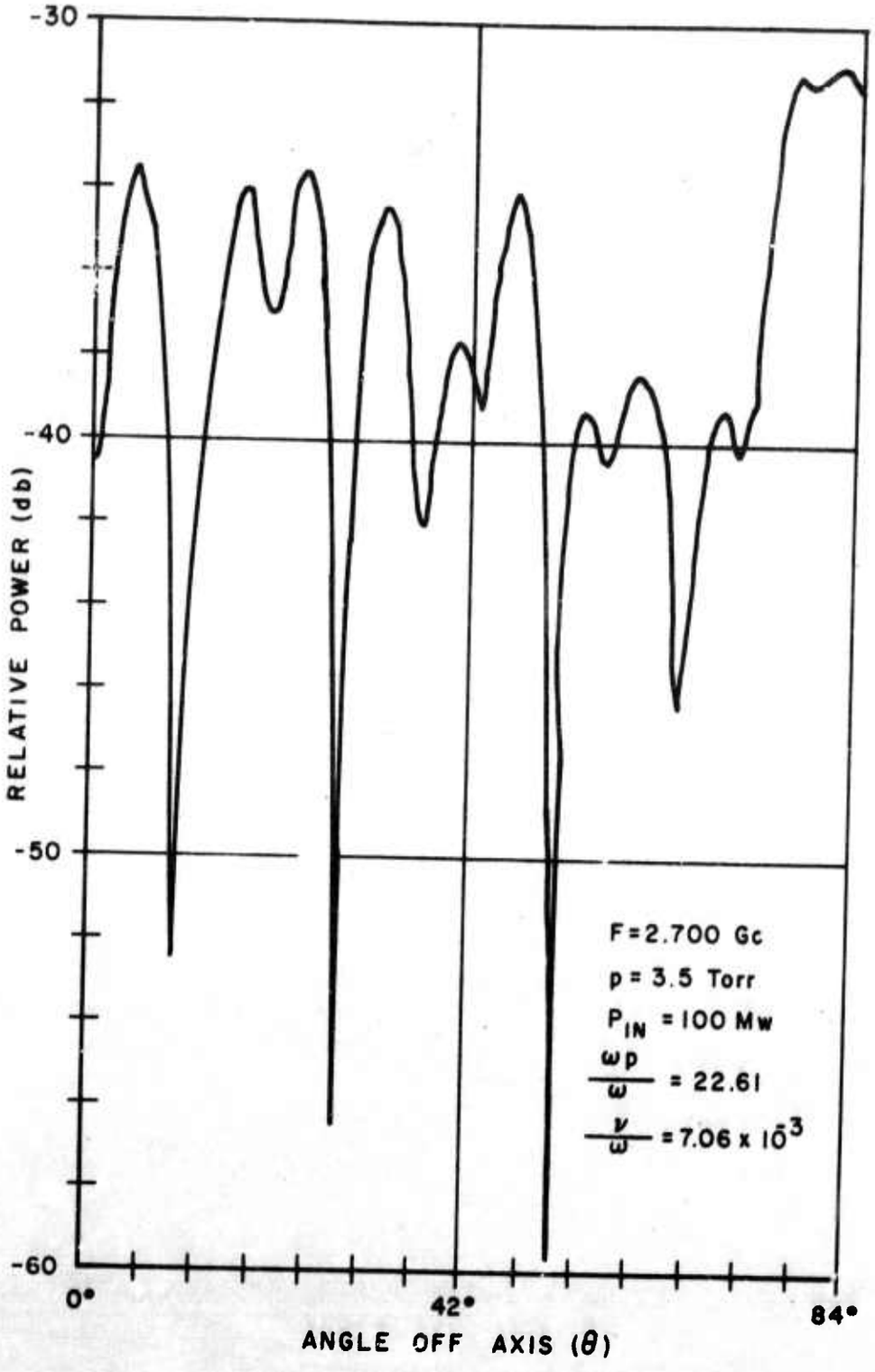

Figure 5-5d H-Plane Pattern of Vertical Slot Antenna

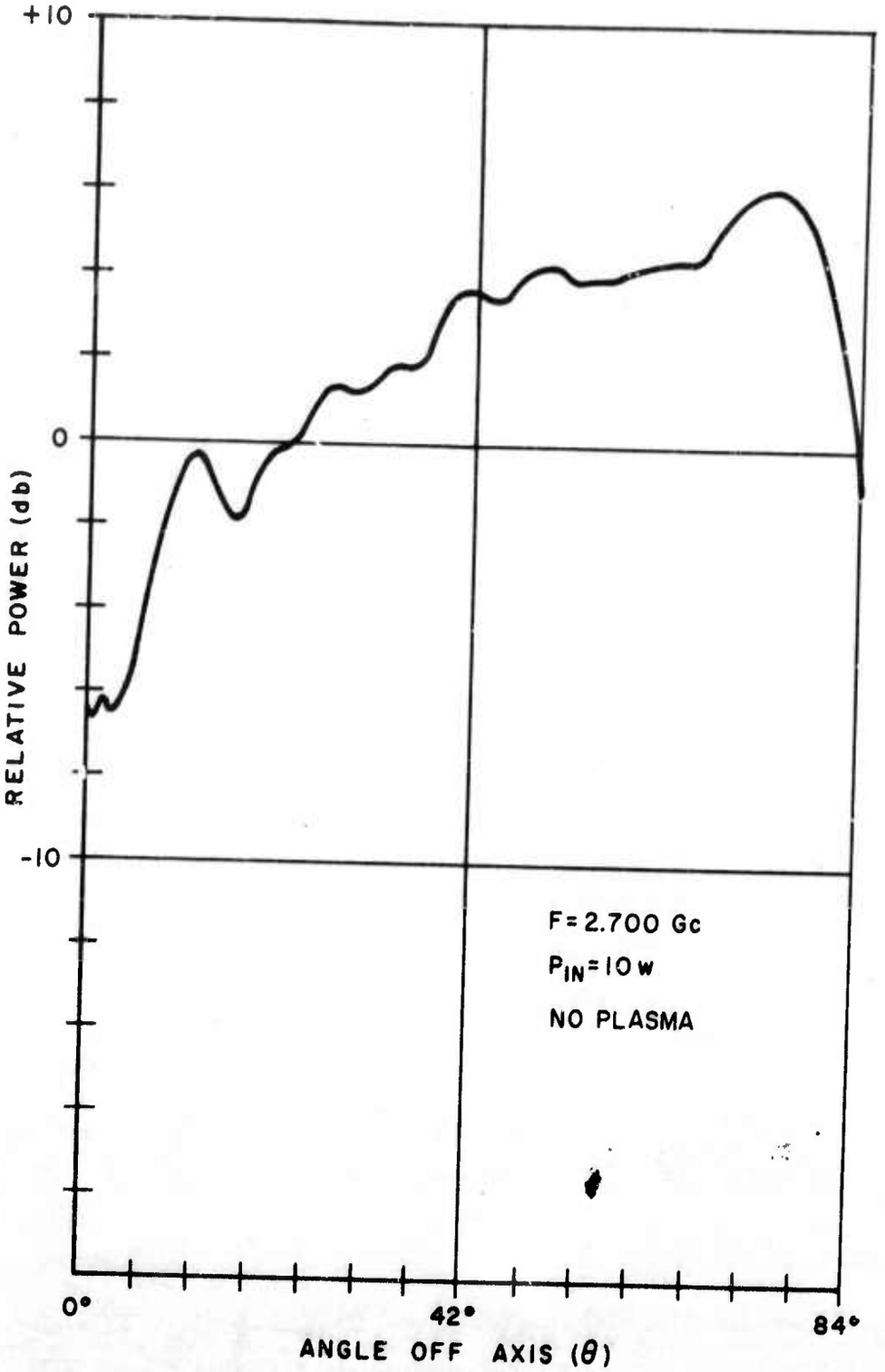

Figure 5-6 H-Plane Pattern of Vertical Slot Antenna

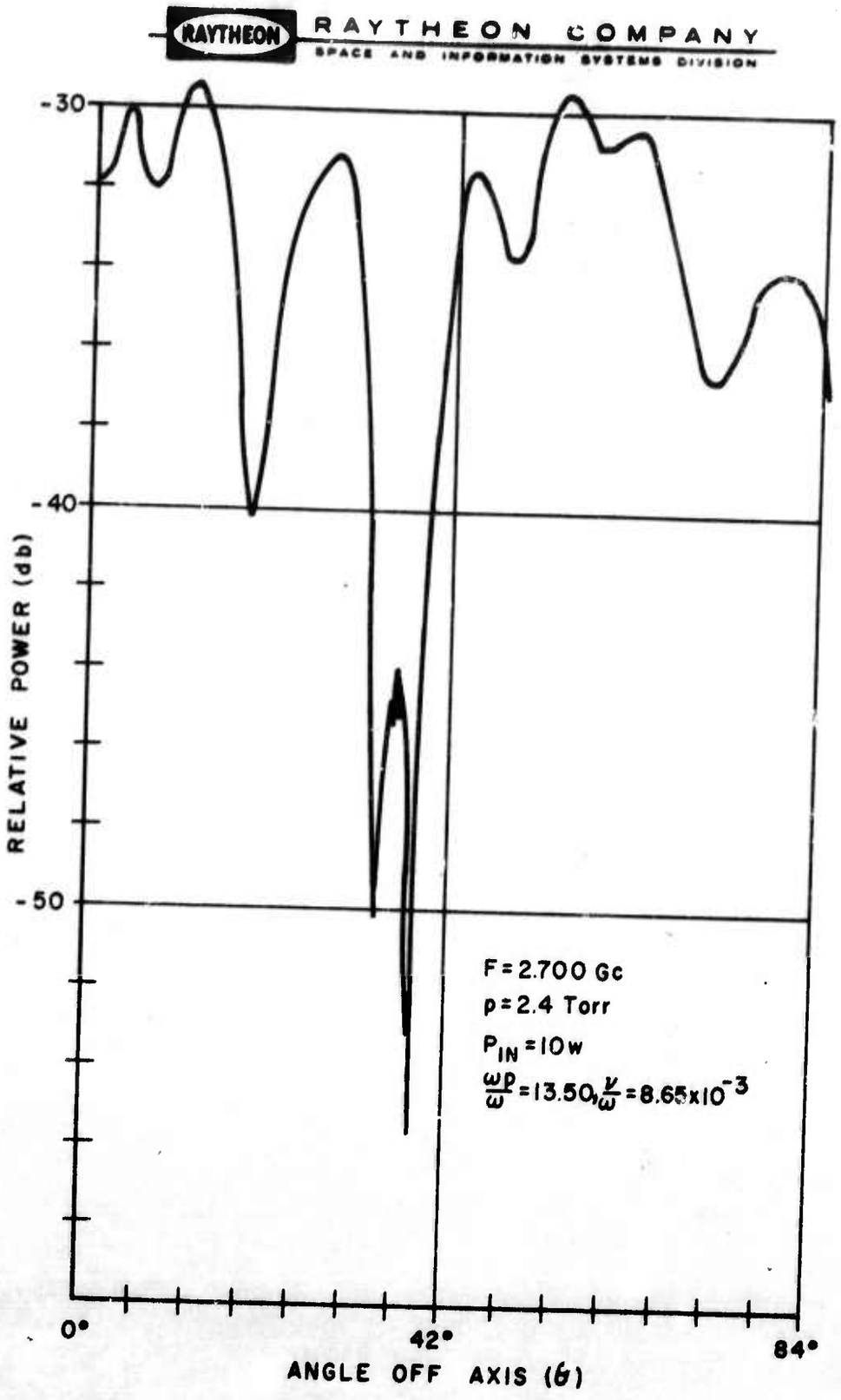

Figure 5-6a H-Plane Pattern of Vertical Slot Antenna

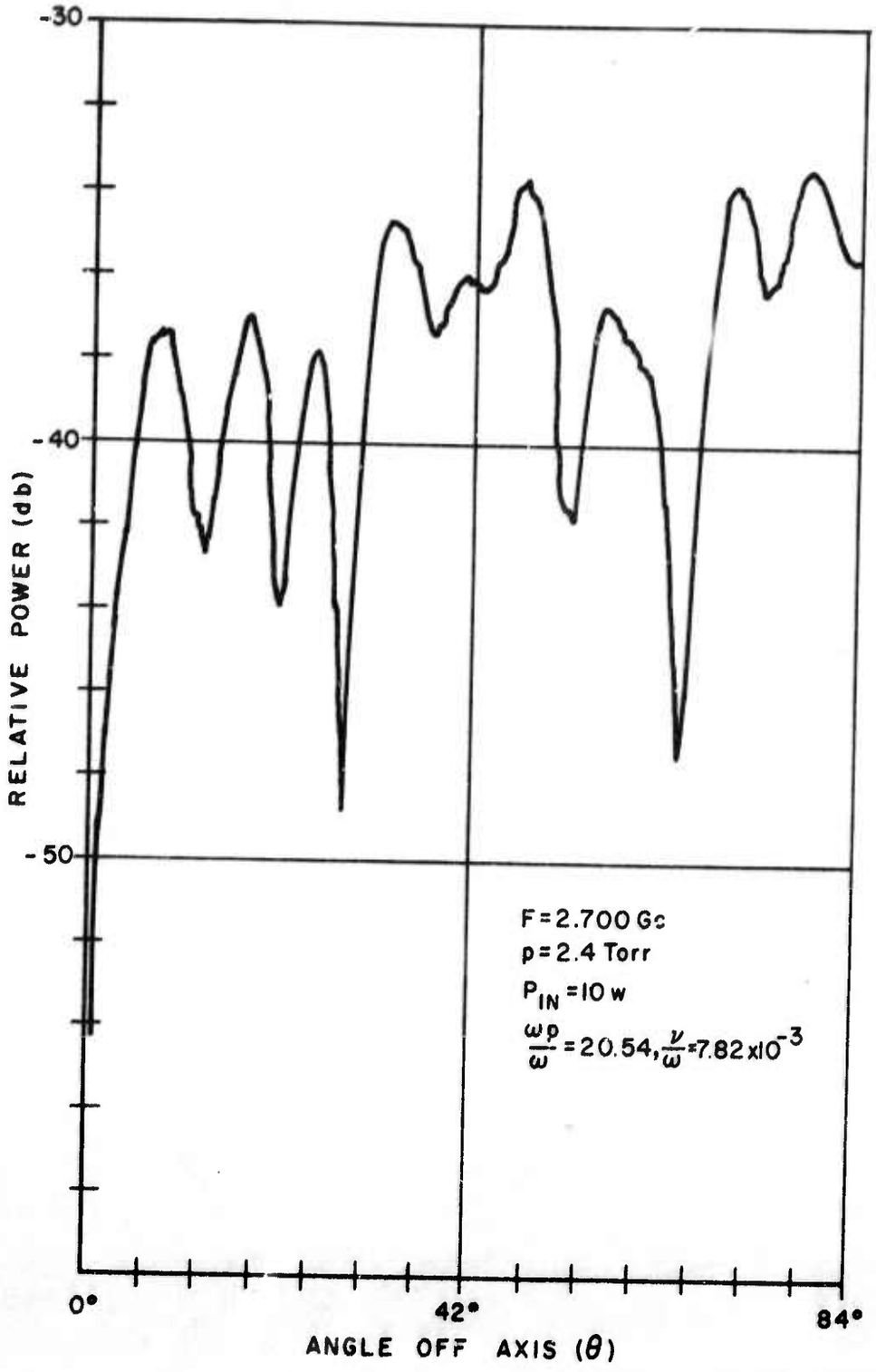

Figure 5-6b H-Plane Pattern of Vertical Slot Antenna

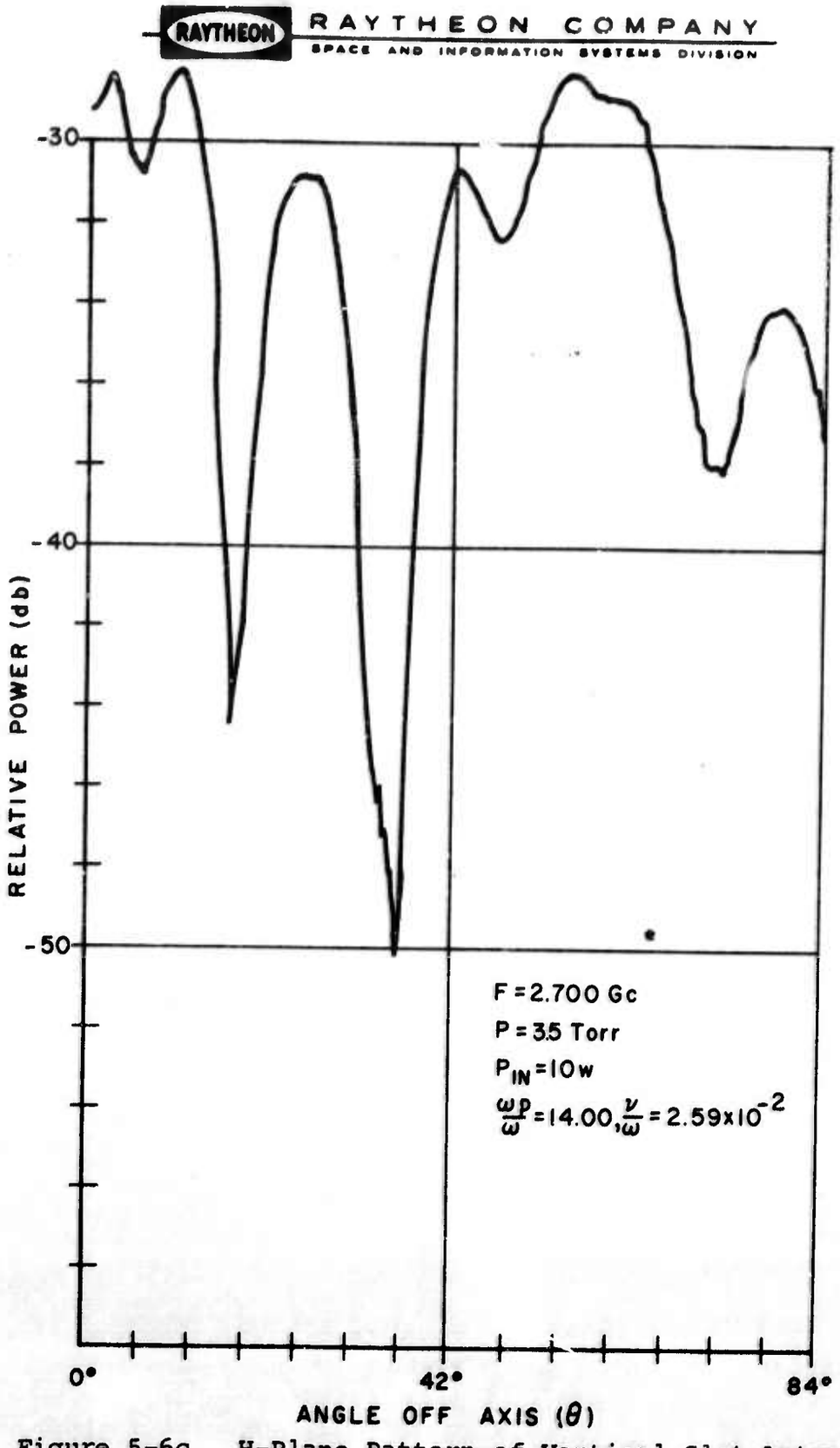

Figure 5-6c H-Plane Pattern of Vertical Slot Antenna

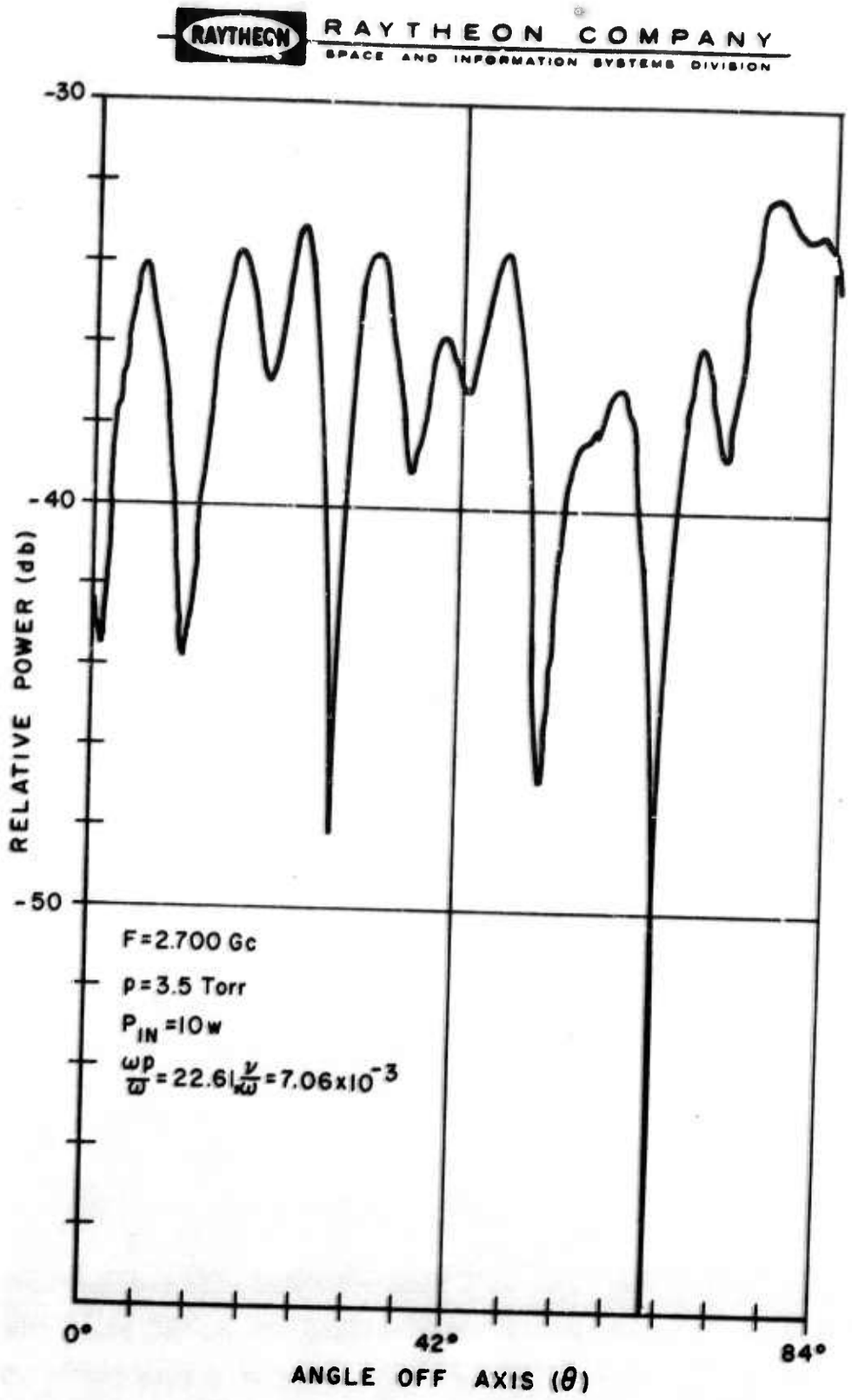

Figure 5-6d H-Plane Pattern of Vertical Slot Antenna

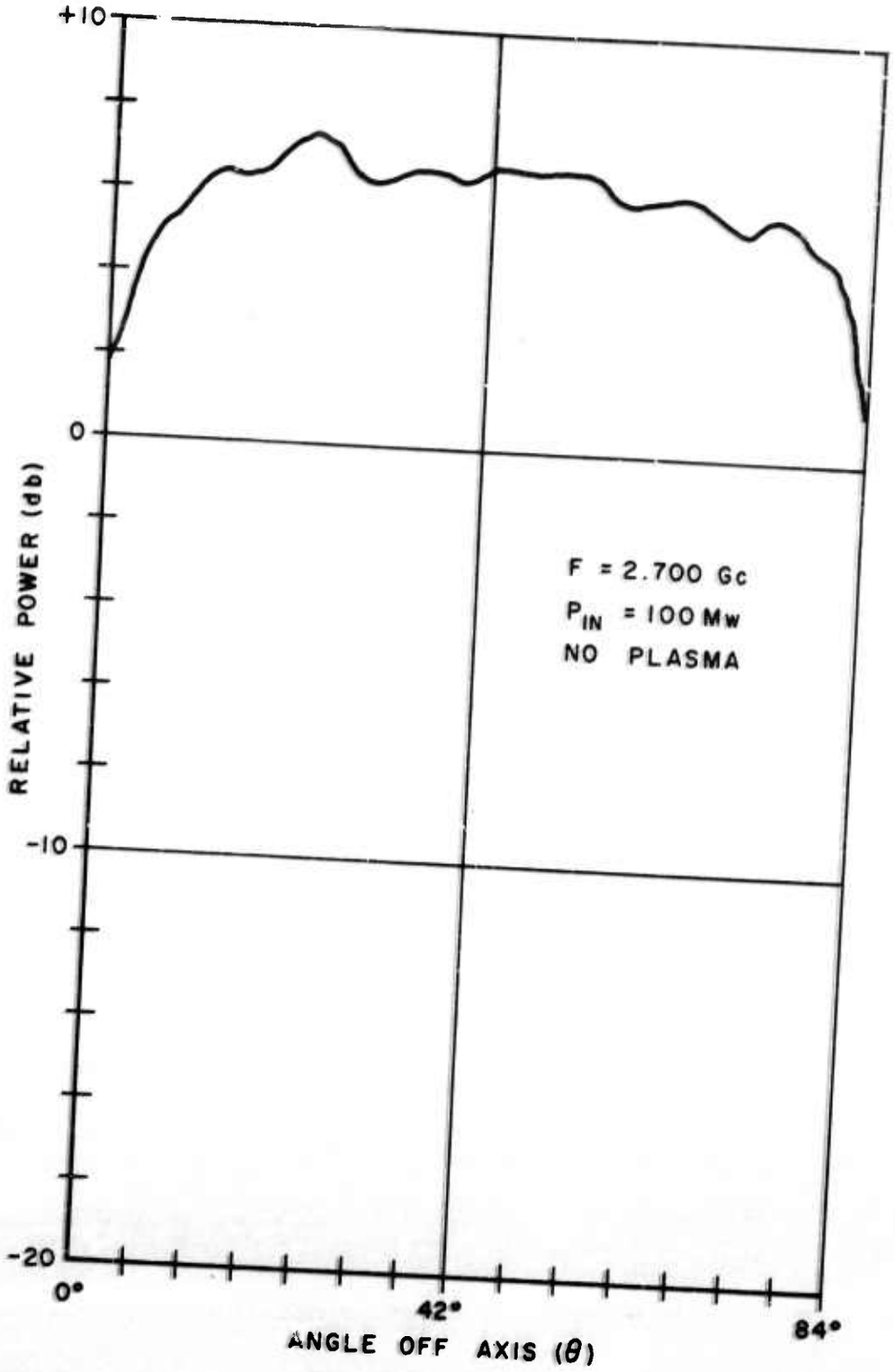

Figure 5-7 E-Plane Pattern of Horizontal Slot Antenna

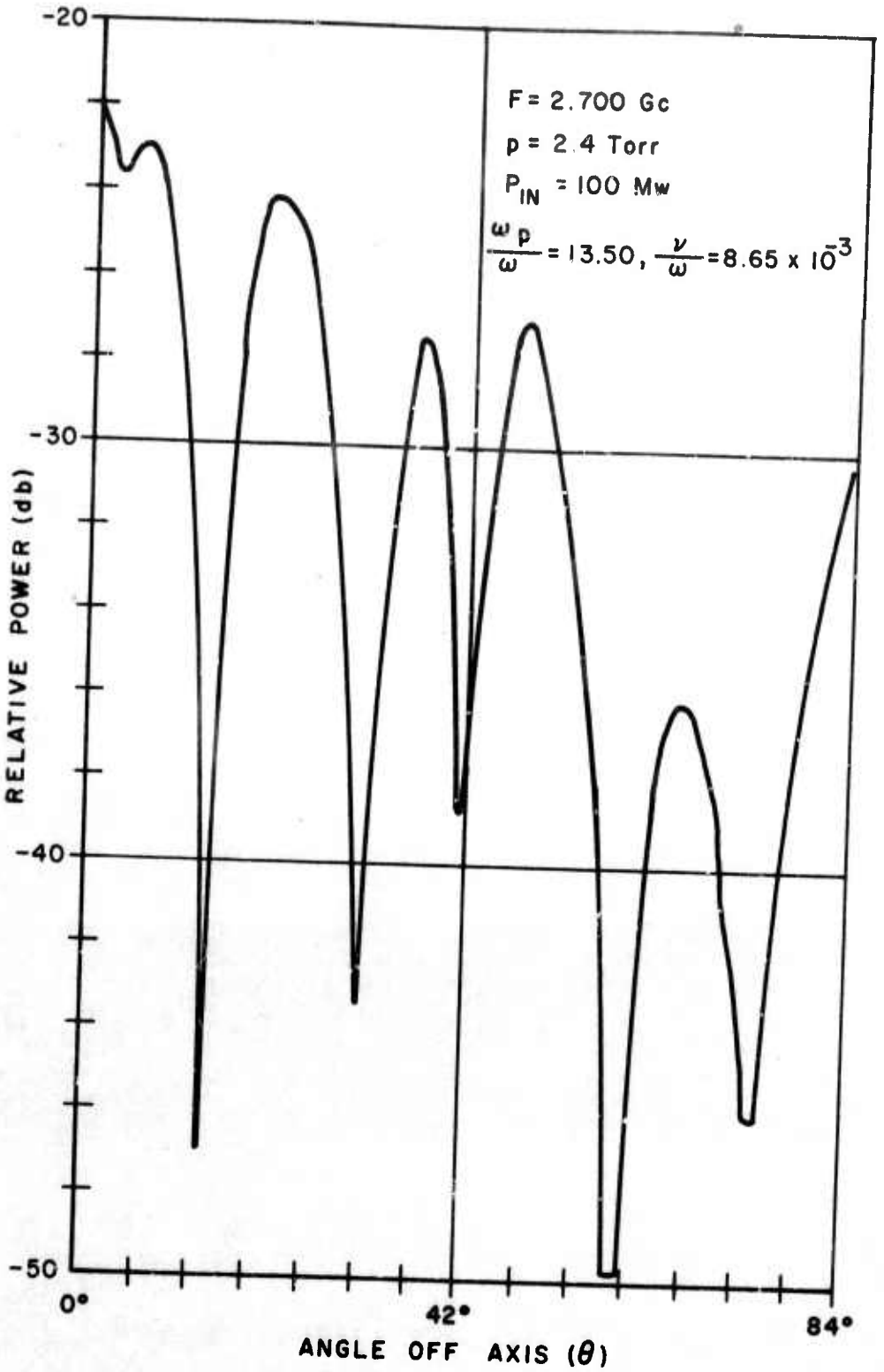

Figure 5-7a E-Plane Pattern of Horizontal Slot Antenna

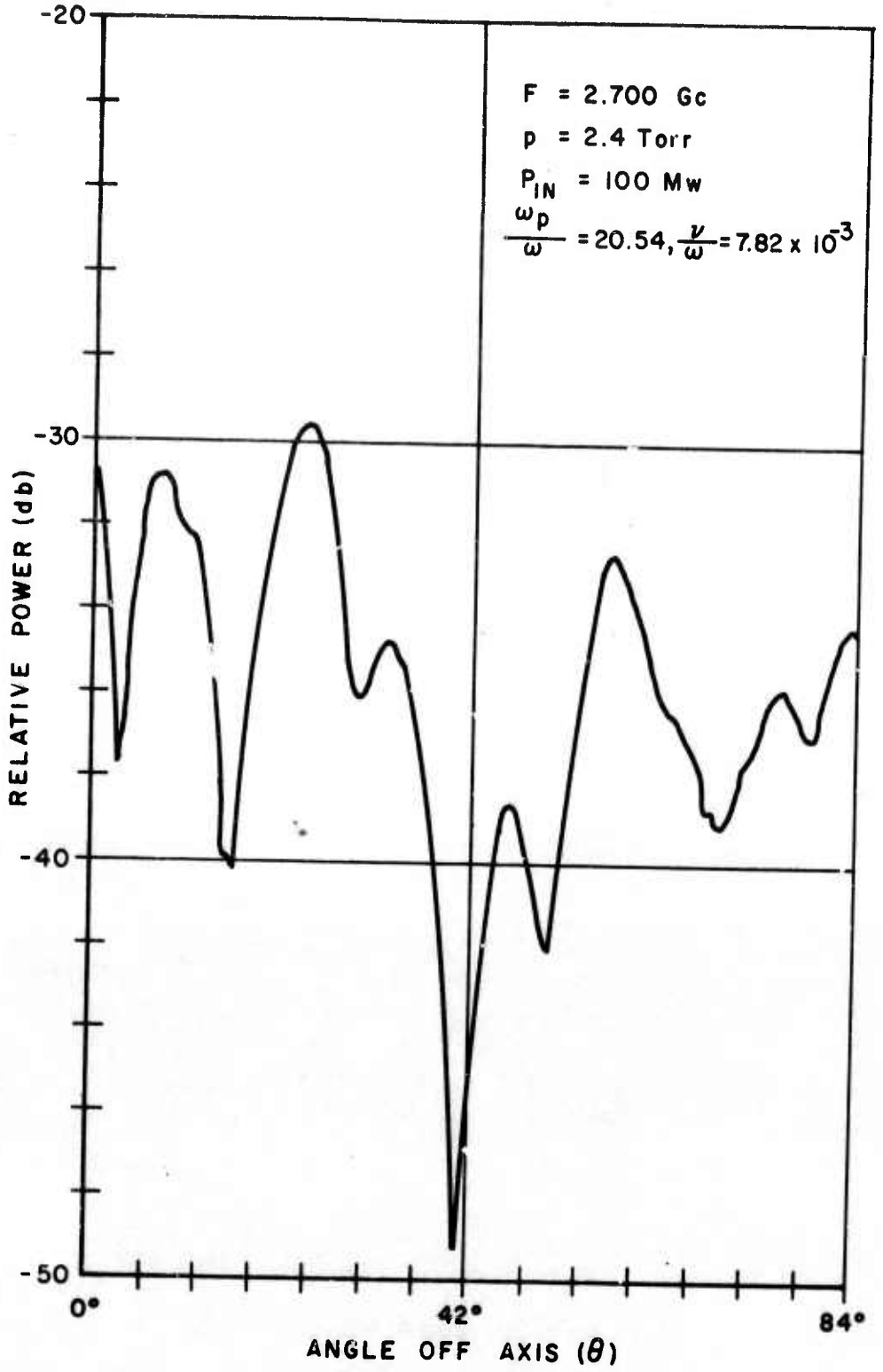

Figure 5-7b E-Plane Pattern of Horizontal Slot Antenna

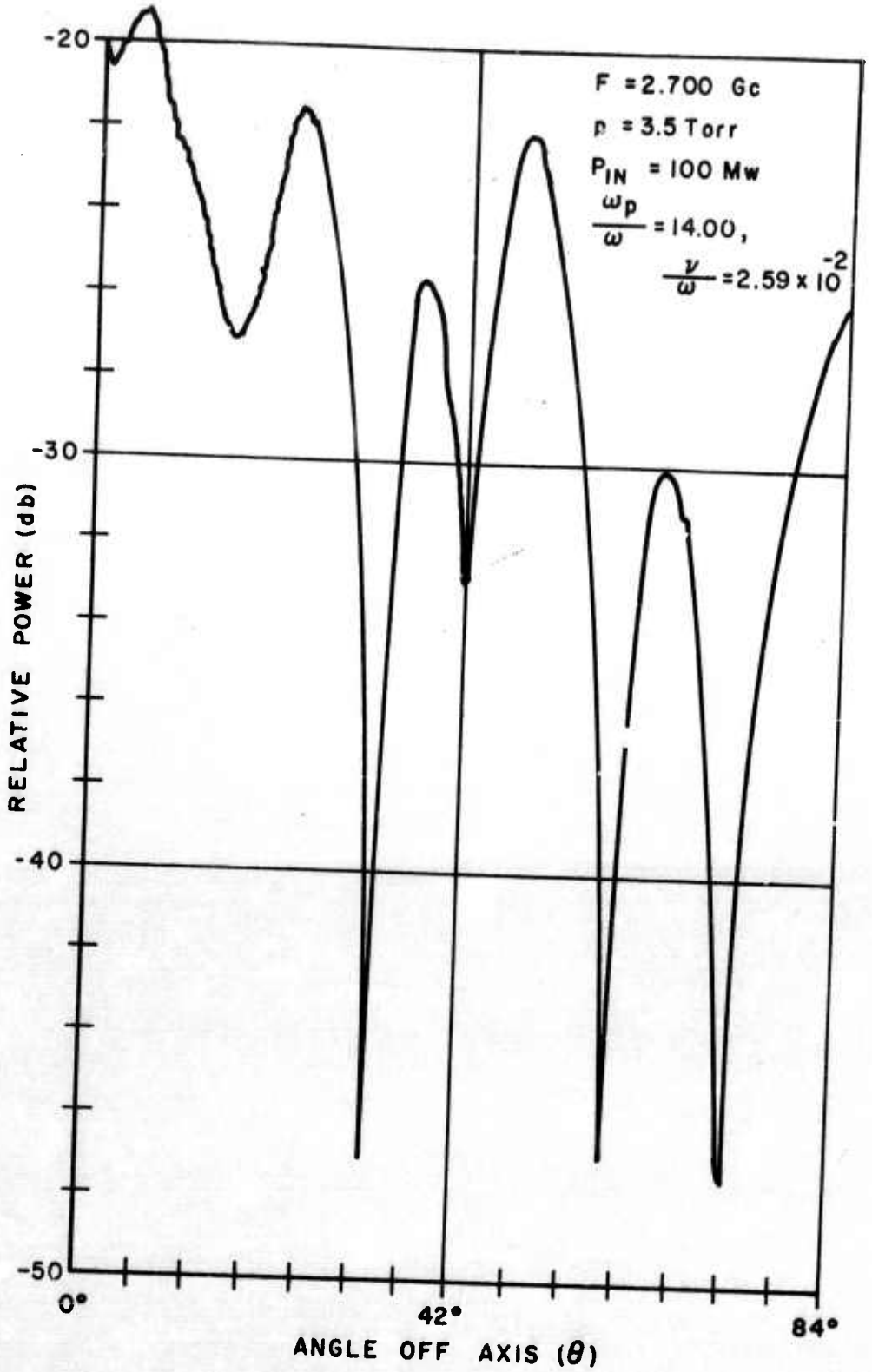

Figure 5-7c E-Plane Pattern of Horizontal Slot Antenna

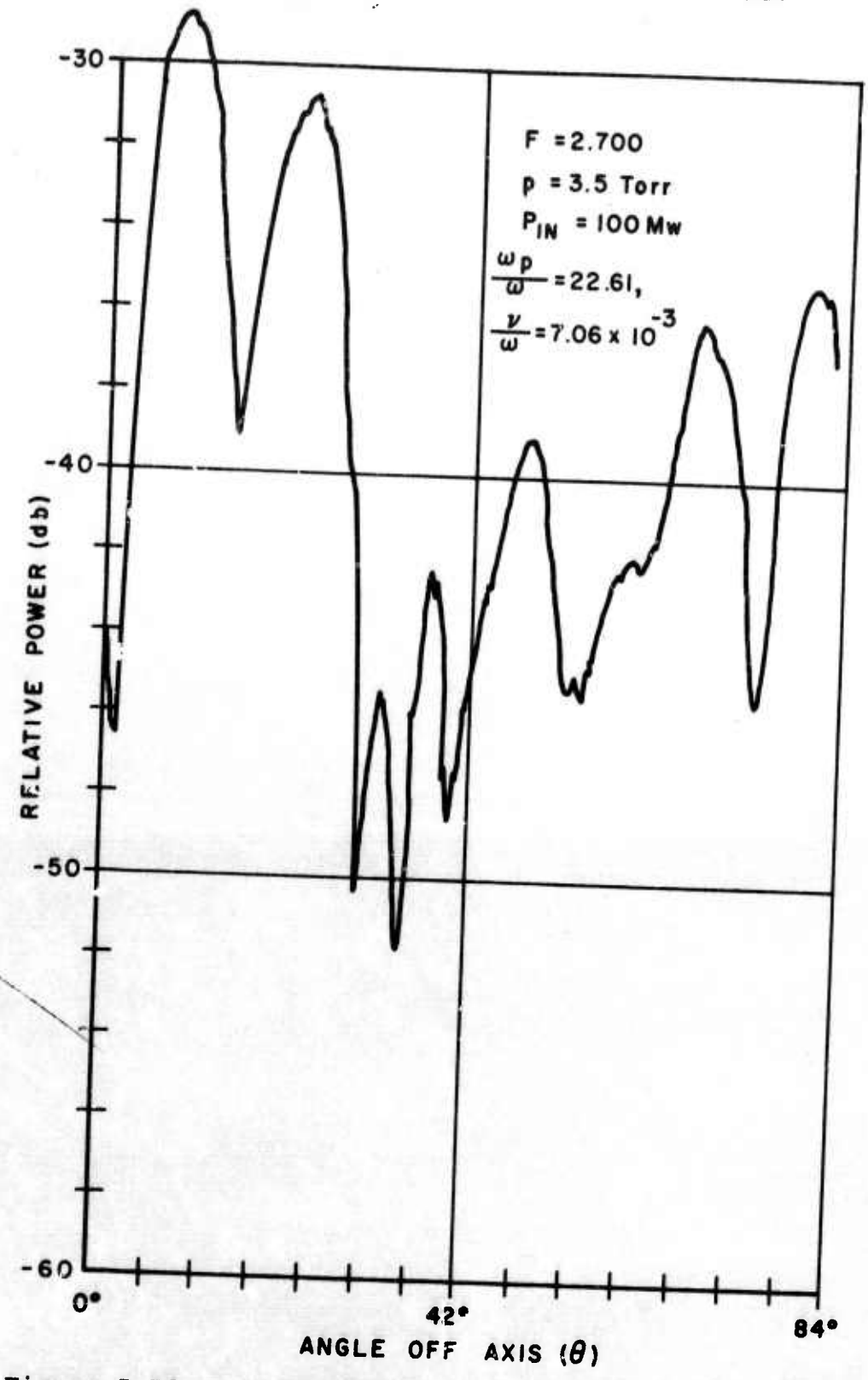

Figure 5-7d E-Plane Pattern of Horizontal Slot Antenna

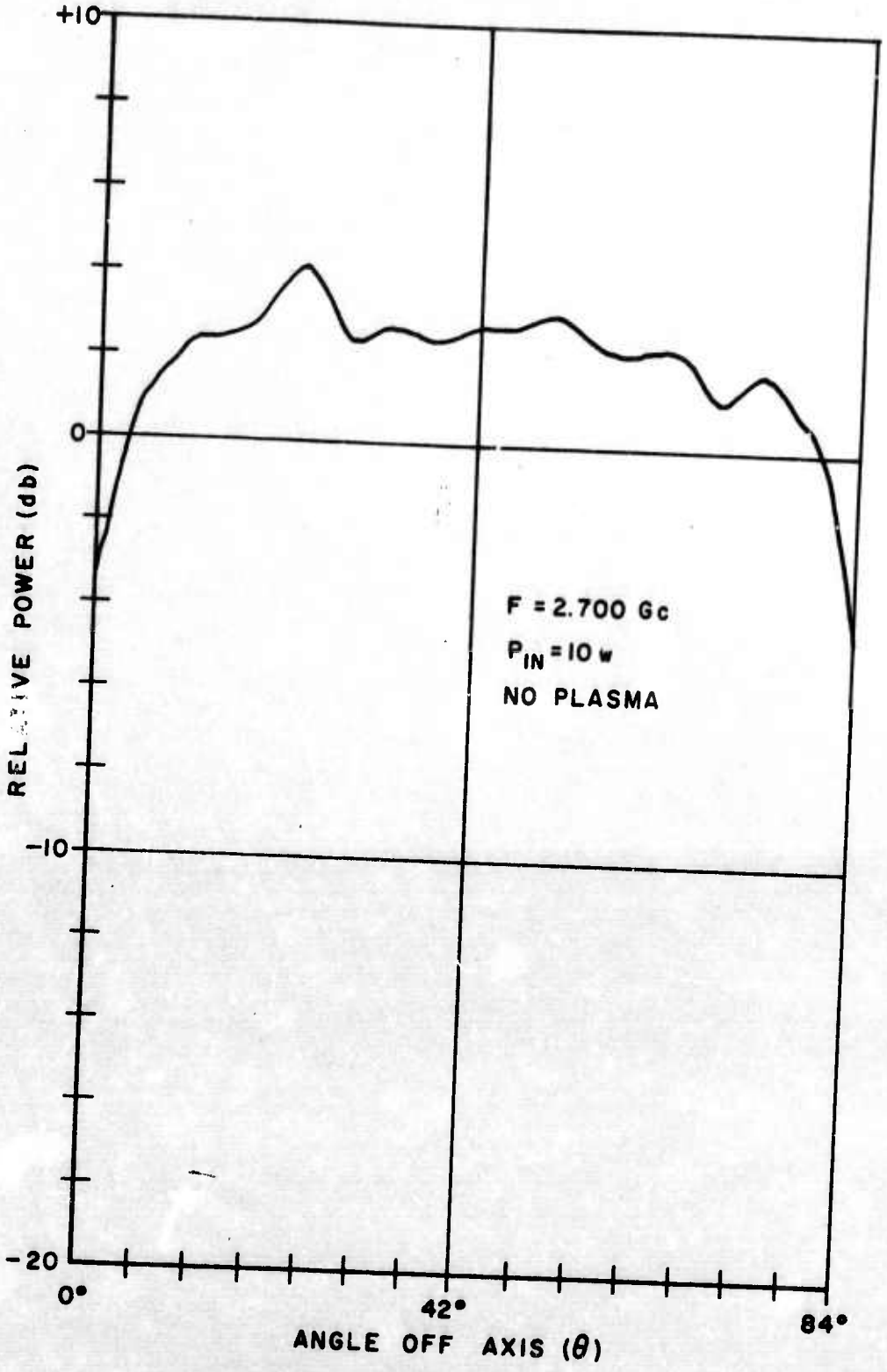

Figure 5-8 E-Plane Pattern of Horizontal Slot Antenna

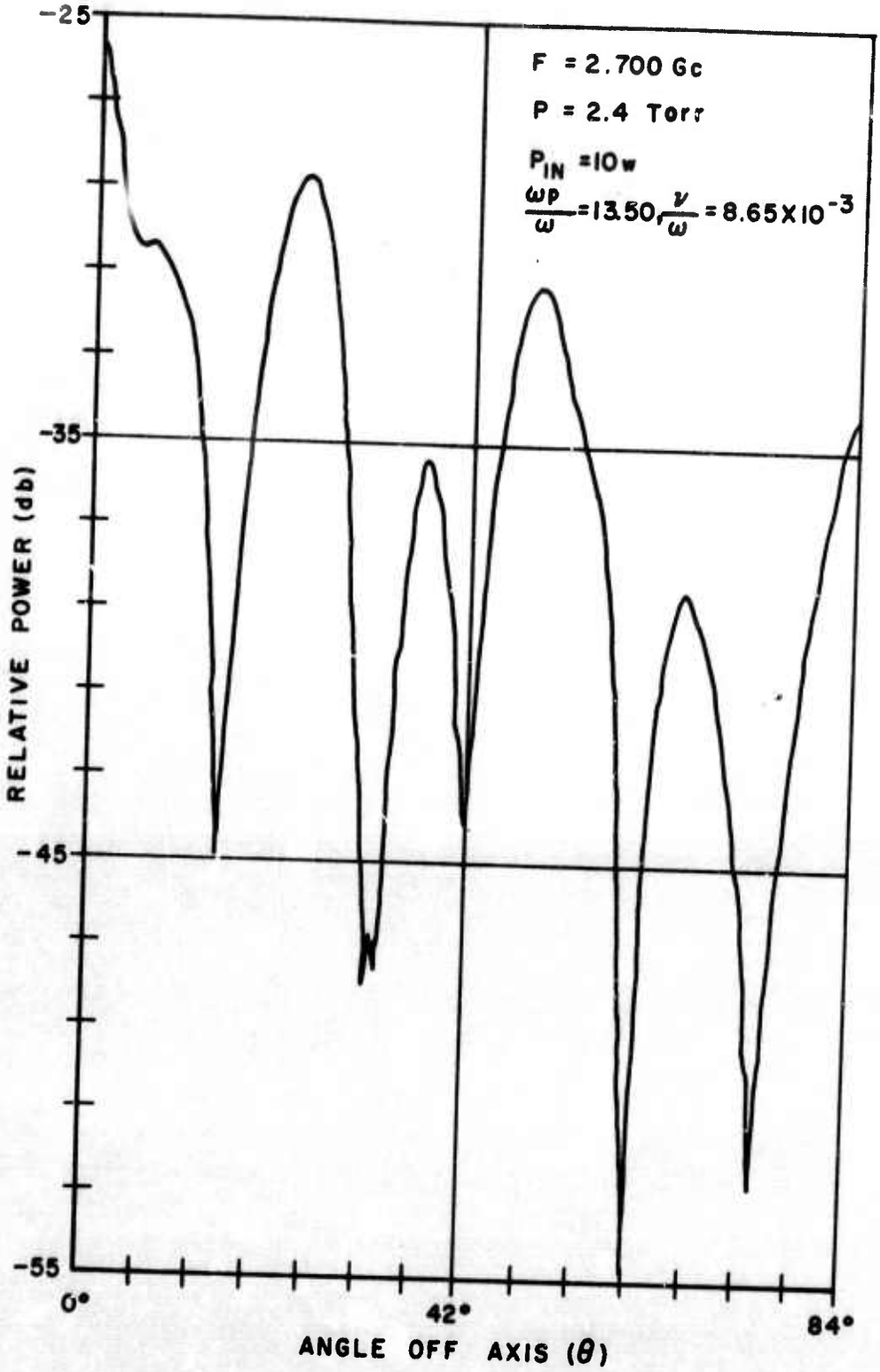

Figure 5-8a E-Plane Pattern of Horizontal Slot Antenna

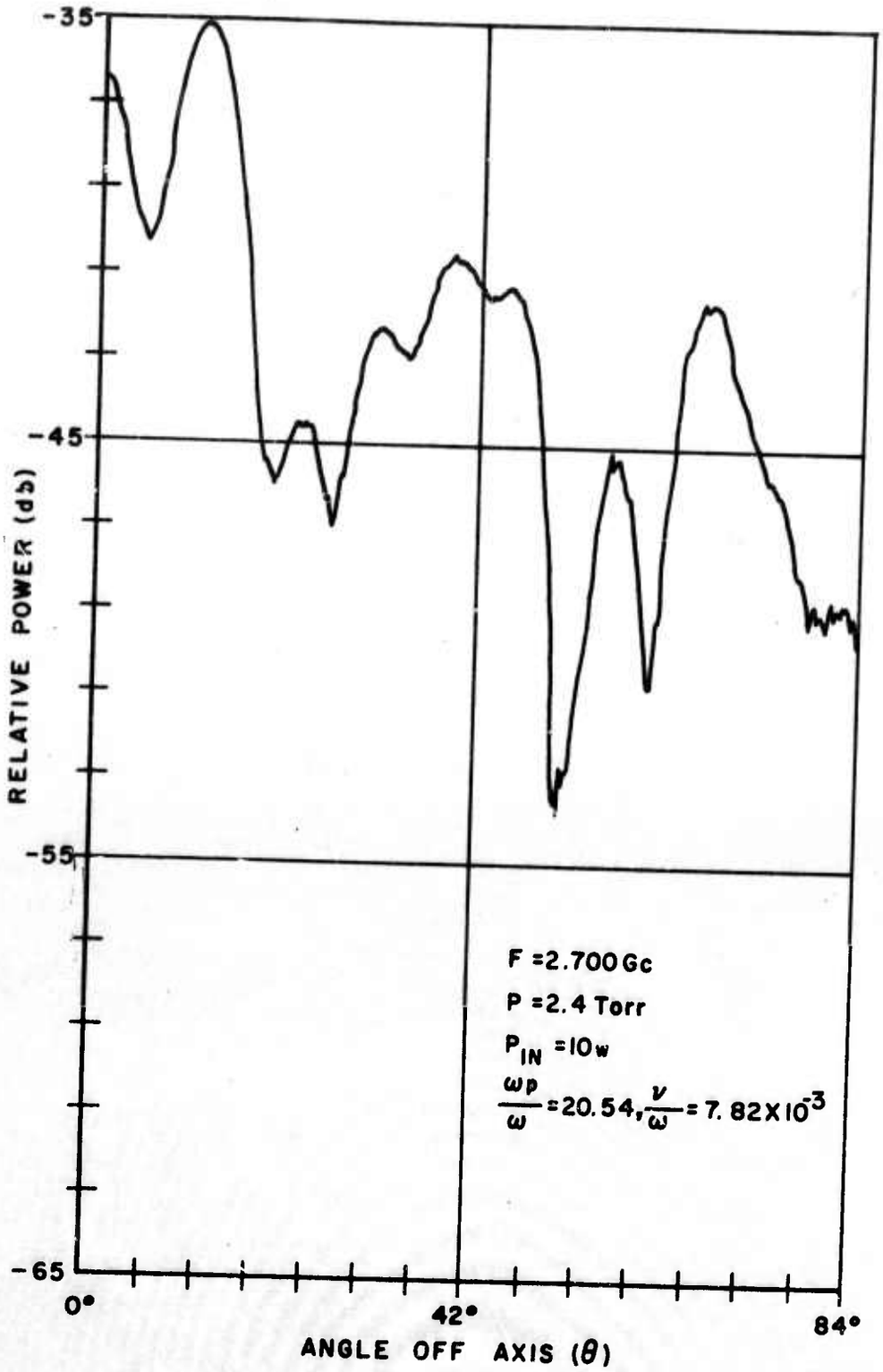

Figure 5-8b E-Plane Pattern of Horizontal Slot Antenna

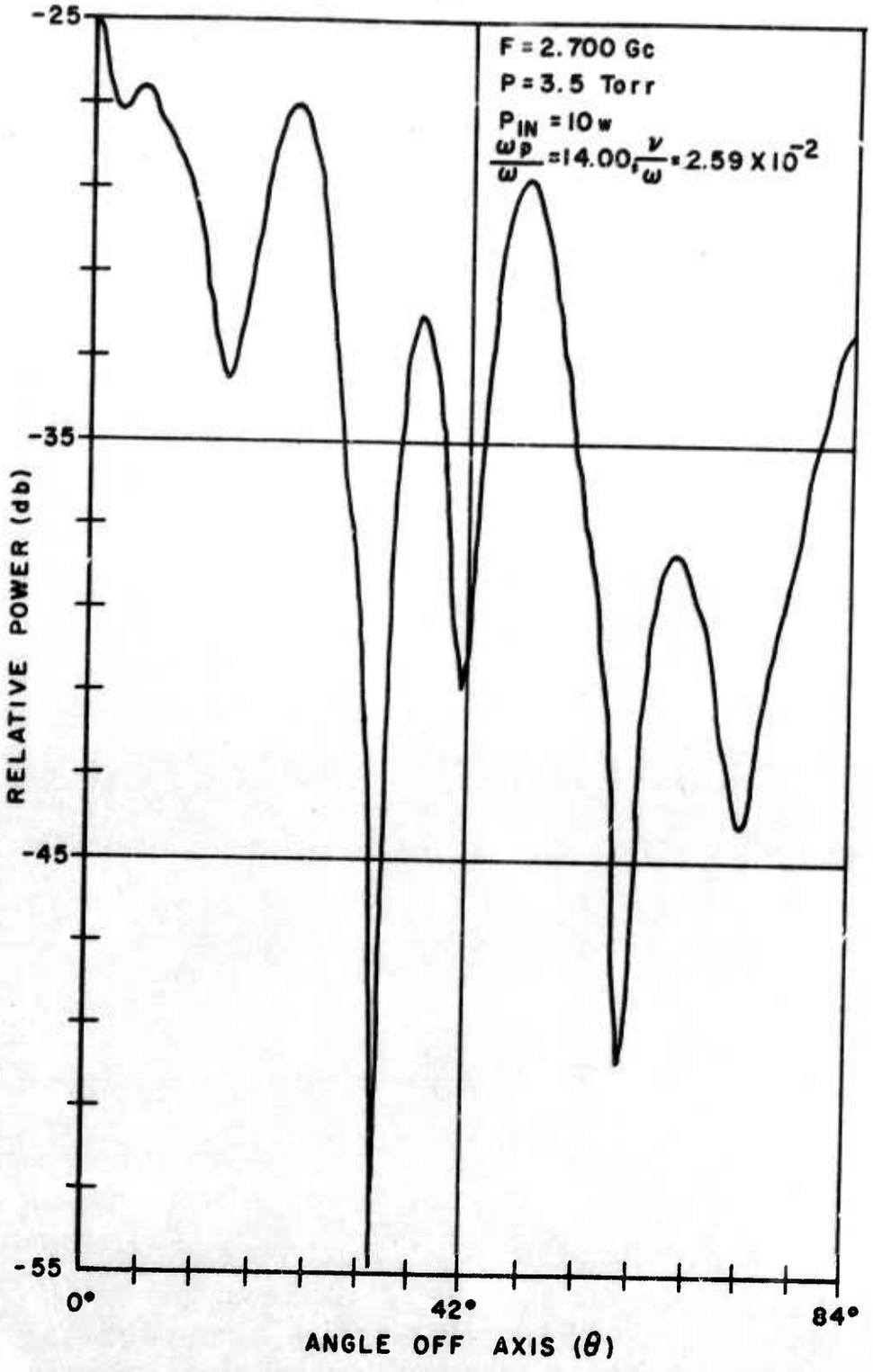

Figure 5-8c E-Plane Pattern of Horizontal Slot Antenna

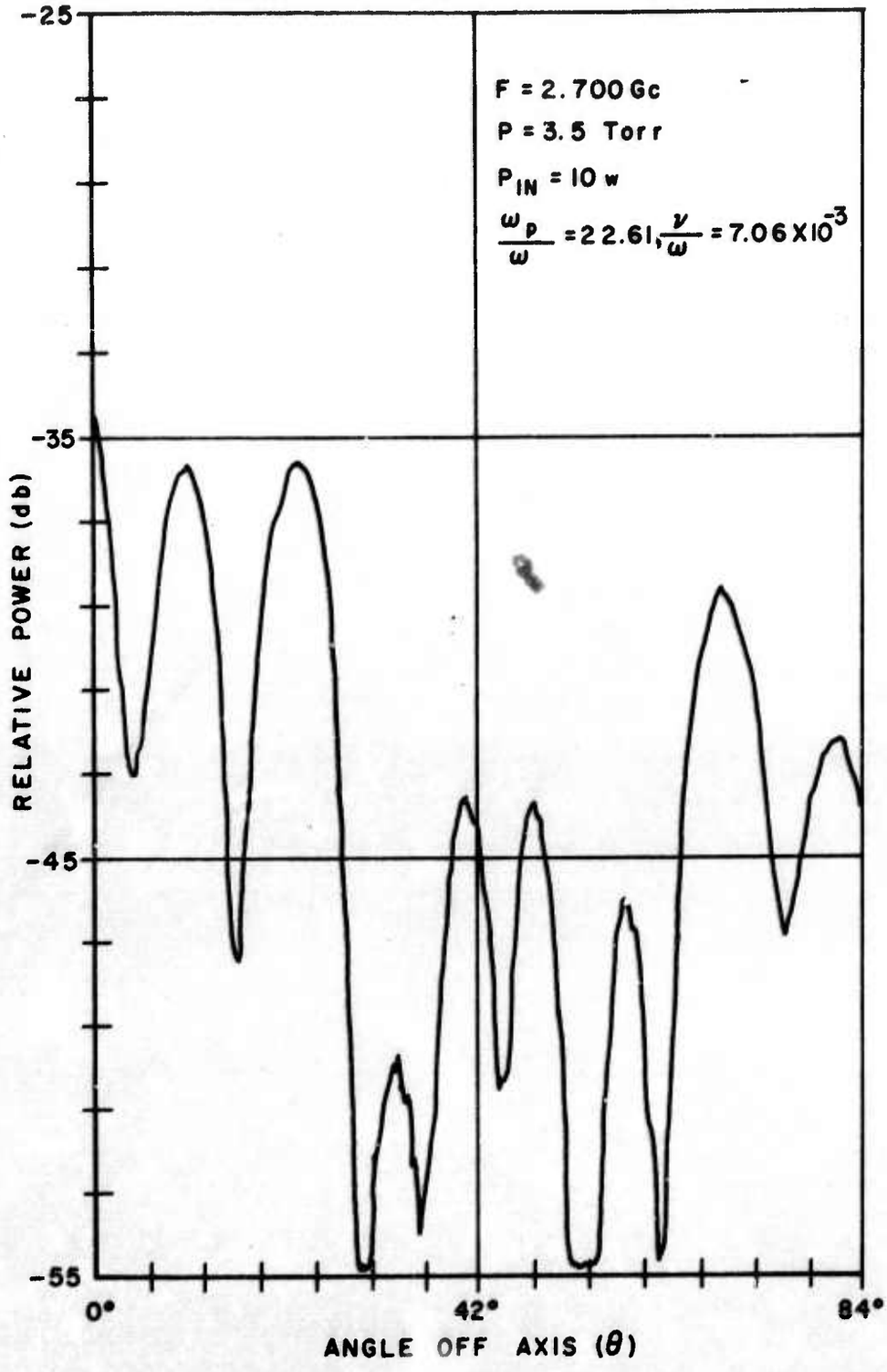

Figure 5-8d E-Plane Pattern of Horizontal Slot Antenna

input power, can be made. In all cases the attenuation was greater for the larger value of ω_p/ω at a given pressure and input power. There was roughly 5 db more attenuation for the vertical slot and 10 db more attenuation for the horizontal slot at the larger value of ω_p/ω. The attenuation was approximately the same for the lower power (P_{in} = 100 MW) and the high power (P_{in} = 10 Watts) cases for the vertical slot at a given pressure and ω_p/ω. Typically, the attenuation was greater than 30 db. The detailed structures of the antenna patterns for the vertical slot were essentially the same at lower power and high power at a given pressure and ω_p/ω. For the horizontal slot the attenuation was roughly greater than 20 db at lower power and greater than 25 db at high power at a given pressure and ω_p/ω. The detailed structures of the antenna patterns for the horizontal slot were essentially the same for the corresponding low power and high power cases.

Although the difference in attenuation between the vertical slot and the horizontal slot might be attributed to the different polarizations, the higher internal loss (4 db) of the vertical slot antenna was probably responsible for the difference in attenuation.

5.3 Isolation Between Orthogonal Slot Antennas

Isolation between the slot antennas was measured using the experimental arrangement shown in Figure 5-9. The transmitter and receiver cables were disconnected from the antenna inputs and shorted together. For a given input power a reference level was obtained on the pattern recorder. A pad had to be placed on the input of the receiver when making the reference measurement to prevent saturating the receiver. The shorting cable was

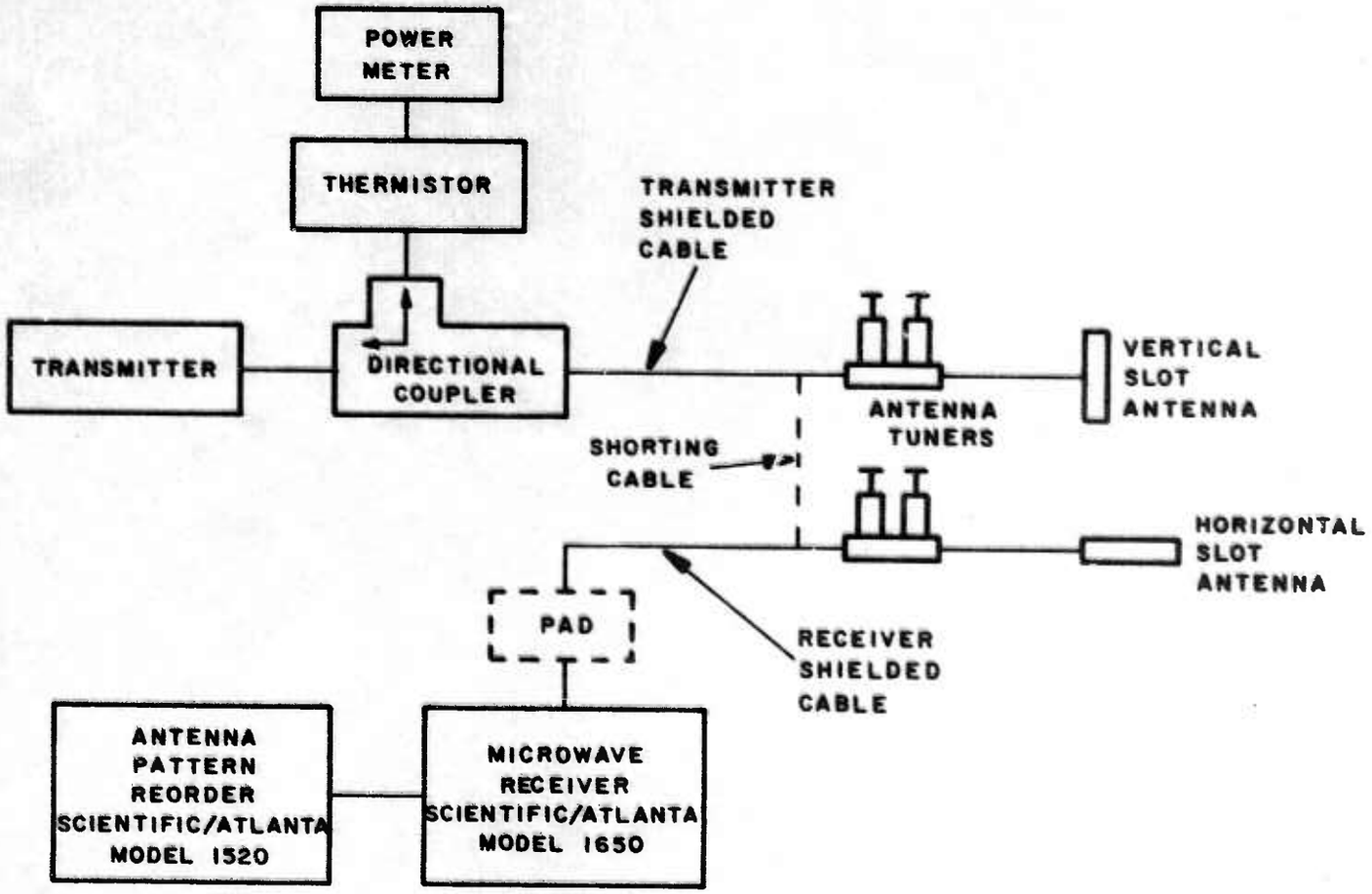

Figure 5-9 Antenna Isolation Measurement

then removed and the transmitter and receiver cables were connected back to the antennas. The pad was then removed and the required amount of attenuation was taken out of the receiver to bring the recorder pen back to the reference mark. The remaining attenuation in the receiver was subtracted from the total attenuation in the receiver (i.e., including the pad) used to obtain the reference level, and the isolation between the slot antennas was obtained directly in db. The plasma was "turned-on" and the receiver attenuation was adjusted to bring the recorder pen back to the reference mark. The isolation between the slot antennas was obtained as previously.

The isolation measured by transmitting with the vertical slot and receiving with the horizontal slot is given in Figure 5-10 and Figure 5-11. The transmitter and receiver cables were interchanged at the transmitter and receiver, and the isolation measured by transmitting with the horizontal slot and receiving with the vertical slot is given in Figure 5-12 and Figure 5-13. In all cases the isolation was essentially independent of input power from 25 milliwatts to 10 watts. No noticeable deviation from the reciprocity principle for transmitting and receiving antennas in a linear medium was observed. Since the plasma was highly overdense the RF fields could not penetrate into the plasma to any appreciable extent and the energy was confined to the air-glass space between the slot apertures and the plasma boundary. Therefore, the energy coupling the antennas was confined within linear media and the antennas behaved reciprocally.

The isolation between the transmitting antenna and the receiver was measured by disconnecting the receiver cable at the receiving antenna input and terminating the cable with an RF load.

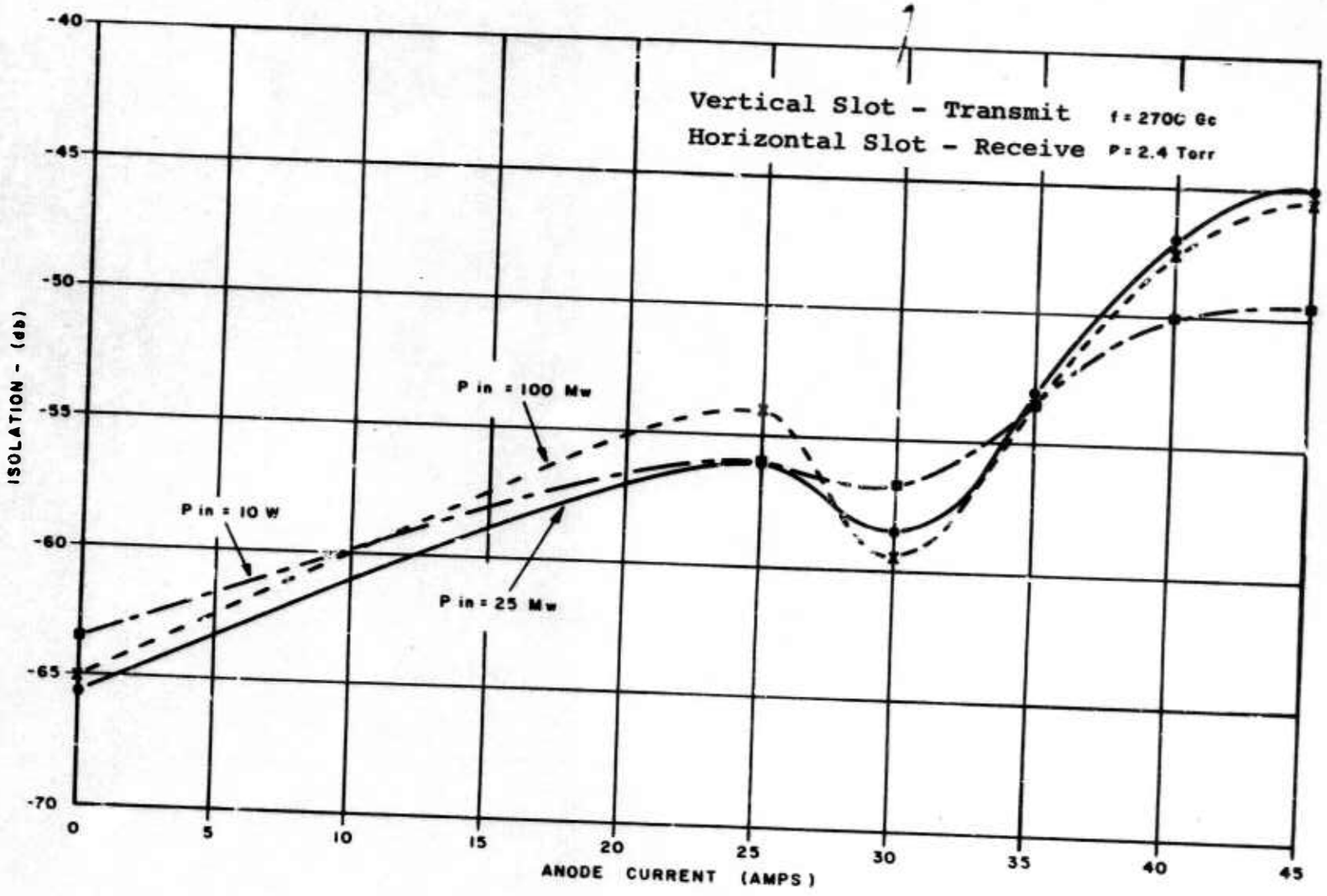

Figure 5-10 Isolation Between Orthogonally Oriented Slot Antennas vs. Simulator Discharge Current

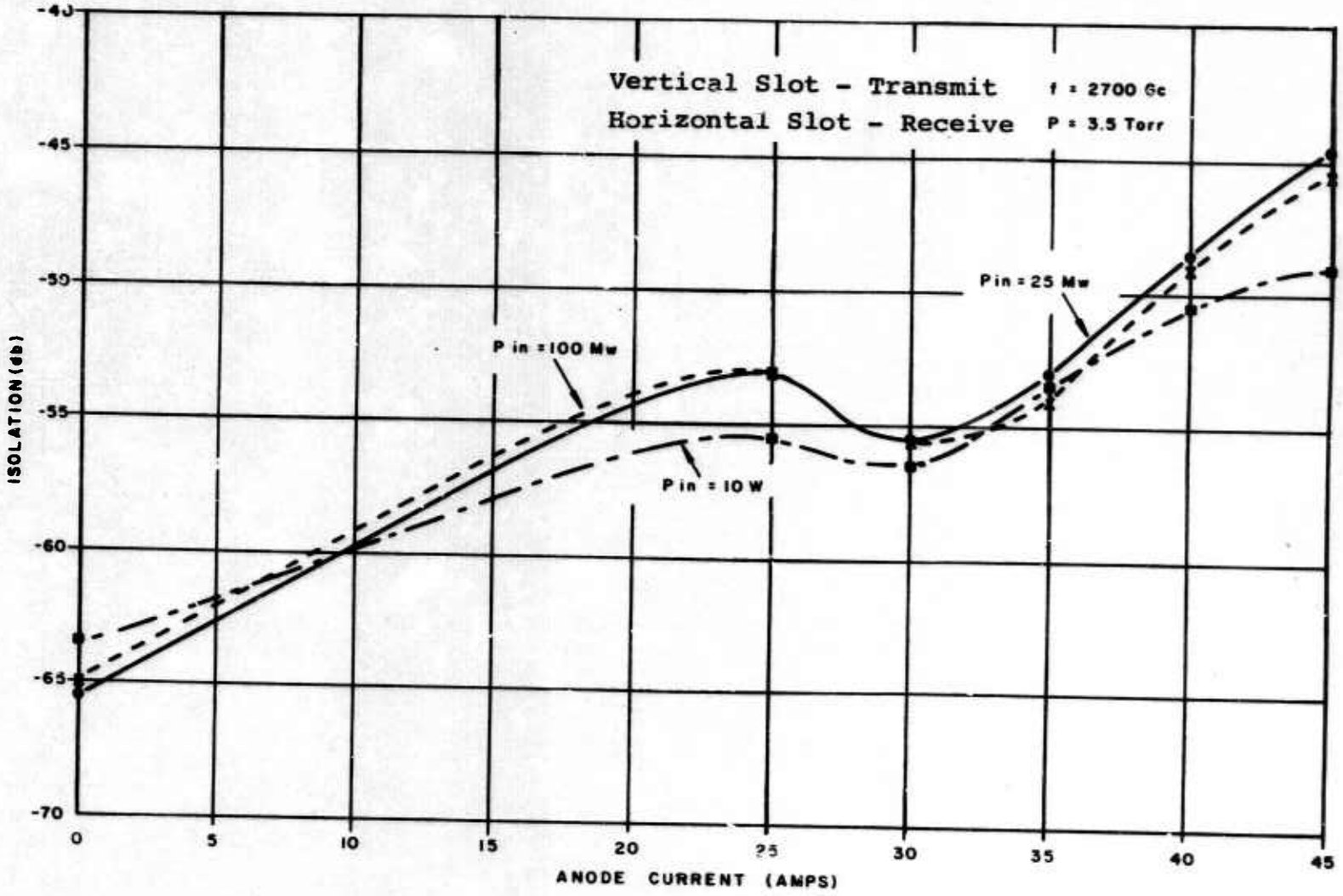

Figure 5-11 Isolation Between Orthogonally Oriented Slot Antennas vs. Simulator Discharge Current

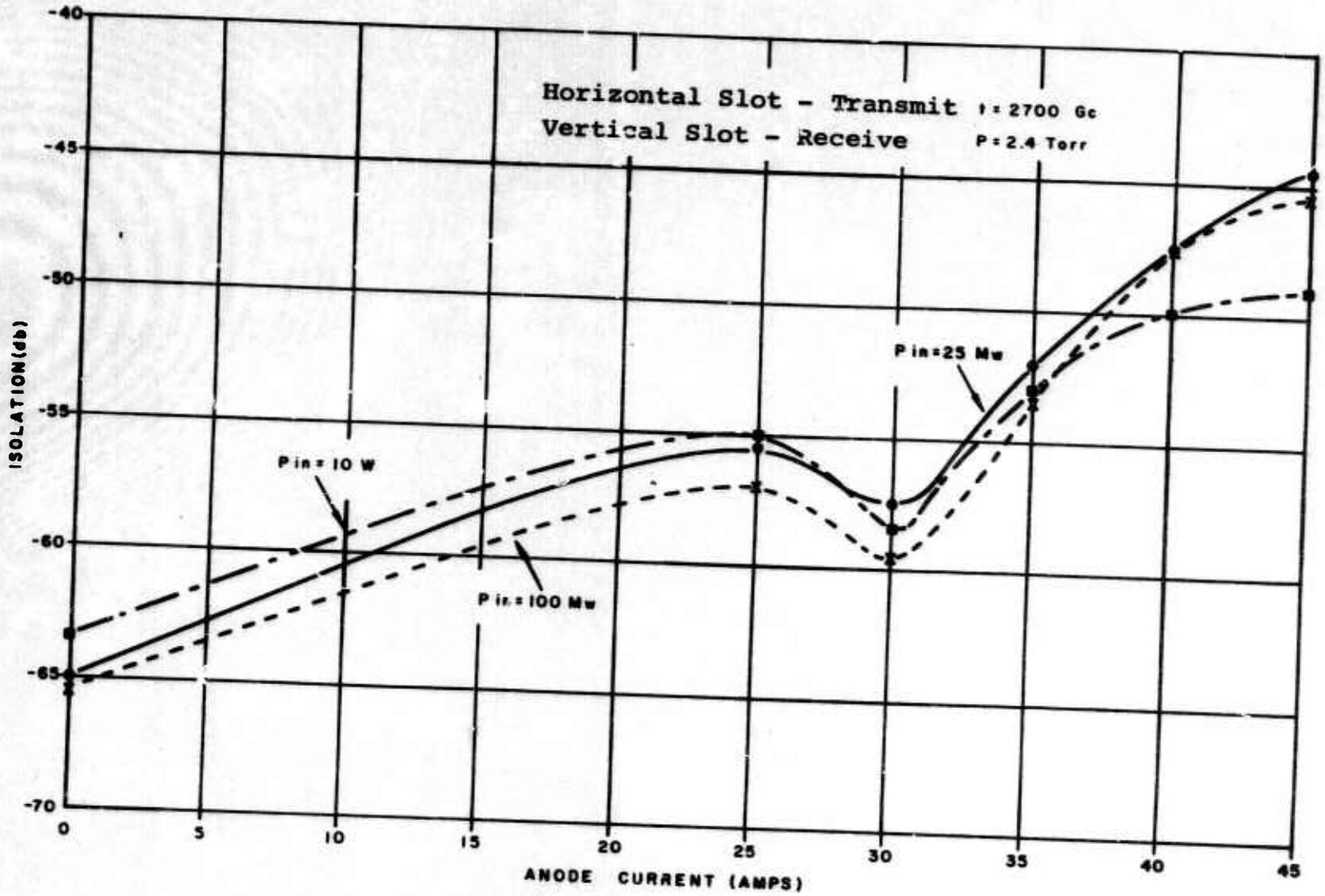

Figure 5-12 Isolation Between Orthogonally Oriented Slot Antennas vs. Simulator Discharge Current

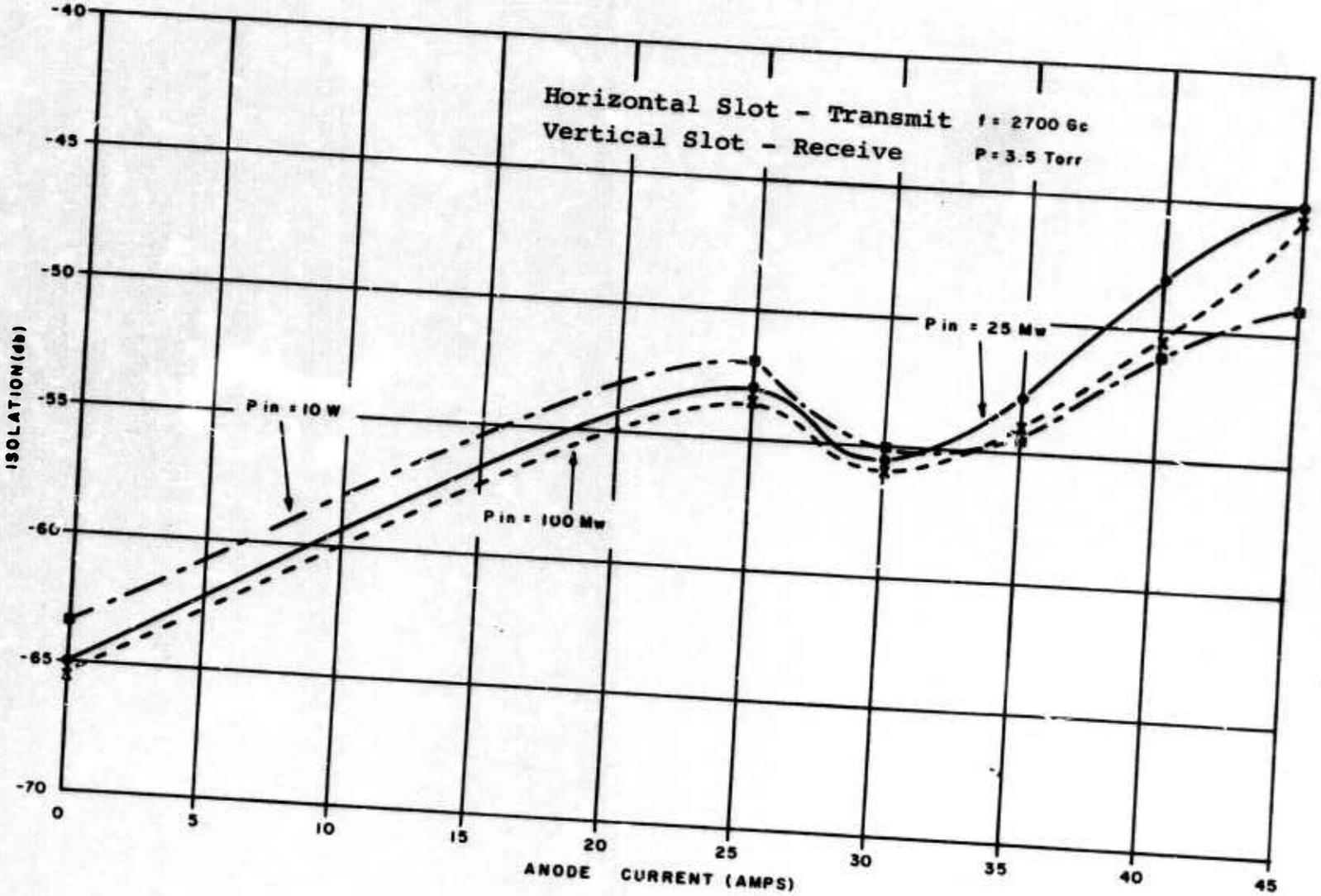

Figure 5-13 Isolation Between Orthogonally Oriented Slot Antennas vs. Simulator Discharge Current

The isolation was -119 db. Therefore, the effect of RF leakage on the isolation measurements was negligible.

5.4 Antenna Input Impedance

For a uniform lossless transmission line terminated in some impedance Z_L, the input impedance $Z(\ell)$ at a distance ℓ from the load is given by (Reference 5)

$$\frac{Z(\ell)}{Z_o} = \frac{1 + |\Gamma| e^{-j\phi(\ell)}}{1 - |\Gamma| e^{-j\phi(\ell)}} \qquad (5.4)$$

where Z_o is the characteristic impedance of the line; Γ is the reflection coefficient and $\phi(\ell)$ is the angle of the reflection coefficient. The normalized load impedance is found by taking $\ell = 0$:

$$\frac{Z_L}{Z_o} = \frac{1 + |\Gamma| e^{-j\phi_L}}{1 - |\Gamma| e^{-j\phi_L}} \qquad (5.5)$$

If the transmission line is not lossless the magnitude of the reflection coefficient in Equation (5.5) must be measured at the load.

Denote the input impedance to the slot antenna by Z_A. Then,

$$\frac{Z_A}{Z_o} = \frac{1 + |\Gamma_A| e^{-j\phi_A}}{1 - |\Gamma_A| e^{-j\phi_A}} \qquad (5.6)$$

Since Γ_A is related to the VSWR, S_A, at the antenna input by the equation

$$|\Gamma_A| = \frac{S_A - 1}{S_A + 1} \qquad (5.7)$$

Equation (5.6) becomes

$$\frac{Z_A}{Z_o} = \frac{1 + \left(\frac{S_A - 1}{S_A + 1}\right) e^{-j\phi_A}}{1 - \left(\frac{S_A - 1}{S_A + 1}\right) e^{-j\phi_A}} \qquad (5.8)$$

If ϕ_A is measured, and using the measured values of S_A given in Section 5.1, the normalized antenna input impedance is given by Equation (5.8).

The angle ϕ_A was measured by measuring the phase difference between the incident and reflected waves with a dual directional coupler and phase bridge as shown in Figure 4-1. To read ϕ_A directly off the phase bridge, the bridge had to be balanced. The bridge was balanced by terminating the coaxial cable to the antenna at the antenna input with a resistive RF load whose impedance was greater than Z_o and adjusting the bridge until the reflection angle meter read zero. The justification for this calibration procedure can be seen from Equation (5.5). If ϕ_L is set equal to zero, then

$$\frac{Z_L}{Z_o} = \frac{1 + |\Gamma_L|}{1 - |\Gamma_L|}$$

But since $|\Gamma_L| \leq 1$, $\frac{Z_L}{Z_o} \geq 1$.

To compute the antenna input impedance, it was found easier to use a Smith Chart than Equation (5.8). A circle of radius S_A was drawn about the center of the chart. A line drawn from the center of the constant VSWR circle to ϕ_A on the "angle of

Equation (5.6) becomes

$$\frac{Z_A}{Z_o} = \frac{1 + \left(\frac{S_A - 1}{S_A + 1}\right) e^{-j\phi_A}}{1 - \left(\frac{S_A - 1}{S_A + 1}\right) e^{-j\phi_A}} \qquad (5.8)$$

If ϕ_A is measured, and using the measured values of S_A given in Section 5.1, the normalized antenna input impedance is given by Equation (5.8).

The angle ϕ_A was measured by measuring the phase difference between the incident and reflected waves with a dual directional coupler and phase bridge as shown in Figure 4-1. To read ϕ_A directly off the phase bridge, the bridge had to be balanced. The bridge was balanced by terminating the coaxial cable to the antenna at the antenna input with a resistive RF load whose impedance was greater than Z_o and adjusting the bridge until the reflection angle meter read zero. The justification for this calibration procedure can be seen from Equation (5.5). If ϕ_L is set equal to zero, then

$$\frac{Z_L}{Z_o} = \frac{1 + |\Gamma_L|}{1 - |\Gamma_L|}$$

But since $|\Gamma_L| \leq 1$, $\frac{Z_L}{Z_o} \geq 1$.

To compute the antenna input impedance, it was found easier to use a Smith Chart than Equation (5.8). A circle of radius S_A was drawn about the center of the chart. A line drawn from the center of the constant VSWR circle to ϕ_A on the "angle of

Equation (5.6) becomes

$$\frac{Z_A}{Z_o} = \frac{1 + \left(\frac{S_A - 1}{S_A + 1}\right) e^{-j\phi_A}}{1 - \left(\frac{S_A - 1}{S_A + 1}\right) e^{-j\phi_A}} \qquad (5.8)$$

If ϕ_A is measured, and using the measured values of S_A given in Section 5.1, the normalized antenna input impedance is given by Equation (5.8).

The angle ϕ_A was measured by measuring the phase difference between the incident and reflected waves with a dual directional coupler and phase bridge as shown in Figure 4-1. To read ϕ_A directly off the phase bridge, the bridge had to be balanced. The bridge was balanced by terminating the coaxial cable to the antenna at the antenna input with a resistive RF load whose impedance was greater than Z_o and adjusting the bridge until the reflection angle meter read zero. The justification for this calibration procedure can be seen from Equation (5.5). If ϕ_L is set equal to zero, then

$$\frac{Z_L}{Z_o} = \frac{1 + |\Gamma_L|}{1 - |\Gamma_L|}$$

But since $|\Gamma_L| \leq 1$, $\frac{Z_L}{Z_o} \geq 1$.

To compute the antenna input impedance, it was found easier to use a Smith Chart than Equation (5.8). A circle of radius S_A was drawn about the center of the chart. A line drawn from the center of the constant VSWR circle to ϕ_A on the "angle of

reflection coefficient" scale intersected the VSWR circle at the normalized input impedance, $\frac{Z_A}{Z_o}$ (Reference 6)

A sample calculation is shown in Figure 5-14.

The normalized real and imaginary parts of the input impedance are given in Figures 5-15 to 5-18 for the vertical slot antenna, and in Figures 5-19 to 5-22 for the horizontal slot antenna. The reactive component of the input impedance was negative for the horizontal slot and positive for the vertical slot at low input power (P_{in} = 100 milliwatts). When the input power was increased to 10 watts, the sign of the reactive component of the input impedance was observed to reverse for both the vertical slot and the horizontal slot. For anode currents below 25 amperes the reactive component of the impedance might be negative, for the horizontal slot, as indicated by the extrapolated portion of the curve in this current range in Figure 5-22. A larger variation in the real and imaginary parts of the impedance with pressure was observed at high input power (P_{in} = 10 Watts) than at low power for both antennas. The real and imaginary parts of the impedance for the vertical slot were less sensitive to variations in the plasma parameters (i.e., n_e and ν), due to changing the simulator anode current at a constant pressure, than the real and imaginary parts of the impedance of the horizontal slot for the same variations in the plasma parameters at both low and high power. This phenomena was possibly due to high losses in the vertical slot antenna.

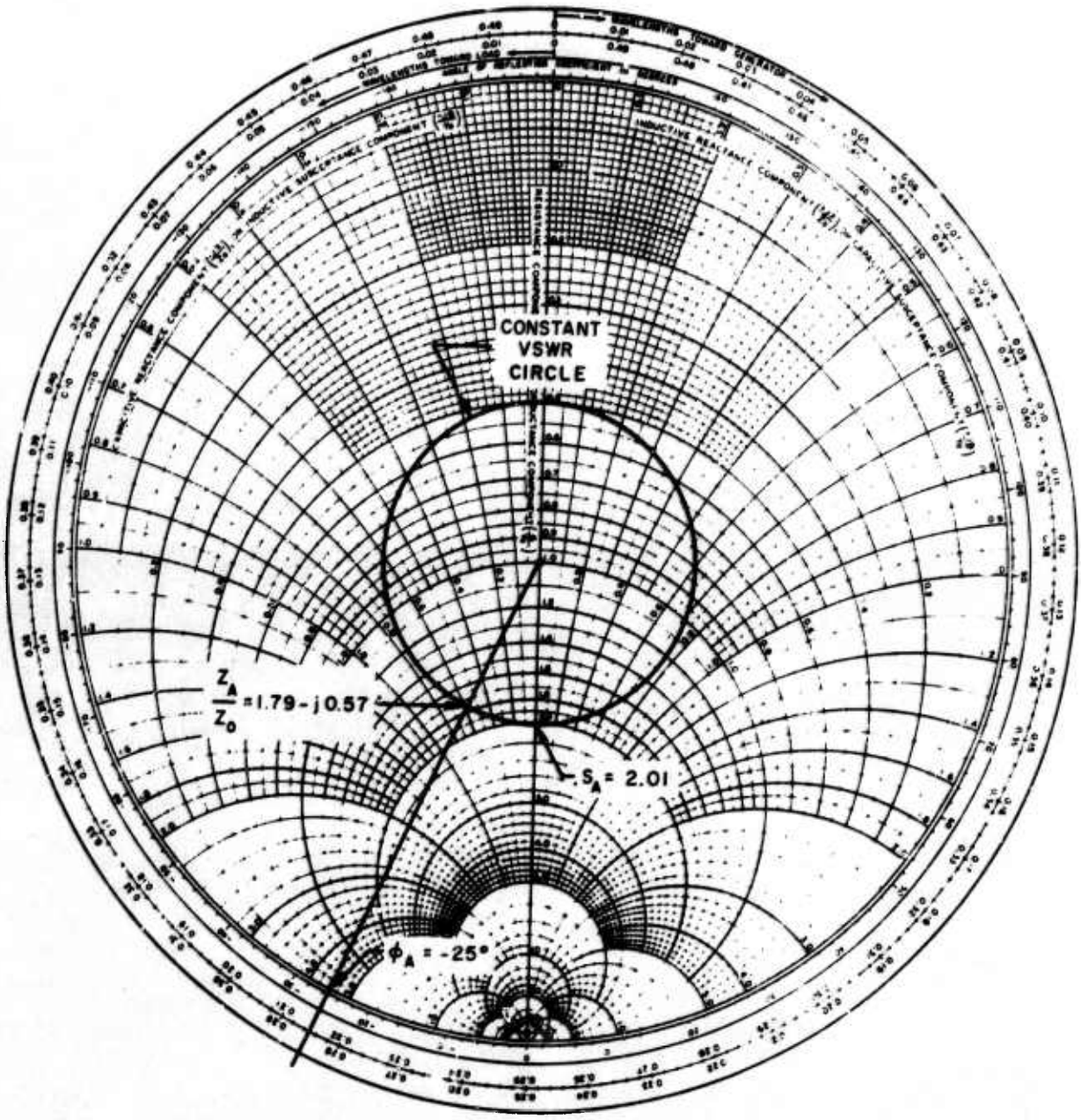

Figure 5-14 Sample Graphical Calculation of Normalized Antenna Input Impedance

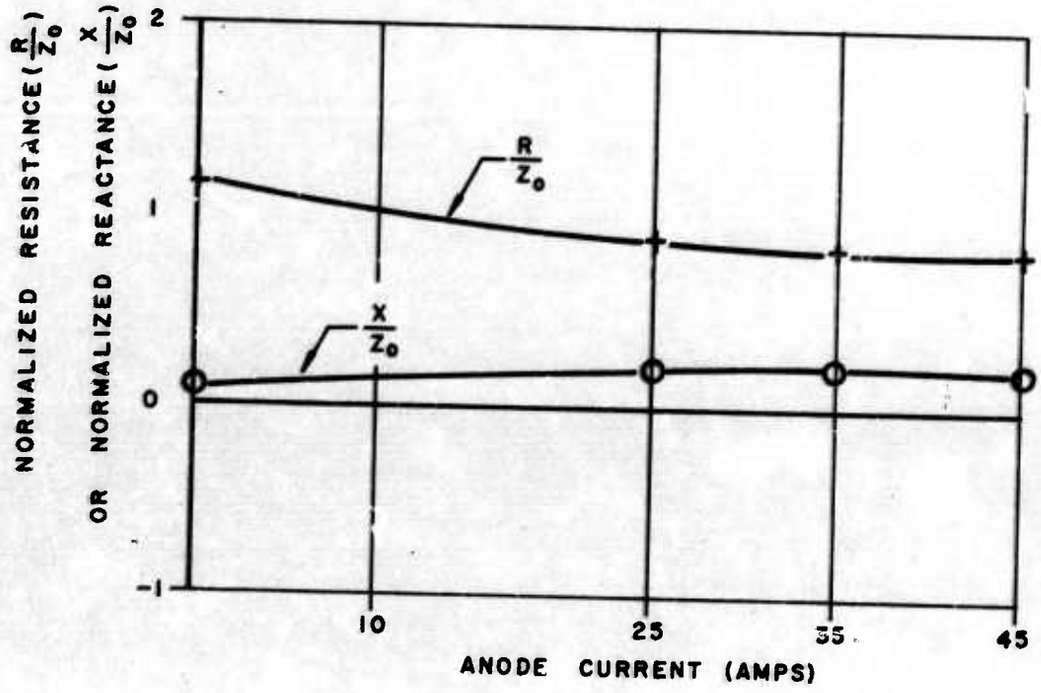

f = 2700 MC
P_{in} = 100 MW
p = 2.4 Torr.

Figure 5-15 Vertical Slot Antenna Input Impedance vs. Simulator Discharge Current

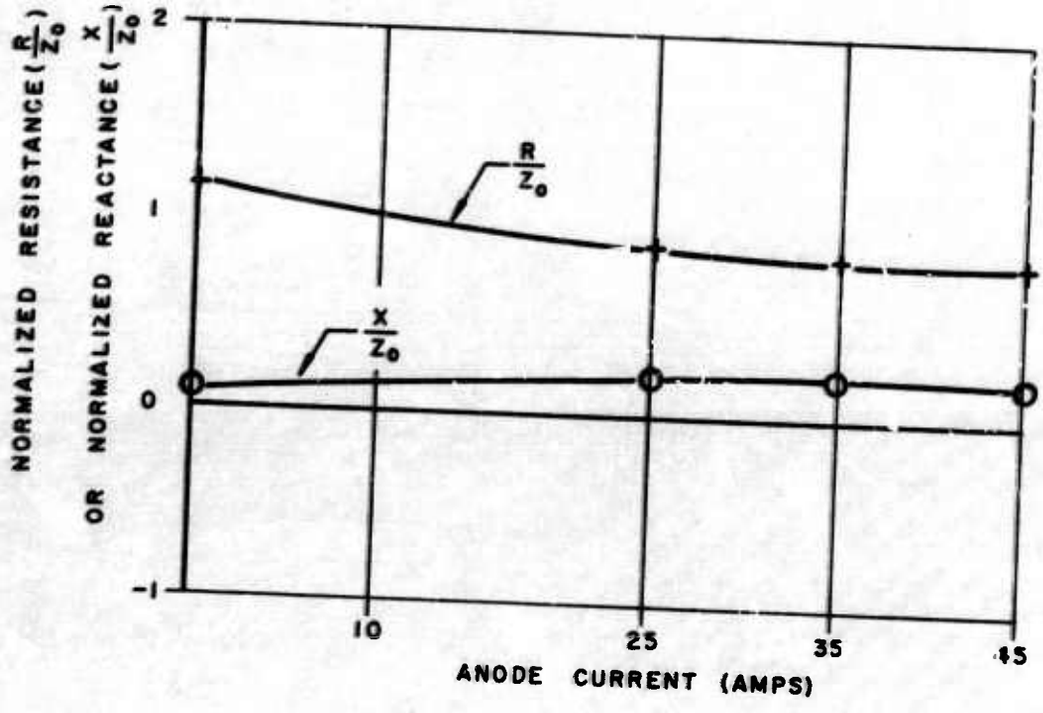

$f = 2700$ MC
$P_{in} = 100$ MW
$p = 2.4$ Torr.

Figure 5-15 Vertical Slot Antenna Input Impedance vs. Simulator Discharge Current

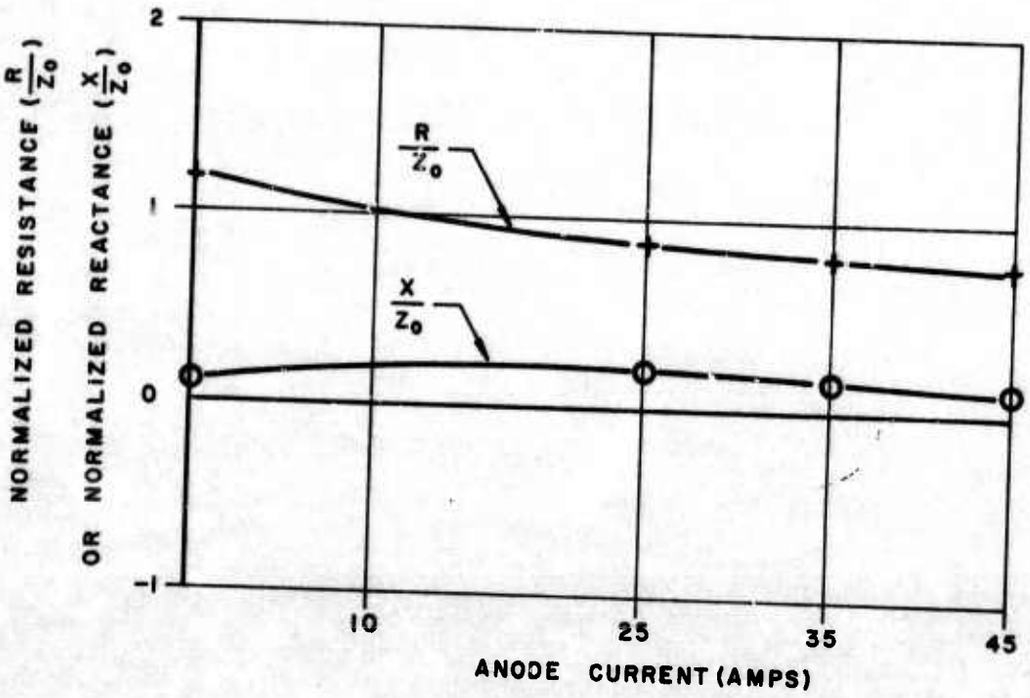

f = 2700 MC
P_{in} = 100 MW
p = 3.5 Torr

Figure 5-16 Vertical Slot Antenna Input Impedance vs. Simulator Discharge Current

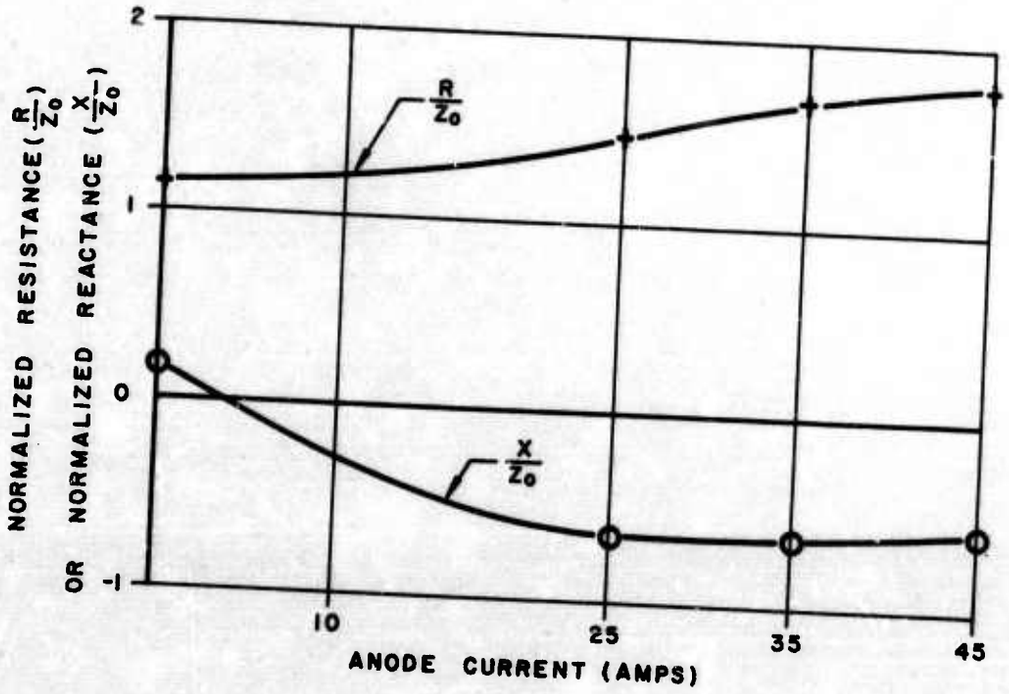

f = 2700 MC
P_{in} = 10 watts
p = 2.4 Torr

Figure 5-17 Vertical Slot Antenna Input Impedance vs. Simulator Discharge Current

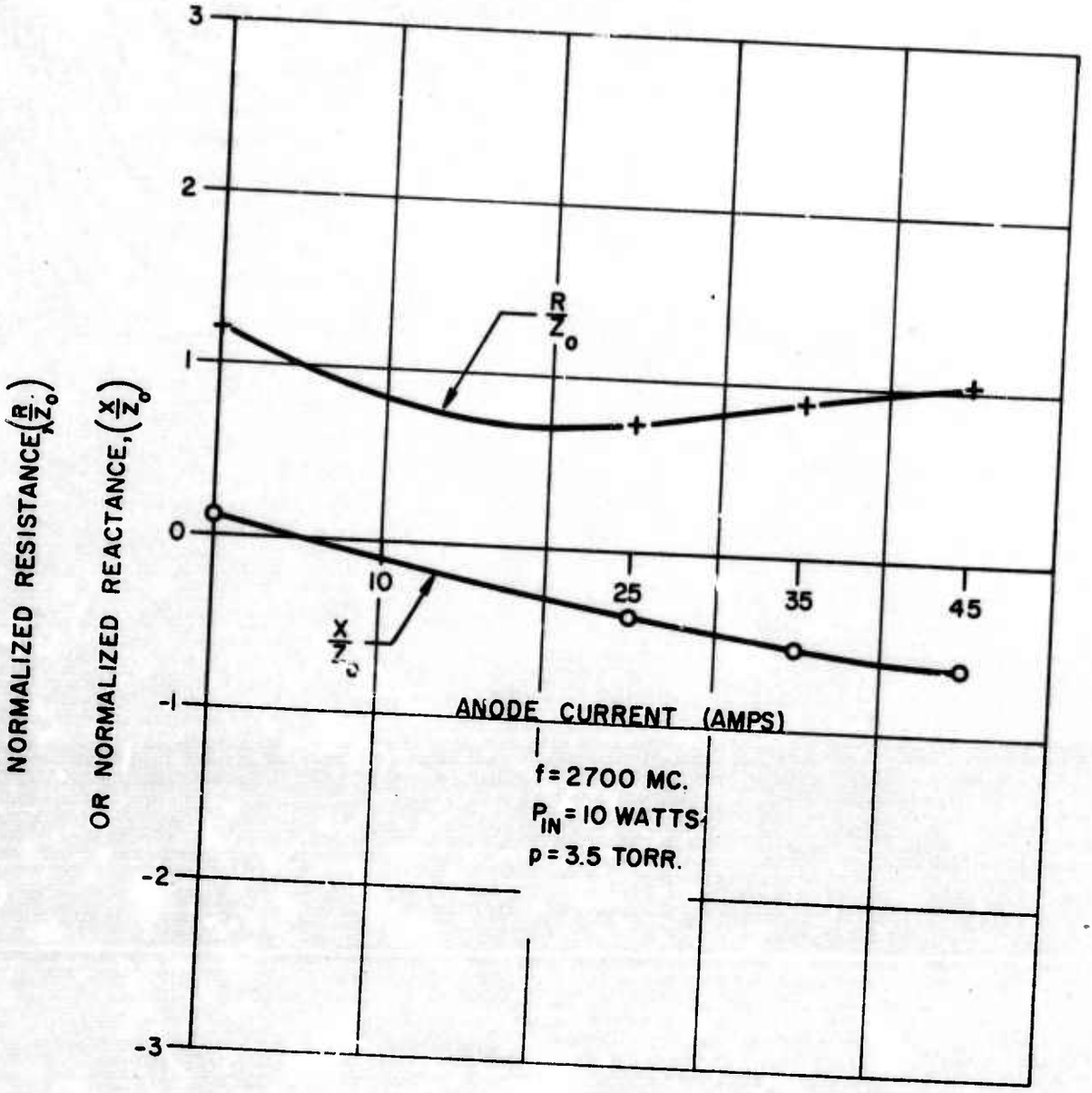

Figure 5-18 Vertical Slot Antenna Input Impedance vs. Simulator Discharge Current

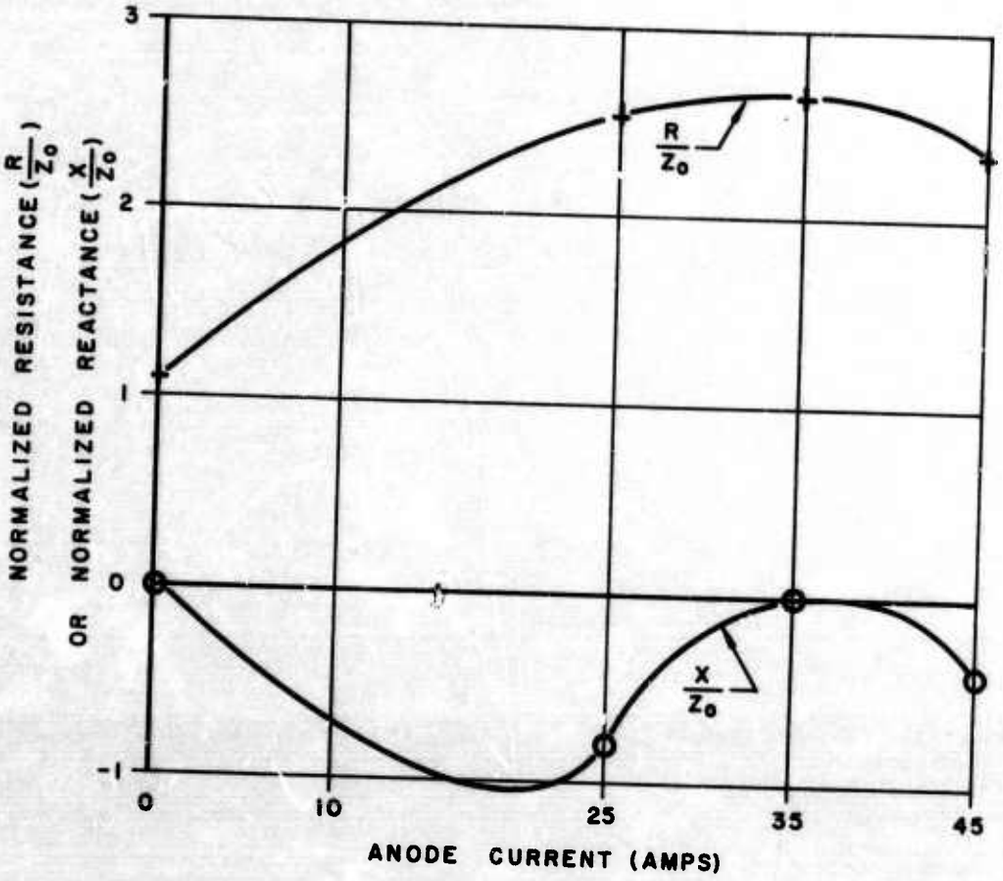

f = 2700 MC
P_{in} = 100 MW
p = 2.4 Torr

Figure 5-19 Vertical Slot Antenna Input Impedance vs. Simulator Discharge Current

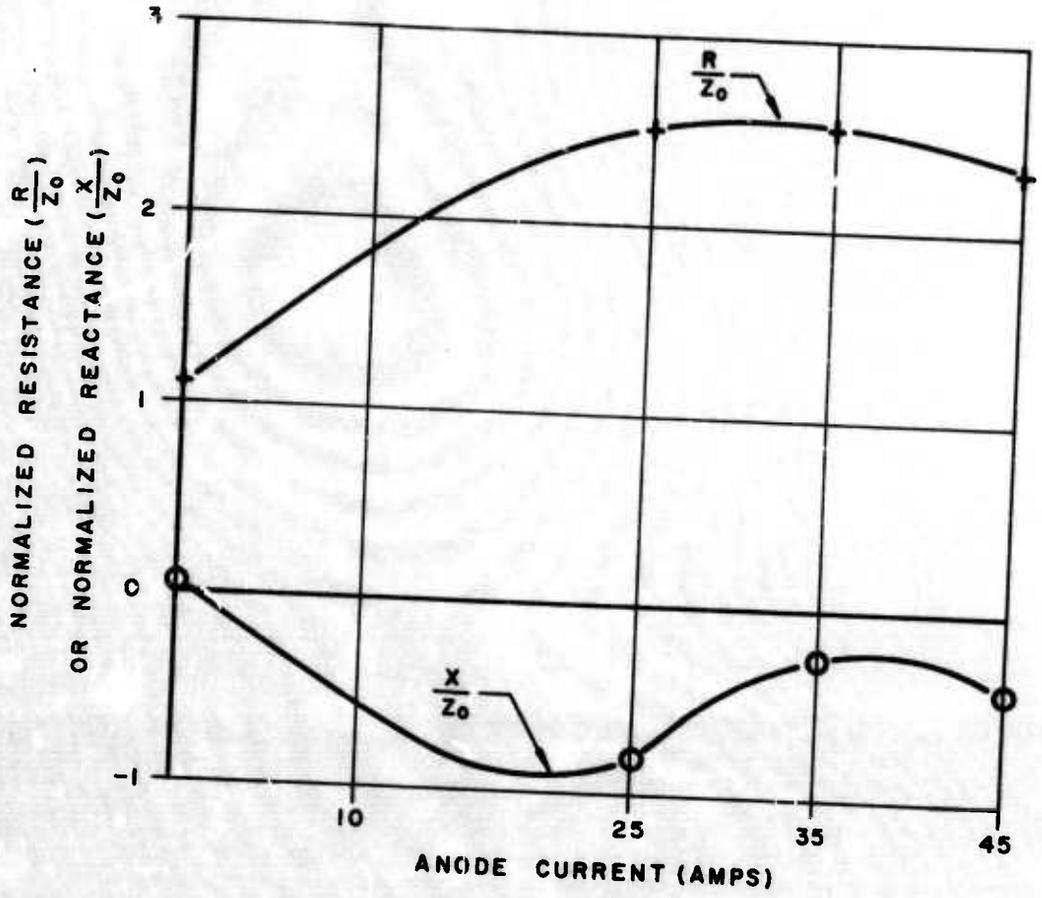

f = 2700 MC
P_{in} = 100 MW
p = 3.5 Torr

Figure 5-20 Horizontal Slot Antenna Input Impedance vs. Simulator Discharge Current

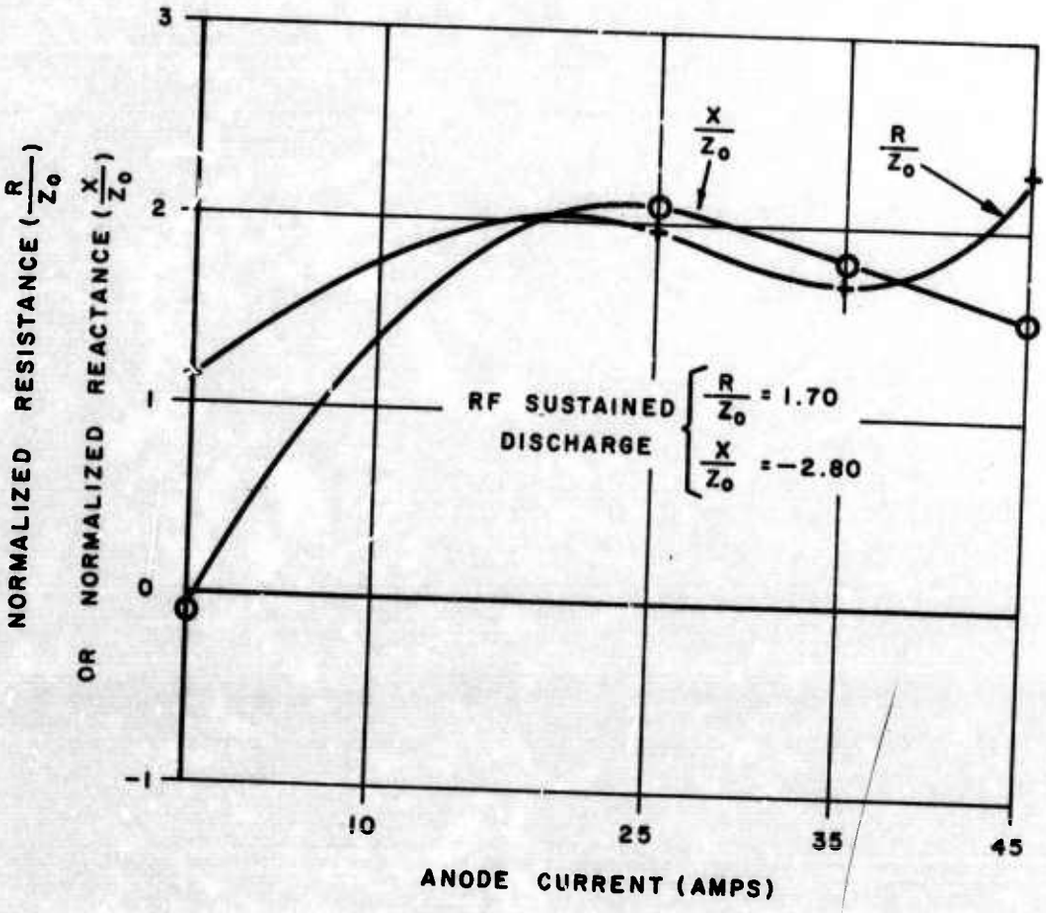

f = 2700 MC
P_{in} = 10 watts
p = 2.4 Torr

Figure 5-21 Horizontal Slot Antenna Input Impedance vs. Simulator Discharge Current

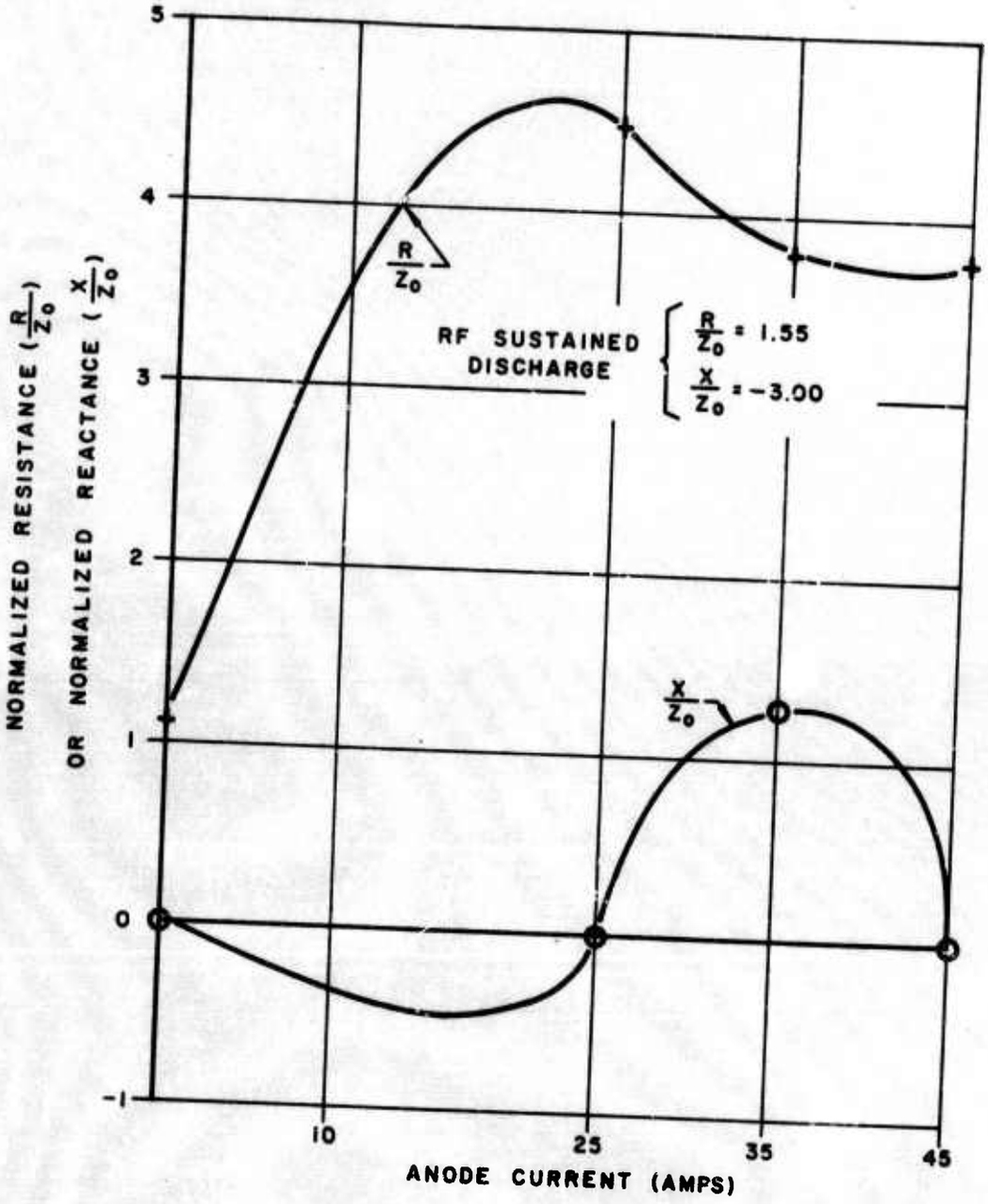

f = 2700 MC
P_{in} = 10 Watts
p = 3.5 Torr

Figure 5-22 Horizontal Slot Antenna Input Impedance vs. Simulator Discharge Current

SECTION 6

SIMULATOR DEVELOPMENT FOR IMPROVED COVERAGE OF REENTRY PARAMETERS

The Raytheon Reentry Plasma Simulator used on this program has many features which are invaluable, if not essential, for reentry electromagnetic and communications measurements. In its present form, however, the range of parameters over which the plasma is stable, and uniformly fills the envelope, is limited. Company effort towards increasing the operating range is already in progress, and the present status is described in this section.

6.1 Present Limitations

The present limitation in range of plasma operating parameters is summarized in Table 5-1.

Figure 6-1 shows the electron concentration and collision frequency ranges over which the simulator will now operate. Also in the figure are shown electron concentrations and collision frequencies generated by typical Reentry ECM vehicles following characteristic trajectories.

It is clear that the operating range of the simulator should be extended to a region of lower electron concentration and higher collision frequency.

It is believed that another operating range exists at pressures below 100 microns, provided suitable changes are made in the anode power supply system to damp out periodic, high frequency oscillations. These are most probably caused by the "load line" of the simulator being too close to the V-I operating

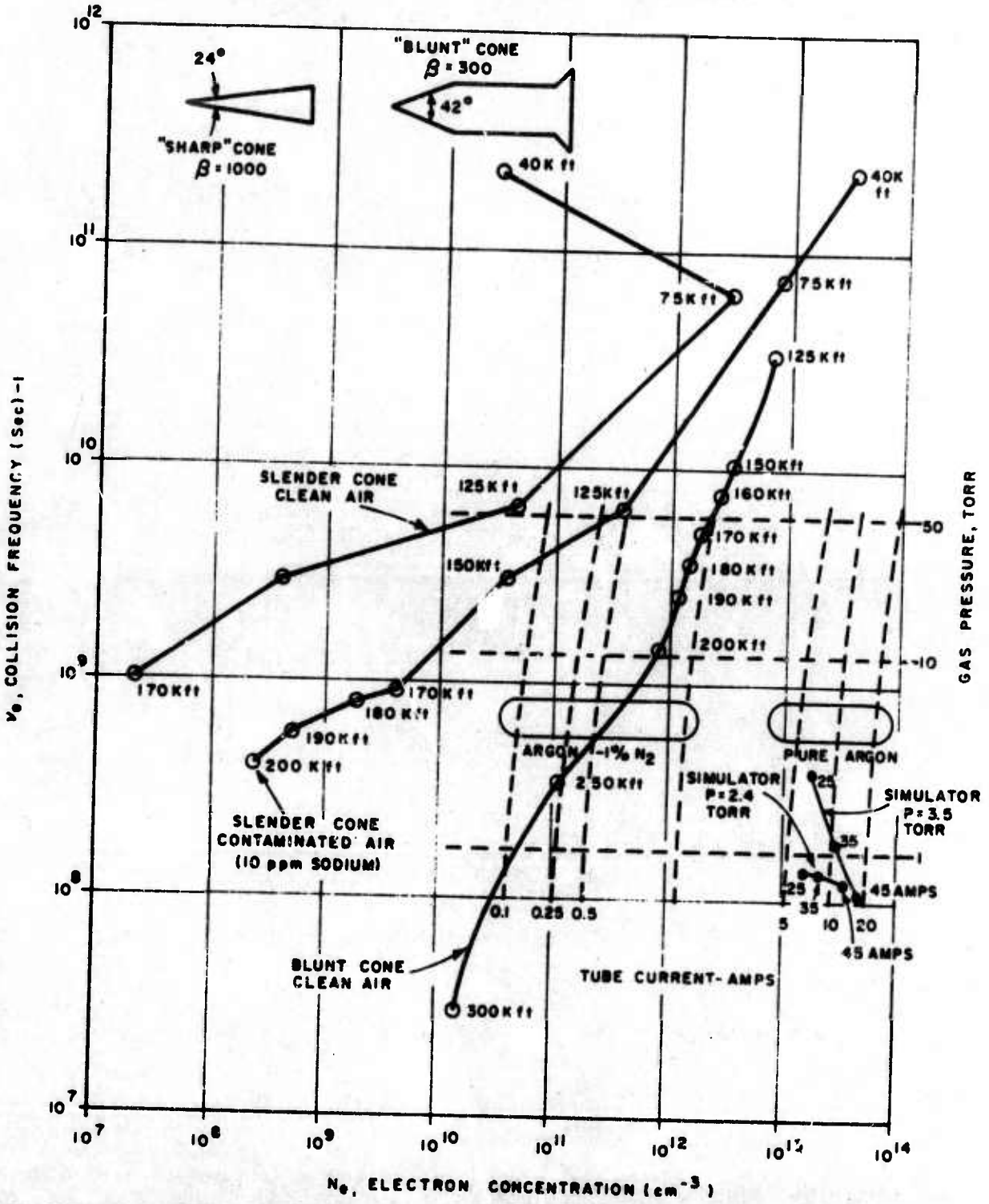

Figure 6-1. Reentry Plasma Simulator Parameters Compared with Vehicle Plasma Sheath Parameters. (Calculated n_e and ν_c for a slender, fast vehicle, and a slow, blunt cone vehicle. Slender vehicle velocity 23,500 ft/sec, blunt vehicle 12,500 ft/sec, both at 125,000 ft. Calculated simulator conditions for Argon plus 1% N_2 as well as for pure Argon are shown by dashed lines.)

characteristic, so that the total circuit resistance is on the threshold of being negative, as discussed in References (4) and (9). Assuming this to be the source of instability, the technique is simply to increase the total power supply voltage and add additional series resistance in the circuit. Since the power supply is a heavy current one, this change was not made during the present work, particularly since operation at lower pressure (and therefore lower collision frequency) was of less interest to the present investigation.

6.2 Design Considerations for the Improved System

In terms of gas discharge parameters, the desired improvements must be brought about as follows:

6.2.1 Lower Electron Concentration

From Equation 2-1, lower electron concentration can be achieved by operating at a lower tube current and/or a higher electron drift velocity. Since the first is not permissible if good filling of the plasma envelope is to be achieved, recourse must be had to increasing drift velocity. Data on drift velocity for a number of gases appears in Reference (2). Unfortunately the data are rather limited, either because precise experiments have not been made with many gases other than rare gases, or because measurements have been made under conditions not applicable to the present problem, such as in a different energy range. A mixture of argon plus one percent nitrogen shown promising possibilities (Reference 2). It should be noted that almost any other gas o. gas mixture other than pure argon would be expected to have a higher drift velocity. This gas was originally chosen with the express purpose of achieving a high electron concentration in the gaseous discharge.

6.2.2 Higher Electron Collision Frequency

The total electron collision frequency is determined in a relatively complex way by several parameters, such as neutral concentration, ion concentration, and electron temperature (Refs. 2, 10, 11). Again, data useful for our specific requirements are relatively limited.

Hence, starting perhaps with Argon plus an admixture of nitrogen, a series of different gas mixtures must be experimentally tried over a range of pressures and tube currents, to determine their operating conditions for good stability and filling of the glass envelope. Then those mixtures and conditions most appropriate for ECM Reentry conditions must be selected, following Figure 6-1.

6.3 Current Development of an Improved System

From the preceding discussion and knowledge of discharge tube design requirements, it is clear that additions must be made to the simulator in the form of a precise gas supply and mixing system. The gases must be of extreme high purity (less than 1 ppm contaminants), so that the system must be fully bakeable for many hours at temperatures up to 400 deg. C. The pressure must be accurately measured and controlled over a relatively wide range (say 1 micron to 760 Torr). It follows, of course, that pressure indicators and valves must also be bakeable.

A further requirement also emerged from some early experiments on the simulator. When a 1% Nitrogen in Argon mixture was used, while a good discharge was obtained, the nitrogen was effectively removed from the system in about a minute by ion bombardment. Clean-up also occurs with pure Argon, of course,

but at a negligible in Vac-Ion pumps. In these pumps, it is well known that rare gases are very difficult to pump, whereas pumping for other gases is quite rapid. Thus the new system must be designed to feed gas in continuously to replenish cleaned-up gases. This immediately dictates the need for a sophisticated, precise, bakeable automatic pressure control system for the simulator.

It would be desirable that gases be used which do not poison the hot thermionic cathodes. Thus this class of gases will be selected first for experiment. Should this prove impossible, or should it be desired for ECM system reasons that a damaging gas such as oxygen be used, then a simulator design has been formulated in which the cathodes would operate under an inert gas blanket, while the system gases are fed into the simulator without contacting the cathodes. Such a technique has proved feasible at the NASA Ames Research Center, although in a different configuration and application, namely a high temperature plasma arc.

Development and construction of the new high purity, bakeable, mixed gas continuous feed system and bakeable pressure gauges and controller has proceeded at the Raytheon Company to the point where the main, critical items have been constructed ready for trial. A photograph of the system is shown in Figure 6-2.

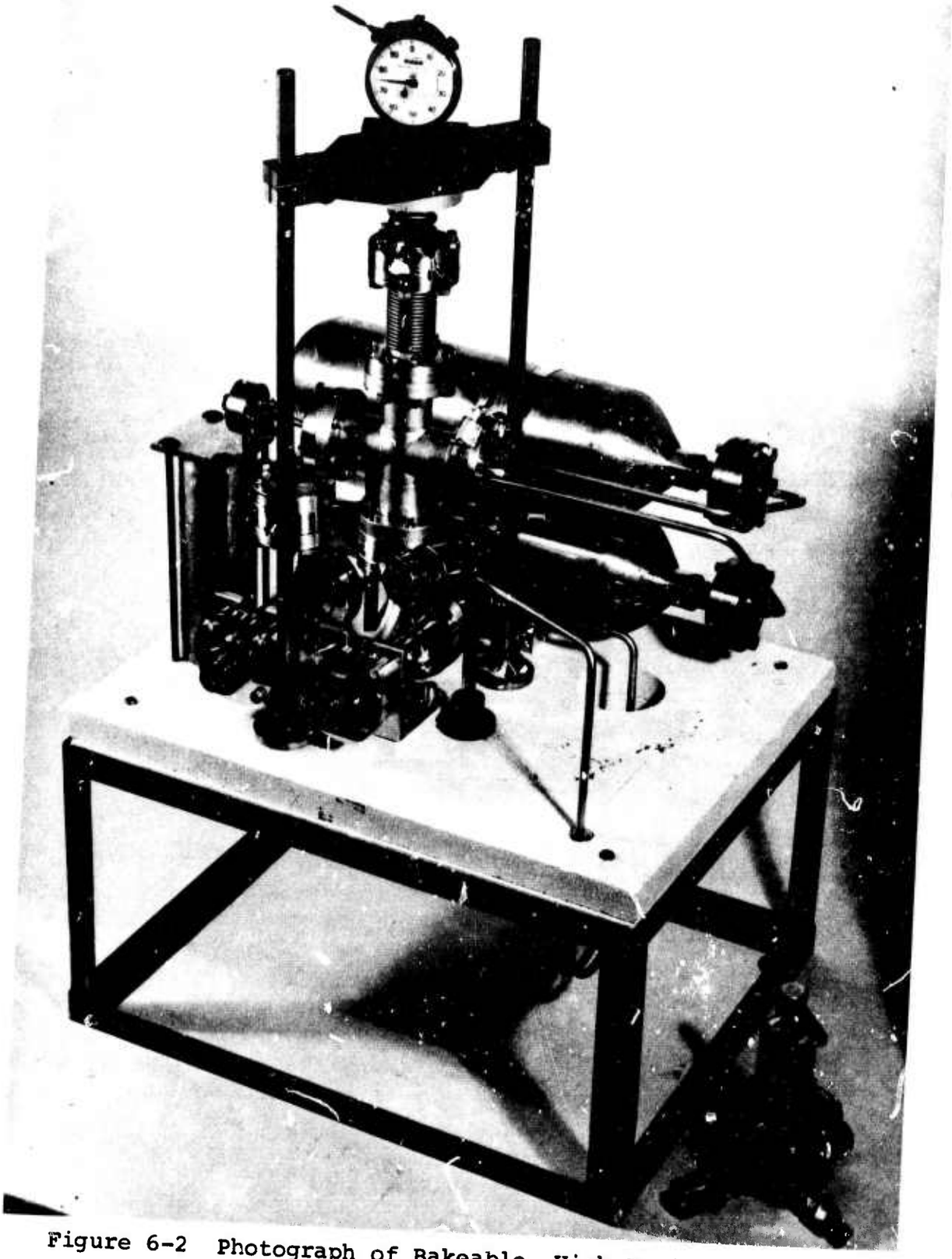

Figure 6-2 Photograph of Bakeable, High Purity, Mixed Gas Continuous Feed and Pressure Control System

SECTION 7

CONCLUSIONS

At present, simulation of reentry plasma sheath collision frequency and electron density, utilizing an argon dc discharge with externally heated cathodes, seems to be limited to collision frequencies below 5×10^8 $(sec.)^{-1}$ and electron densities above $10^{13}(cm)^{-3}$. The use of a gas other than argon or gas mixtures such as argon and one percent nitrogen may shift and perhaps extend the range of simulation of reentry plasma parameters. The nitrogen in the argon-nitrogen mixture, however, is driven into the simulator walls by the discharge within a few seconds. Such a gas mixture is unuseable unless nitrogen can be fed into the simulator at a precisely controlled rate. Raytheon development work on a system of this kind is described in Section 6.0.

The simulator fills with plasma between 75% and 90% depending on the discharge current. It is felt, however, that antenna measurements are not significantly affected by the unfilled portion of the simulator since most of the power dissipated is due to absorption in the plasma.

Strong interference effects are observed in the "no plasma" antenna patterns if all metal structures at the base of the simulator are not well covered with absorber material. The "pack-in place" absorber ring at the base of the simulator has a negligible effect on the antenna patterns, and no change in signal attenuation in the far field results when the ring of absorber is removed.

It is difficult to extract the effect of the polarization of the vertical slot antenna on the measurements from the "padding" effect due to the internal loss (4db) of the antenna. Due to the mismatch between the coaxial feed cables and the slot antennas the input impedance is very frequency-sensitive, thus requiring the frequency to be held constant to within a few mega-cycles.

RF shielding of cables and connectors in coaxial systems is extremely important when antenna pattern measurements are made for plasma attenuations greater than approximately 20db. For coaxial systems, measurements of input VSWR and impedance should be made at the antenna inputs. Errors introduced in the VSWR measurements due to mismatches at the connectors are as high as 15%.

In the presence of a highly overdense plasma (i.e., $\omega_p/\omega > 20$) the isolation between orthogonally oriented slot antennas decreases by more than 20db. The maximum input VSWR attainable (for a low loss slot antenna) is about 4.5. Since the antenna patterns show an average attenuation on the order of 30db, most of the power loss is due to absorption in the plasma. RF heating of the plasma appreciably affects the antenna input impedance. At high input power (i.e., 10 watts) the impedance is also appreciably affected by a change in gas pressure of 1 Torr.

7.1 Recommendations

It was difficult to shield the steel flanges of the cathode stems on the simulator from the antenna fields, since the flanges are only about 5 inches from the antenna slots. It would be desirable to lengthen the cylindrical portion of the simulator envelope at least 5 inches. At present, the Langmuir probes

are located near the simulator anode requiring electron density measurements to be extrapolated down to the region of the antenna apertures. It would be preferable to have a probe at the same height of the antenna apertures but 90 degrees to the right or left of the apertures. New gases and gas mixtures should be investigated for obtaining higher collision frequencies and lower electron densities while obtaining satisfactory filling of the simulator. The nature and causes of the plasma instabilities observed in the argon discharge should be investigated and means for eliminating such instabilities should be implemented.

If two or more antennas of the same type are to be mounted at various places, and with a prescribed relative orientation, on the surface of a vehicle model for the purpose of studying the effect of the plasma sheath on antenna location and orientation it is imperative that the electrical characteristics of the antennas be identical. Furthermore, if small plasma effects at the antenna apertures are to be measured at the antenna inputs, the antennas should have small internal losses. To facilitate making measurements over the frequency band of interest the antennas should be matched to the transmission line at their inputs over the entire frequency band. The use of stub tuners at the inputs make the measurements highly frequency-sensitive. These antenna design considerations can be more easily met if the antennas can be constructed from waveguide only, from the input to the radiating aperture on the surface of the vehicle model. Furthermore, an all waveguide S-Band system is imperative if errors due to mismatches of connectors in a coaxial system are to be eliminated.

It is recommended that the vehicle model be constructed in two easily detachable parts. Such a construction would

facilitate the repairing or modification of any particular antenna on the model without requiring the other antennas to be removed or essentially dismantling the entire model.

SECTION 8

SUMMARY OF ANALYTICAL STUDIES

8.1 Analytical Approach - Cone Problem

The model considered for this problem of radiation from slot antennas consists of a semi-infinite metallic (perfectly conducting) cone with a spherical cap of radius r_o at the tip of the cone (see Figure 8-1). This conducting cone represents an ECM vehicle. The cone is assumed to be covered by a uniform plasma sheath occupying the region $r>r_o$ and $\alpha<\theta<\beta$, where the angle θ is measured from the axis of the cone. The angles $\theta = \alpha$ and $\theta = \beta$ define the surfaces of the conical vehicle and the plasma sheath respectively. Two orthogonally oriented slot antennas are mounted on the surface of the conducting cone. These radiating elements radiate through the plasma sheath into the free space.

The method of approach (see References 4, 7, 8, 9) consists of introducing appropriate radial eigen functions for each region (i.e., for plasma and free space regions). In order to remove some mathematical difficulties encountered in the construction of radial eigen functions, a spherical cap on the nose of the cone is introduced as a mathematical model of the problem. For details the reader is referred to References (4) and (9).

At present the problem is incomplete. However, the approach is discussed clearly in References (4) and (9).

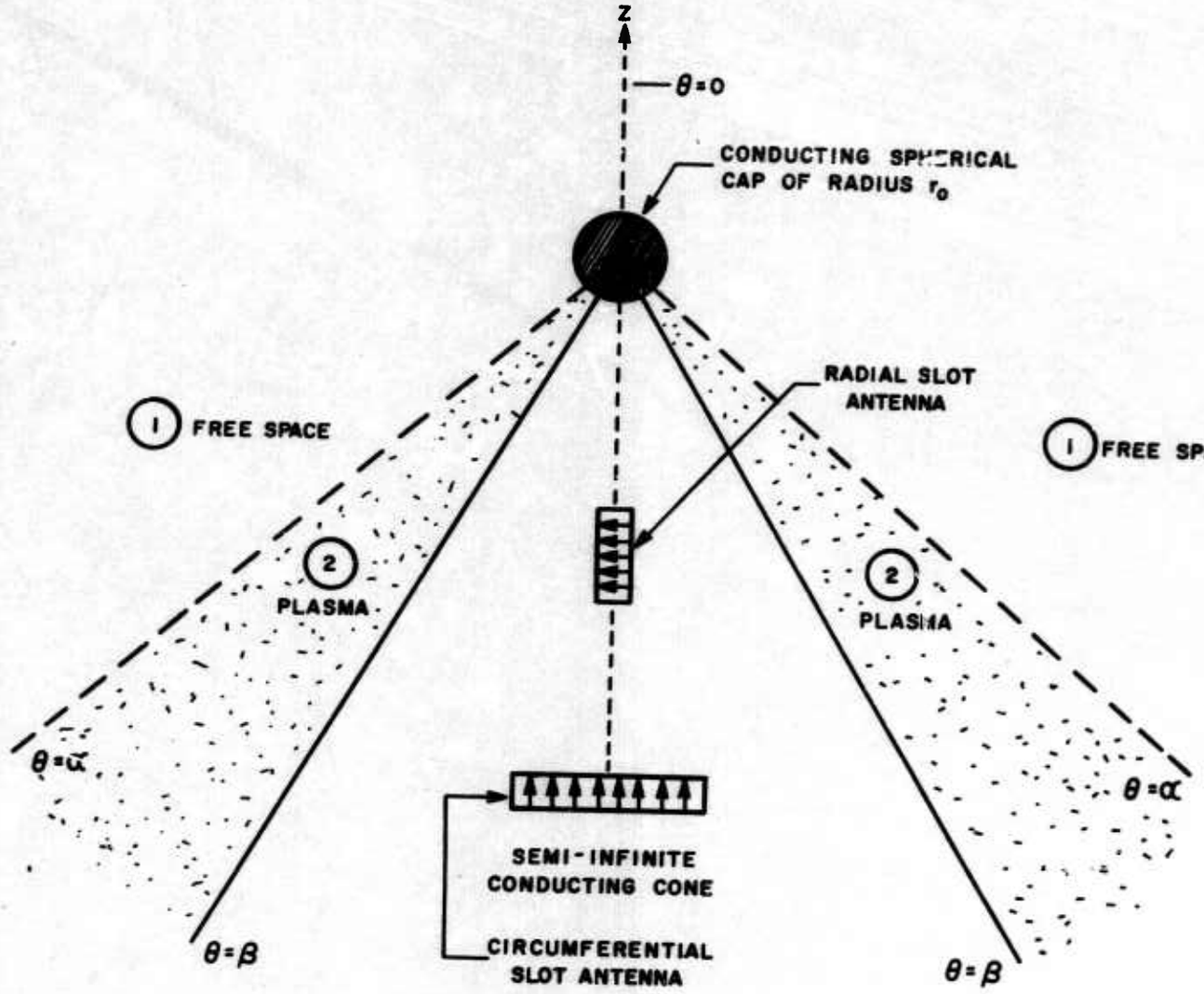

Figure 8-1 Mathematical Model of the Cone Problem

The purpose of this problem was to calculate the radiation pattern, the phase of the radiated fields and the mutual impedance between the two antennas.

RAYTHEON COMPANY
SPACE AND INFORMATION SYSTEMS DIVISION

SECTION 9 (SECRET)

See Supplemental Volume

S67-4138A

SECTION 10

REFERENCES

1. von Engel, "Ionized Gases," second edition, Clarendon Press 1965.

2. S.C. Brown, "Basic Data of Plasma Physics," John Wiley and Sons, 1959.

3. Rolfe, et al, "Final Technical Report, Energy Processes in Shock Waves," RADC, Contract AF30-(602)-2716, RADC TDR-64-269, Volumes I and II (1963).

4. Rolfe, et al, Third Quarterly Report, "Study of ECM Antenna Optimization (U)" AFCRL-66-80, Contract No. AF19(628)5519, Project #8671, Raytheon Report No. FR-66-209 (1966).

5. M. Sucher and J. Fox, "Handbook of Microwave Measurements," Third Edition, Vol. III, Polytechnic Press of the Polytechnic Institute of Brooklyn (1963).

6. H. Jasik, "Antenna Engineering Handbook," McGraw-Hill, 1961.

7. Yeh, C. "An Application of Sommerfeld's Complex-order Wave-functions to an Antenna Problem." J. Math. Phys., Vol. 5, pp.344-350, March 1964.

8. Samaddar, S.N., "Mathematical Analysis of the Radiation from a Magnetic Line Source on a Cylindrically Capped Wedge Covered by a Plasma," App. Sc. Research, Vol. 16, pp.89-101, 1966.

9. Rolfe, E., et al, Second Quarterly Report, "Study of ECM Antenna Optimization (U)", AFCRL-66-80, Contract No. AF19(628)-5519, Project #8671, Raytheon Report No. FR-66-12 (1966).

10. Ratcliff, "The Magneto-Ionic Theory," Cambridge University Press.

11. Massey & Burhop, "Electronic and Ionic Impact Phenomena," Oxford Clarendon Press (1956).

UNCLASSIFIED
Security Classification

DOCUMENT CONTROL DATA - R&D

(Security classification of title, body of abstract and indexing annotation must be entered when the overall report is classified)

1. ORIGINATING ACTIVITY (Corporate author)
RAYTHEON COMPANY, SISD
528 BOSTON POST ROAD
SUDBURY, MASSACHUSETTS 01776

2a. REPORT SECURITY CLASSIFICATION
UNCLASSIFIED

2b. GROUP

3. REPORT TITLE

STUDY OF ECM ANTENNA OPTIMIZATION

4. DESCRIPTIVE NOTES (Type of report and inclusive dates)
SCIENTIFIC REPORT, FINAL, JUNE 1965 — MARCH 1967

APPROVED
20 JULY 1967

5. AUTHOR(S) (Last name, first name, initial)
SFORZA, PHILLIP F.
SAMADDAR, SURENDRA N.
ROLFE, EDWARD
WEISS, JOHN G.

6. REPORT DATE
20 MARCH 1967

7a. TOTAL NO. OF PAGES
135

7b. NO. OF REFS
11

8a. CONTRACT OR GRANT NO.
AF19(628)5519 ARPA ORDER

b. PROJECT NO.
No. 693
8671

c. DoD ELEMENT 6250301R

d. DoD SUBELEMENT NONE

9a. ORIGINATOR'S REPORT NUMBER(S)
U67-4138 UNCLASSIFIED
FINAL REPORT (I)

9b. OTHER REPORT NO(S) (Any other numbers that may be assigned this report)
AFCRL-67-0348

10. AVAILABILITY/LIMITATION NOTICES THIS DOCUMENT IS SUBJECT TO SPECIAL EXPORT CONTROLS AND EACH TRANSMITTAL TO FOREIGN GOVERNMENTS OR FOREIGN NATIONALS MAY BE MADE ONLY WITH PRIOR APPROVAL OF HQ. AFCRL, OAR (CRDM) USAF, L.G. HANSCOM FIELD, BEDFORD, MASS. 01730

11. SUPPLEMENTARY NOTES THIS RESEARCH WAS SPONSORED BY THE ADVANCED RESEARCH PROJECTS AGENCY.

12. SPONSORING MILITARY ACTIVITY
AIR FORCE CAMBRIDGE RESEARCH LABORATORIES (CRD)
L.G. HANSCON FIELD, BEDFORD, MASS 01730

13. ABSTRACT MEASUREMENTS ON THE EFFECTS OF A CONICAL PLASMA SHEATH ON TWO ORTHOGONALLY ORIENTED SLOT ANTENNAS FLUSH-MOUNTED ON THE SURFACE OF A CONICAL VEHICLE MODEL WERE MADE. THE PLASMA PARAMETERS WERE VARIED OVER THE RANGE $13 < \omega_p/\omega < 23$, $.007 < \nu/\omega < .026$. THE MEASUREMENTS WERE PERFORMED AT 2700 MC WITH INPUT POWERS OF 100 MILLIWATTS AND 10 WATTS.

THE ANTENNA PATTERNS SHOW STRONG INTERFERENCE EFFECTS AND SIGNAL ATTENUATION ON THE ORDER OF 30 DB. ISOLATION BETWEEN THE SLOT ANTENNAS IS FOUND TO DECREASE 20 DB FOR $\omega_p/\omega > 20$ AND $\nu/\omega < .008$. THE ANTENNA INPUT IMPEDANCE IS OBSERVED TO BE APPRECIABLY AFFECTED BY PRESSURE CHANGES OF 1 TORR IN ARGON FOR HIGHPUT POWER (I.E., 10 WATTS). THE IMPEDANCE IS ALSO OBSERVED TO UNDERGO AN APPRECIABLE CHANGE FOR HIGH POWER BUT CONSTANT PRESSURE. THE GREATEST CHANGE IN INPUT IMPEDANCE IS PRODUCED BY AN RF SUSTAINED PLASMA AT THE ANTENNA APERTURE AT HIGH POWER. THE PLASMA SHEATH PRODUCED A MAXIMUM VSWR OF 4.5 INDICATING THAT THE MAJOR LOSS OF POWER WAS DUE TO ABSORPTION IN THE PLASMA. THE RF SUSTAINED PLASMA PRODUCED A MAXIMUM VSWR OF 7.8.

DEVELOPMENTS IN PROGRESS TO EXTEND THE OPERATING RANGE OF THE SIMULATOR ARE DESCRIBED.

THE ANALYTICAL PROBLEM OF DETERMINING THE INPUT IMPEDANCE AND RADIATION FIELD PATTERN OF A SLOT ANTENNA ON THE SURFACE OF AN INFINITE CONDUCTING CONE COVERED BY A PLASMA SHEATH IS FORMULATED.

A SUMMARY OF A SYSTEMS ANALYSIS IS PRESENTED. (THIS ANALYSIS IS INCLUDED IN SECRET DOCUMENT S67-4138A).

DD FORM 1 JAN 64 1473

UNCLASSIFIED
Security Classification

14. KEY WORDS	LINK A		LINK B		LINK C	
	ROLE	WT	ROLE	WT	ROLE	WT
RE-ENTRY TECHNOLOGY	4,8	3				
ECM SYSTEMS	2	2				
PLASMA	5,6,8	3				
PLASMA SIMULATION	8,10	3				
ANTENNA	2,4,8	3				
ANTENNA DECOUPLING	2,7	3				
VEHICLE PARAMETERS	1	3				
PLASMA PARAMETER ANALYSIS		2				
PLASMA EFFECTS ANALYSIS	10	2				

INSTRUCTIONS

1. ORIGINATING ACTIVITY: Enter the name and address of the contractor, subcontractor, grantee, Department of Defense activity or other organization *(corporate author)* issuing the report.

2a. REPORT SECURITY CLASSIFICATION: Enter the overall security classification of the report. Indicate whether "Restricted Data" is included. Marking is to be in accordance with appropriate security regulations.

2b. GROUP: Automatic downgrading is specified in DoD Directive 5200.10 and Armed Forces Industrial Manual. Enter the group number. Also, when applicable, show that optional markings have been used for Group 3 and Group 4 as authorized.

3. REPORT TITLE: Enter the complete report title in all capital letters. Titles in all cases should be unclassified. If a meaningful title cannot be selected without classification, show title classification in all capitals in parenthesis immediately following the title.

4. DESCRIPTIVE NOTES: If appropriate, enter the type of report, e.g., interim, progress, summary, annual, or final. Give the inclusive dates when a specific reporting period is covered.

5. AUTHOR(S): Enter the name(s) of author(s) as shown on or in the report. Enter last name, first name, middle initial. If military, show rank and branch of service. The name of the principal author is an absolute minimum requirement.

6. REPORT DATE: Enter the date of the report as day, month, year, or month, year. If more than one date appears on the report, use date of publication.

7a. TOTAL NUMBER OF PAGES: The total page count should follow normal pagination procedures, i.e., enter the number of pages containing information.

7b. NUMBER OF REFERENCES: Enter the total number of references cited in the report.

8a. CONTRACT OR GRANT NUMBER: If appropriate, enter the applicable number of the contract or grant under which the report was written.

8b, 8c, & 8d. PROJECT NUMBER: Enter the appropriate military department identification, such as project number, subproject number, system numbers, task number, etc.

9a. ORIGINATOR'S REPORT NUMBER(S): Enter the official report number by which the document will be identified and controlled by the originating activity. This number must be unique to this report.

9b. OTHER REPORT NUMBER(S): If the report has been assigned any other report numbers *(either by the originator or by the sponsor)*, also enter this number(s).

10. AVAILABILITY/LIMITATION NOTICES: Enter any limitations on further dissemination of the report, other than those imposed by security classification, using standard statements such as:

(1) "Qualified requesters may obtain copies of this report from DDC."

(2) "Foreign announcement and dissemination of this report by DDC is not authorized."

(3) "U. S. Government agencies may obtain copies of this report directly from DDC. Other qualified DDC users shall request through _____."

(4) "U. S. military agencies may obtain copies of this report directly from DDC. Other qualified users shall request through _____."

(5) "All distribution of this report is controlled. Qualified DDC users shall request through _____."

If the report has been furnished to the Office of Technical Services, Department of Commerce, for sale to the public, indicate this fact and enter the price, if known.

11. SUPPLEMENTARY NOTES: Use for additional explanatory notes.

12. SPONSORING MILITARY ACTIVITY: Enter the name of the departmental project office or laboratory sponsoring *(paying for)* the research and development. Include address.

13. ABSTRACT: Enter an abstract giving a brief and factual summary of the document indicative of the report, even though it may also appear elsewhere in the body of the technical report. If additional space is required, a continuation sheet shall be attached.

It is highly desirable that the abstract of classified reports be unclassified. Each paragraph of the abstract shall end with an indication of the military security classification of the information in the paragraph, represented as *(TS)*, *(S)*, *(C)*, or *(U)*.

There is no limitation on the length of the abstract. However, the suggested length is from 150 to 225 words.

14. KEY WORDS: Key words are technically meaningful terms or short phrases that characterize a report and may be used as index entries for cataloging the report. Key words must be selected so that no security classification is required. Identifiers, such as equipment model designation, trade name, military project code name, geographic location, may be used as key words but will be followed by an indication of technical context. The assignment of links, rules, and weights is optional.